EFFECT OF THE PILE PROPERTIES AND SOIL PARAMETERS ON THE DYNAMIC BEHAVIOR OF PILED FOUNDATIONS

KAZIK ÖZELLİKLERİ VE ZEMİN PARAMETRELERİNİN KAZIKLI TEMELLERİN DİNAMİK DAVRANIŞINA ETKİSİ

SERKAN NURİ TAŞTEKİN

PROF. DR BERNA UNUTMAZ

Supervisor

ASSOC. PROF. DR NABİ KARTAL TOKER

Co-Supervisor

Submitted to

Graduate School of Science and Engineering of Hacettepe University

as a Partial Fulfillment to the Requirements

for the Award of the Degree of Master of Science

in Civil Engineering

2024

Dedicated to my family

ABSTRACT

EFFECT OF THE PILE PROPERTIES AND SOIL PARAMETERS ON THE DYNAMIC BEHAVIOR OF PILED FOUNDATIONS

Serkan Nuri TAŞTEKİN

Master of Science, Department of Civil Engineering

Supervisor: Prof. Dr. Berna UNUTMAZ

Co- Supervisor: Assoc. Prof. Dr. Nabi Kartal TOKER

June 2024, 175 pages

The rapid urbanization in today's world has resulted in decrease of suitable lands for new constructions, forcing people to construct new buildings on challenging soils with bearing capacity and settlement issues. To overcome these challenges, various methods are implemented in the past few decades. Piled foundations are one of the most frequently used solutions for the structures built on problematic soils. The proper design of piled foundation system is an important aspect from engineering point of view.

In the design of structures, it is crucial to consider the interactions between the structure, foundation system and soil under seismic effects. For instance, a building with identical foundation systems on the same soil layer may exhibit varying behavior during different earthquake scenarios. Moreover, numerous variables impact the seismic behavior of piled

foundations, such as soil parameters and structural properties. To ensure the structural integrity and safety of a structure against seismic effects, thorough analysis of the earthquake-soil-structure interaction is significantly important.

In this study, the behavior of piled foundations under the effect of seismic forces was investigated using Plaxis 2D finite element software. A parametric study was conducted involving kinematic interaction analysis of piles of different diameters, spacing, and lengths in layered soil profiles consisting of loose sand, dense sand, and rock units using earthquake records with different peak ground accelerations. Analysis results, including the accelerations in the soil and the internal forces of piles (bending moments and shear forces), were compared and the influence of different variables on the analysis results were discussed.

ÖZET

KAZIK ÖZELLİKLERİ VE ZEMİN PARAMETRELERİNİN KAZIKLI TEMELLERİN DİNAMİK DAVRANIŞINA ETKİSİ

Serkan Nuri TAŞTEKİN

Günümüz dünyasında hızlı kentleşme, yeni yapılara uygun arazilerin azalmasına neden olmuş, bu durum da insanların taşıma gücü ve oturma sorunları olan zorlu zeminlerde yeni yapılar inşa etmek durumunda kalmalarıyla sonuçlanmıştır. Bu sorunların üstesinden gelebilmek için son dönemlerde çeşitli yöntemler uygulanmıştır. Kazıklı temeller sorunlu zeminler üzerine inşa edilen yapılar için en sık kullanılan çözüm yöntemlerinden birisidir ve bu temel sistemlerinin tasarımı mühendislik açısından önemli bir husustur.

Yapıların tasarımında sismik etkiler altında yapı, temel sistemi ve zemin arasındaki etkileşimlerin dikkate alınması büyük önem taşımaktadır. Örneğin, aynı zemin tabakası üzerinde aynı temel sistemine sahip bir bina, farklı deprem senaryolarında farklı davranışlar sergilemektedir. Ayrıca, kazıklı temellerin sismik davranışını zemin

parametreleri ve yapısal özellikler gibi çok sayıda değişken etkilemektedir. Bir yapının yapısal bütünlüğünü ve sismik etkilere karşı güvenliğini sağlamak için deprem-yapı-zemin etkileşiminin ayrıntılı analizi oldukça önemlidir.

Bu çalışmada, kazıklı temellerin deprem yükleri etkisi altındaki davranışları Plaxis 2D sonlu elemanlar yazılımı kullanılarak incelenmiştir. Bu kapsamda, farklı büyüklükte yer ivmelerine sahip deprem kayıtları kullanılarak gevşek kum, sıkı kum ve kaya birimlerinin çeşitli kombinasyonlarından oluşan tabakalı zemin profillerinde farklı çap, aralık ve boylara sahip kazıkların kinematik etkileşim analizlerini içeren bir parametrik çalışma yapılmıştır. Analiz sonuçlarında zeminlere etkiyen ivmeler ve kazıklara etkiyen iç kuvvetler (momentler ve kesme kuvvetleri) kıyaslanmış ve farklı değişkenlerin analiz sonuçları üzerindeki etkileri incelenmiştir.

Anahtar Kelimeler: Kazıklı temeller, Kinematik etkileşim, Dinamik analiz, Plaxis 2D, Deprem, Geoteknik tasarım

ACKNOWLEDGEMENTS

TABLE OF CONTENTS

LIST OF FIGURES

xiii

LIST OF TABLES

SYMBOLS AND ABBREVIATIONS

Symbols

A	Cross sectional area (m^2)
a	Acceleration (m/s^2)
A_s	Surface area (m^2)
A_p	Pile tip area (m^2)
$\underline{C}$	Damping matrix (-)
c'	Effective soil cohesion (kPa)
D	Pile diameter (m)
E	Elasticity modulus (kPa)
E_{50}	Secant modulus (kPa)
E_{oed}	Oedometric modulus (kPa)
E_{ur}	Unloading-reloading elastic modulus (kPa)
f	Natural frequency (Hz)
f_{max}	Fundamental frequency of input signal (Hz)
f_p	Predominant frequency of input signal (Hz)
G	Shear modulus (kPa)
G_0	Maximum shear modulus (kPa)
G_{sec}	Secant shear modulus (kPa)
G_t	Tangent shear modulus (kPa)
G_{ur}	Unloading-reloading shear modulus (kPa)
H	Layer thickness (m)
H_1	Thickness of the top layer (m)
H_2	Thickness of the bottom layer (m)
I	Inertia (m^4)

$\underline{K}$	Stiffness matrix (-)
K_s	Coefficient of earth pressure at rest (-)
$K_{0,nc}$	Coefficient of earth pressure at rest for normally consolidated soils (-)
L	Pile length (m)
M	Bending moment (kNm)
$\underline{M}$	Mass matrix (-)
m	Stress level dependency (-)
N_q	Bearing capacity factor (-)
N_{60}	Corrected SPT blow count (-)
$N_{1,60}$	Overburden corrected SPT blow count (-)
p_{ref}	Reference pressure (kPa)
Q	Load (kN)
Q_p	Tip resistance (kN)
q_p	Unit tip resistance (kPa)
Q_s	Skin friction (kN)
q_s	Unit skin friction (kPa)
Q_u	Ultimate load capacity (kN)
s	Pile spacing (m)
u	Displacement (m)
$\dot{u}$	Velocity (m/s)
$\ddot{u}$	Acceleration (m/s^2)
V	Shear force (kN)
V_p	Primary wave velocity (m/s)
V_s	Shear wave velocity (m/s)
V_{s1}	Shear wave velocity of the top layer (m/s)

V_{s2}	Shear wave velocity of the bottom layer (m/s)
w	Weight of the plate element (kN/m/m)
α_r	Rayleigh damping coefficient (-)
β_r	Rayleigh damping coefficient (-)
β	Friction coefficient (-)
ε	Strain (-)
ϕ'	Effective soil internal friction angle (°)
ρ	Mass density (kg/m^3)
σ'	Effective vertical effective stress (kPa)
τ	Shear strength (kPa)
ν	Poisson's ratio (-)
ω	Angular frequency (rad/s)
Ψ	Dilatancy angle (°)
δ	Soil-pile friction angle (°)
Δt	Time step (s)
ξ	Damping ratio (%)
λ	Wave length (m)
γ	Unit weight (kN/m^3)
γ_{sat}	Saturated unit weight (kN/m^3)
γ_{unsat}	Unsaturated unit weight (kN/m^3)
$\upgamma$	Shear strain (-)

Abbreviations

AES	Average element size
API	American Petroleum Institute
BEM	Boundary element method
FDM	Finite difference method
FEM	Finite element method
PDE	Partial differential equation
PGA	Peak ground acceleration
P-waves	Primary waves
SPT	Standard Penetration Test
SSI	Soil-structure interaction
S-waves	Shear waves
TBDY	Turkish Building Earthquake Code

1. INTRODUCTION

1.1. Problem Statement

Foundations play a crucial role in providing support to structures and transferring the loads imposed by superstructure to the soil beneath them. Soil characteristics beneath foundations often dominate the behaviors of foundations and structures. The soil where the structural loads are transferred needs to have adequate characteristics in terms of settlement, bearing capacity and liquefaction potential issues. However, the rapid urbanization in today's world has resulted in decrease of suitable lands for new constructions, forcing people to construct new structures in areas with high seismic activity and challenging soil conditions. To overcome these challenges, various methods have been implemented in the past few decades. Piled foundations are one of the most frequently used solutions for the structures built on soils with poor qualities as they effectively transfer or distribute the loads coming from superstructure to deeper and usually stiffer soil layers reducing the risk of structural damage caused by the aforementioned potential issues.

The proper design of piled foundation system is an important aspect from engineering point of view. Since structures are built at or below ground level, they cannot behave independently from the soil. When external dynamic forces like earthquakes or vibrations affect structures, response of soil and pile becomes interdependent. This interaction is known as dynamic Soil-Structure Interaction (SSI). Piles experience stresses during seismic events. These stresses are caused by different factors including the forces generated by movement of structure (inertial interaction) and interaction with soil in which they are embedded (kinematic interaction). Designers usually focus on stresses resulting from superstructure. However, especially in cases where the soil layers exhibit significant variations in stiffness properties, past earthquakes have revealed the importance of kinematic interaction for designing safe structures against seismic events. It has been observed that this interaction can result in pile failure. Therefore, even though piled foundations are considered as a reliable option for supporting structures, numerous buildings utilizing this system have experienced failures during devastating earthquakes

1

in the past, resulting in substantial human and financial losses. An example of earthquake damaged piles is presented in Section 2.3.

Given the complex nature of nonlinear soil behavior under dynamic loads, it is essential to consider multiple factors for the seismic design of piled foundations. Since there are numerous variables affecting SSI like soil parameters and structural properties, a thorough analysis of SSI is essential for the design of earthquake resistant structures.

This study delves into the detailed examination of the seismic performance exhibited by different piled foundation configurations subjected to varying soil and earthquake conditions. In the literature, there are various analytical, experimental, and numerical methods to investigate seismic behaviors of piles during an earthquake. Makris and Gazetas (1992) performed a study to examine SSI under either lateral or earthquake loads and proposed a new analytical method for estimating dynamic interaction between soils and piles. Suzuki et al. (2014) carried out large scale 3D shake table tests with the purpose of examining factors affecting the stress distribution on pile groups in dry sand. Fan et al. (1991) performed a comprehensive investigation in order to predict displacements at pile head under seismic effects. They proposed dimensionless graphs which are containing free field soil response-pile head displacement relation for different soil profiles. Giannakos et al. (2012) conducted a numerical study to examine seismic pile behavior in dry dense sand under cyclic loading. They proposed a nonlinear constitutive soil model for simulating piles' lateral response to cyclic loading in cohesionless soils. Then, they utilized this model in 3D FEA to compare analysis results with centrifuge test data of a pile which is constructed within a sandy soil. Haeri et al. (2012) investigated a pile group behavior exposed to liquefaction by conducting shaking table tests and they developed a numerical approach to predict pile behavior under liquefaction.

In this thesis, kinematic interaction analyses of piled foundations are performed in 2D model geometries. Analyzing the SSI in 2D does not fully capture the complexities of 3D behaviors of soil and piles. Nonetheless, conducting analysis in 2D is a highly practical method and can provide a reasonable estimation of 3D behavior under adequate assumptions. This estimation can be achieved through various means, such as implementing a reduction in strength of the structural element to take into account the spacing between piles and validation of 2D pile behavior with experimental data or 3D analysis. In Plaxis 2D, "embedded beam row" element was developed in 2012 to be able to reflect the soil-pile interaction and the spacing between piles more accurately. In the literature, effectiveness of modeling piles in 2D model geometries is investigated by different researchers. For instance, Kwaak (2015) proposed a parametric study and proved that the SSI can be successfully modeled in Plaxis 2D by using embedded beam row elements. He demonstrated that results of dynamic analyses using this element were similar to the ones in 3D analyses. Sluis (2012) performed a comparison study to evaluate the reliability of embedded beam row. He conducted analyses in which this element modeled in two-dimensional and three-dimensional model geometries. Soil displacements in two-dimensional analyses were quite similar to the once in three-dimensional analyses. This study has also demonstrated that proper selection of the most suitable method for simulating pile behavior accurately is contingent upon pile spacing. Zein et al. (2021) compared the performances of the plate elements and embedded beam row in their studies. They concluded that the embedded beam row feature is a better alternative to capture actual pile behavior, particularly in loose to medium dense sands.

Therefore, due to its effectiveness in terms of time and computational costs and the studies in the literature validating its performance, it can be concluded that the analysis of the kinematic interaction between piles and soils can be performed in 2D model geometries using appropriate elements and adequate assumptions.

In this thesis study, Plaxis 2D finite element software is utilized to conduct kinematic interaction analyses of piled foundations. A comparison study is performed with different variables such as soil profiles, pile properties and earthquake characteristics. Soils are modeled as layered soil profiles with varying stiffness characteristics. Piles are modeled

via embedded beam row elements, which are capable of reflecting the spacing between piles and the kinematic interaction between soil and piles. Three distinct input motions having different peak ground accelerations (PGA) are used to explore the influence of PGA magnitude on analysis results. After the completion of analysis of various scenarios, accelerations in the soil and pile internal forces (bending moments & shear forces) are examined for comparison purposes.

1.2. Aim of the Study

In this study, kinematic interactions of piled foundation systems during earthquakes in different soil profiles will be investigated and effects of different variables like pile properties (diameter, spacing and length), on the soil-pile interaction will be evaluated by performing two-dimensional finite element analyses. In the large-scale projects in which structures seated on piled foundations, piles having different properties can be utilized under the structures and the properties of the piles, especially the lengths of piles can be modified during the design stages of the project. Since the kinematic interaction analyses are required for the proper design of the structures, it may be required to perform lots of analyses for all modifications during the design process. However, these kinematic interaction analyses can be time consuming and require a lot of computer memory. Hence, possessing the capability of predicting the effects of distinct variables on the analysis results is of significant importance. For example, having the capability to make simple predictions on how small changes in the pile length affect the internal forces acting on the piles can be highly efficient and time saving for designers. The primary aim of this study is investigating the influence of pile properties, especially pile length, on the analysis results and providing a sample guide for designers to be able to make predictions about the effects of different parameters on the dynamic response of piles and soils. A parametric study was performed to achieve this goal.

The focal point of considerations of this study are:

- Analyzing soil-pile interaction with 2D model geometries.

- Investigating the influences of pile diameter, pile spacing and pile length on the

analysis results. Several different combinations of these variables are used to evaluate the influence of pile properties on internal forces.

- Exploring the effects of soil characteristics on soil accelerations and internal forces acting on piles.

- Evaluating the effect of earthquake PGA on the response of piles and soils.

1.3. Delimitations of the Study

Due to the vast and complex nature of the topic of this master thesis, it is important to clearly specify the delimitations of the study. The delimitations of this study are presented below.

- Two-dimensional model geometry. It does not fully represent the actual 3D nature of the soil and piled foundations. However, conducting analysis in 2D is quite practical in terms of time and computational cost. In addition, it can provide highly reasonable estimations with adequate assumptions and there are different studies proposed by different researchers in the literature validating the performance of 2D finite element analyses, as mentioned in Section 1.1. Therefore, analyses are performed with 2D analysis models.

- Idealized soil profiles, soil parameters and piled foundation configurations utilized in the analyses are not based on real world scenarios. As a result, no validation process is performed with real test data.

- Groundwater is not considered in the analyses, resulting in the neglect of its potential impacts.

- This study only focuses on the kinematic interactions of soils and piled foundation systems (i.e., inertia effect of superstructure is disregarded).

- Liquefaction potentials of sand layers are not taken into account.

1.4. Thesis Outline

Organizational framework of this study is explained in following paragraphs.

Chapter 2 includes theoretical background of the subject of this study. In addition to general information about earthquakes and soil-structure interaction, this chapter provides analysis methods for soil-structure interaction. This chapter concludes with a concise overview of previous researches regarding dynamic analysis of piled foundations is provided.

Chapter 3 delineates the parametric study performed in this thesis study. It includes methodology and variables used in the analyses. The chapter concludes with the determination of soil parameters and properties of structural elements.

Chapter 4 focuses on the fundamentals of dynamic finite element modeling. It covers the element types, constitutive soil models and dynamic formulations in Plaxis 2D. This chapter also discusses boundary conditions, average element size, and time steps utilized in the analyses.

Chapter 5 provides the analysis results together with the interpretation of the influence of different variables on analysis results.

Chapter 6, the last chapter of this study, concludes this thesis study by summarizing the main findings of analyses and gives recommendations for potential future studies regarding the topic discussed in this master thesis study.

2. THEORETICAL BACKGROUND

2.1 General Information About Earthquakes

2.1.1. Introduction

Earthquake refers to the sudden movement along a fault line and the ground shaking results from the seismic energy being released during this movement. This sudden movement can be triggered by changes in the stress within the earth or by volcanic or magmatic activity (USGS, n.d.).

2.1.2. Primary Components of Earthquake

Primary components and their definitions, proposed by Sucuoğlu and Akkar (2014) are presented in this section.

Plate: Plates refer to the segments that divide the lithosphere, with their movements relative to one another leads to various hazards such as volcanic eruptions, earthquakes, and tsunamis.

Fault: Faults are the fractures or cracks in the earth's crust along which plates move relative to each other.

Hypocenter: The starting point of the rupture is referred to hypocenter. Seismic waves start to propagate from the hypocenter of an earthquake.

Epicenter: The projection point located directly above the hypocenter at ground level is called as epicenter.

Magnitude: Earthquake magnitude is a metric used to quantify the energy released in an earthquake. Magnitudes of earthquakes are measured with seismographs.

Intensity: Earthquake intensity at a specific location is a numerical measure which describes the level of shaking at that location by taking into account the impact of the shaking on individuals, buildings and the environment. The main factor influencing the

intensity of an earthquake is the distance from the hypocenter. It is measured by Modified Mercalli Scale. The intensity of earthquakes can vary widely, ranging from barely noticeable shakings to extremely powerful events.

Seismic Waves: Seismic waves can be divided into two main groups, known as body and surface waves. Body waves travel through interior of the earth. Velocities of body waves can be influenced by soil's density and stiffness. Body waves can also be divided into two groups. They are P-waves (pressure or primary waves) and S-waves (secondary or shear waves). P-waves are seismic waves which cause earth particles, through which they pass, to move back and forth in the same direction with the direction they are traveling. These waves propagate faster and are recorded first during earthquakes. S-waves, are a type of transverse wave moving ground in a direction perpendicular to their path of propagation. Moreover, since they propagate slower than P-waves, they are recorded in seismographs later.

Velocities of body waves (V_p and V_s), which depends on the characteristics of the medium through which they propagate, can be calculated by using equations provided below.

$$V_p = \sqrt{\frac{E(1-v)}{\rho(1+v)(1-2v)}} \tag{2.1}$$

$$V_s = \sqrt{\frac{E}{2\rho(1+v)}} \tag{2.2}$$

where;

V_p = P-wave velocity (m/s)

V_s = S-wave velocity (m/s)

E = Modulus of elasticity of soil (kPa)

ρ = Mass density of soil (kg / m^3)

v = Poisson's ratio (dimensionless)

Furthermore, S- (surface) waves propagate along earth's surface. These waves can also be divided into two main groups, which are Rayleigh and Love waves. Particle movement in surface waves is greater than that of body waves, resulting in more significant damage according to body waves. The simulations of seismic wave propagation are presented in Figure 2.1.
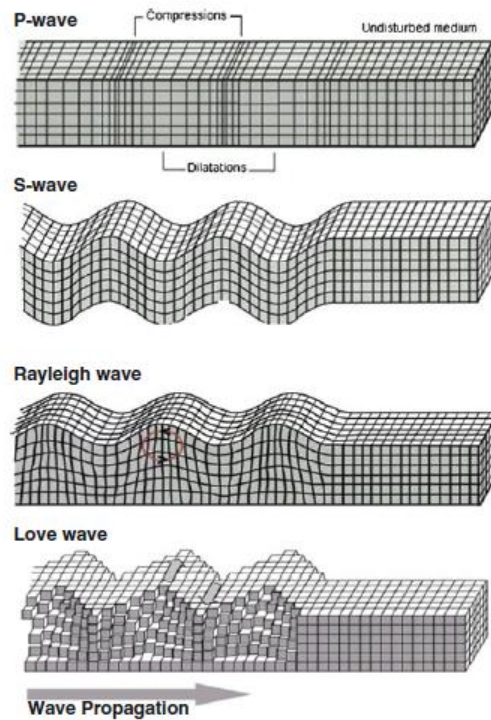
Figure 2.1. Seismic wave propagation (Sucuoğlu and Akkar, 2014)

Visual representation of primary components of an earthquake can be seen in Figure 2.2.
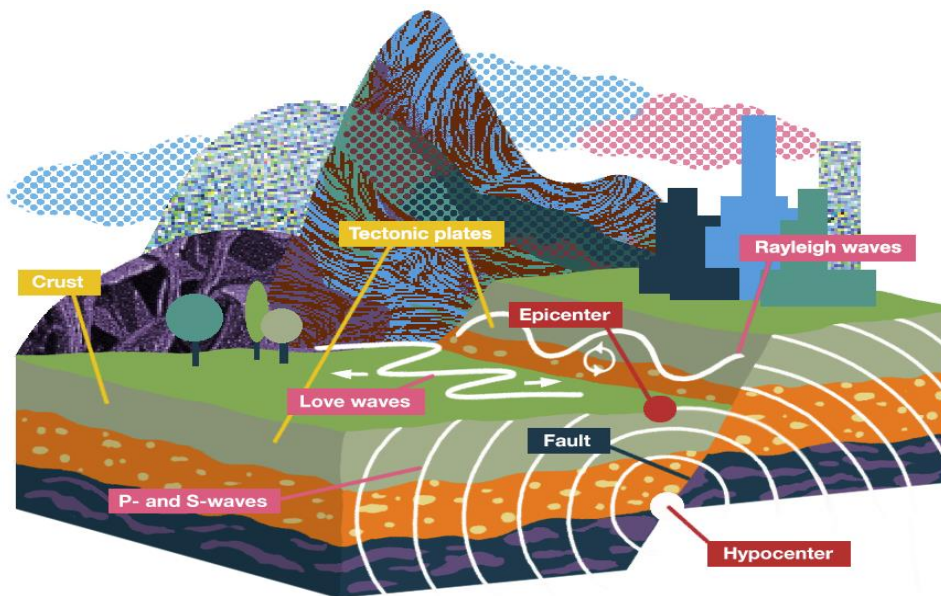
Figure 2.2. Primary components of an earthquake (Caltech science exchange)

2.2. Soil-Structure Interaction

Since structures are built at or below ground level, they cannot behave independently of the soil. When external dynamic forces like earthquakes or vibrations affect structures, behaviors of the structures and soils become interdependent. In other words, soil behavior affects structural response and vice versa. This mutual interaction is defined as Soil-Structure Interaction (Fu, 2018). Two main types of SSI are kinematic interaction and inertial interaction. Kinematic interaction involves the effects of soil deformation on the structure, whereas inertial interaction involves the impact of structural forces on the soil (Firoozi and Firoozi, 2024).

2.2.1. Kinematic Interaction

Motion in the soil caused by an earthquake when there is no structure present is known is termed free-field motion and motion experienced by a foundation due to a massless superstructure is termed Foundation input motion. (FEMA, 2020). During an earthquake, these motions are not the same. This difference between free field and foundation input motions is called as kinematic interaction (Lin and Miranda, 2008).

2.2.2. Inertial Interaction

During an earthquake, mass of the superstructure transfers inertial forces to soil, leading to additional soil deformations known as inertial interaction (Kausel, 2009).

2.3. Influence of SSI on Piled Foundations

SSI can have a significant impact on how structures respond to seismic activity. Hence, they should be accounted for in design process (Heintz and Hortacsu, 2020). In cases where the soil layers exhibit significant variations in the stiffness properties, past earthquakes have revealed the importance of stresses resulting from kinematic interaction between piles and soil, in designing piles to withstand seismic effects. Even though piled foundations are considered as a reliable option for supporting structures, numerous buildings utilizing such foundations have experienced failures during devastating earthquakes in the past, resulting in substantial human and financial losses. An example of these piled foundation failures is presented in Figure 2.3.

Figure 2.3. Damaged piles under NHK building after Niigata earthquake (Hamada, 1991)

Herreros (2020) mentioned that pile damages were discovered under NHK building almost 20 years after Niigata earthquake. When foundation excavation was performed for retrofitting purposes, damaged piles were observed under this building. Moreover, damages on the piles were generally located at two regions which are near the pile head and near the pile tip. He mentioned that while failures near the pile head were probably due to inertial effects and liquefaction of sand layers, the failures near the pile tip were at a location where there is a significant stiffness difference between the soil layers. This stiffness difference might have increased the effect of kinematic interaction between the soil layers and piles.

Therefore, although piled foundations are reliable foundation systems to support structures, kinematic interactions of piles and soils can cause them fail during severe earthquakes. Hence, proper design and thorough analysis of SSI is essential to ensure the structural integrity and safety of a structure against seismic effects.

2.4. Analysis of Dynamic SSI

Dynamic SSI analysis encapsulates various analytical, experimental and numerical methods. These methods help engineers understand complex and mutually dependent behaviors of soil and structures during seismic events, providing a basis for designing and evaluating structures that are exposed to such events. For the sake of integrity and brevity of the study, only the main approaches for analyzing SSI and numerical methods for analyses will be summarized in this section.

Direct and substructure methods are two frequently employed methods for modeling SSI problems (Wolf, 1989).

2.4.1. Direct Method

The direct method is a quite powerful approach for analyzing SSI problems, especially in the cases of complicated structural geometries and nonlinear soil models. Soil, foundation and structure are modeled and analyzed simultaneously in this approach (Asli et al., 2019). Visual representation of direct method can be seen in Figure 2.4.
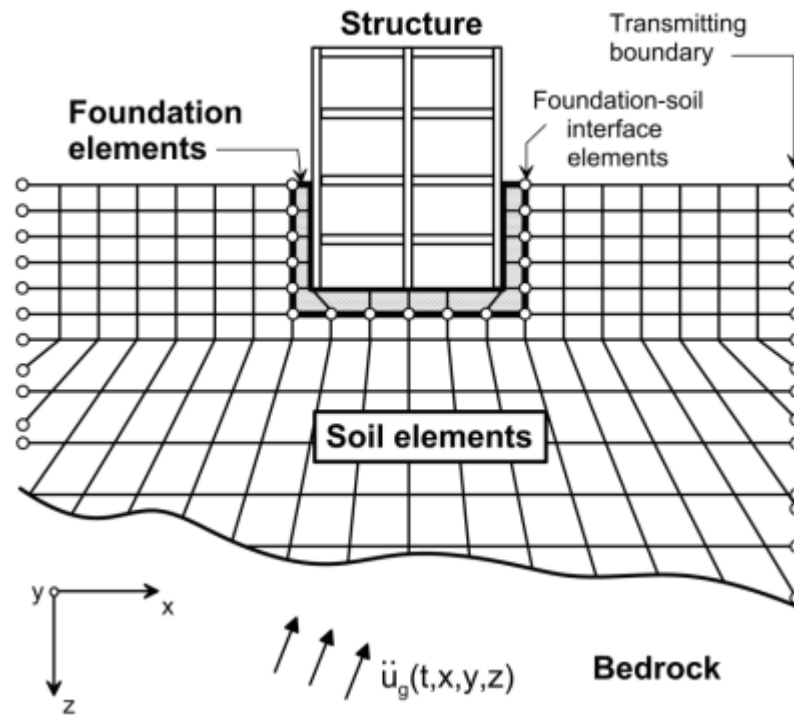
Figure 2.4. Direct method (NIST, 2012)

The direct method is an effective way to handle a variety of SSI concerns, such as linear and nonlinear soil models for different types of foundations. This approach provides the most precise representation of SSI and capable of capturing complicated soil behavior and model geometries. However, the direct method is not frequently employed in engineering applications due to intricate nature of the analysis and the extensive amount of computational time and resources it requires (NIST, 2012).

2.4.2. Substructure Method

The substructure method decomposes SSI analysis into two separate analyses: one for the soil response in free field motion, another for interaction among the soil and superstructure. Firstly, free field analyses are performed, after which analysis results are utilized as input for soil-structure analysis. Then, structural response is obtained by using principle of superposition. In essence, substructure method has the capability of analyzing the inertial and kinematic interactions separately and combining the results of these analyses (Anand and Kumar, 2018). The visual representation of substructure method is presented in Figure 2.5.
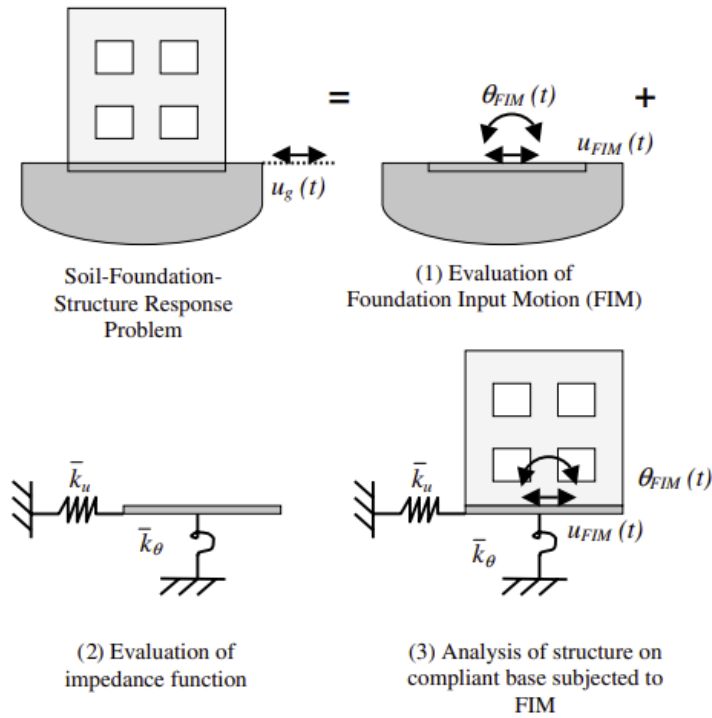
Figure 2.5. Substructure method (Stewart and Kramer, 2004)

Substructure method is much faster than the direct method since it allows the separate analysis of the soil and structure, but it provides a less precise representation of SSI and cannot capture complicated soil-structure geometries and soil behavior (Bapir et al., 2023).

2.5. Methods for Numerical Analysis of SSI

With the advancements and innovations in computer technology, numerical analyses have become increasingly important in the disciplines of soil mechanics and foundation engineering. Numerical analysis models allow us to analyze soil problems by describing factors such as soil behavior, failure modes, stress levels, anisotropy, and time-dependent behaviors like creep and plastic deformations. They are able to generate both 2D and 3D representations of soils and structures, as well as perform dynamic analysis. A brief discussion on certain numerical analyses methods which are utilized for analyzing dynamic behavior of piled foundations is provided in this section.

2.5.1. Finite Element Method

Finite element method (FEM) is one of the well-known computational methods to analyze civil engineering problems. FEM's fundamental concept consists of discretizing a region into a limited number of elements having arbitrary shapes and sizes, connecting these elements with nodes and then, estimating the solutions by solving differential equations within each element (Czichos et al., eds., 2006).

FEM is a powerful tool that can accurately model the behavior of soil and structures, especially when dealing with complex geometries and loading conditions. In addition, it is capable of successfully modeling nonlinear soil behavior and analyzing dynamic SSI (Menglin, et al., 2011).

This method has the advantages of the ability to represent complex geometries concerning soil profiles and structural components, flexibility in mesh size, improved convergence accuracy and providing more accurate results. However, it has some disadvantages, too. In order to include radiation damping, which is the energy loss during the propagation of waves, in a finite element analysis accurately, specific boundary conditions and significant model dimensions are required. These boundary conditions primarily absorb the waves that reaches the boundaries (Boominathan et al., 2018). Moreover, this method can be time-consuming and require a lot of computer memory.

2.5.2. Finite Difference Method

This method (FDM) is one of the frequently used numerical analysis methods and it discretizes the problem domain into a grid of smaller elements. In civil engineering, this method can be utilized in order to solve differential equations describing soil behavior, including stress-strain relation, fluid flow etc. The fundamental concept of finite difference method relies on dividing the problem domain into a grid of uniformly spaced points and calculating the derivatives using finite difference approximation (Ge, 2023).

FDM also has the ability of performing dynamic SSI analyses and model soil and structures accurately. This method has advantages such as reduced computational time, simple implementation and lower memory usage. On the other hand, its efficacy in

tackling complex geometries or heterogeneous soil profiles may be limited in comparison to the finite element method (Firoozi and Firoozi, 2024).

2.5.3. Boundary Element Method

This method is one of the numerical approaches which can solve linear PDEs which are transformed into integral formulations. When dealing with an infinite problem domain, it provides a robust alternative to other numerical methods. BEM's fundamental concept involves discretizing only the boundary of the problem into smaller elements instead of the entire domain. Moreover, the equations describing the domain's motion will be expressed as integral equations rather than differential equations (Yu, 2010).

Wave propagation and dynamic SSI problems in soils can be effectively addressed using the boundary element method, assuming linear elastic or viscoelastic soil behavior (Beskos, 1993).

Boundary element method has particular advantages for problems involving domains that are either infinite or semi-infinite. It inherently meets the radiation damping criteria without using complex non-reflective boundaries (Menglin et al., 2011). Furthermore, it requires less time and memory for analyses, but it is not a commonly used method for engineering problems since problems containing nonlinear behavior cannot be addressed due to its formulation (Firoozi and Firoozi, 2024).

2.6. Previous Studies in the Literature

There are numerous studies in the literature performed to investigate the dynamic analysis of soil-structure interaction. Within this chapter, a concise overview will be presented about these studies.

Dezi et al. (2010) conducted a parametric numerical analysis study to evaluate kinematic soil-pile interaction in various conditions. Dynamic behaviors of fixed head single piles were investigated by concentrating mainly on bending moments of piles embedded in various soil profiles. Firstly, a numerical model introduced by the same authors for analyzing soil-pile interaction of pile groups in layered soil profile was specialized and

then, that model was validated for its applicability in analyzing dynamic behavior of a single pile embedded within a stratified soil profile. After validation process, proposed procedure is used for other kinematic interaction analyses. A detailed examination was carried out by manipulating the key variables affecting seismic pile response, including soil characteristics, properties of the piles (diameter and length of the socket in the bedrock) and layer thicknesses of soils. After the comparisons, they came up with conclusions such as the maximum bending moment occurs at the top of the pile for floating piles and at a point very close to the soil-bedrock interface for the end bearing piles. For the case where surface layer depth was small, a secondary peak was obtained at pile head in for end bearing piles. In addition, they demonstrated also bending moments acting on pile increase with increasing diameter and bedrock depth while they decrease with increasing shear wave velocity. Sample bending moment diagrams from mentioned study, are presented in Figure 2.6.
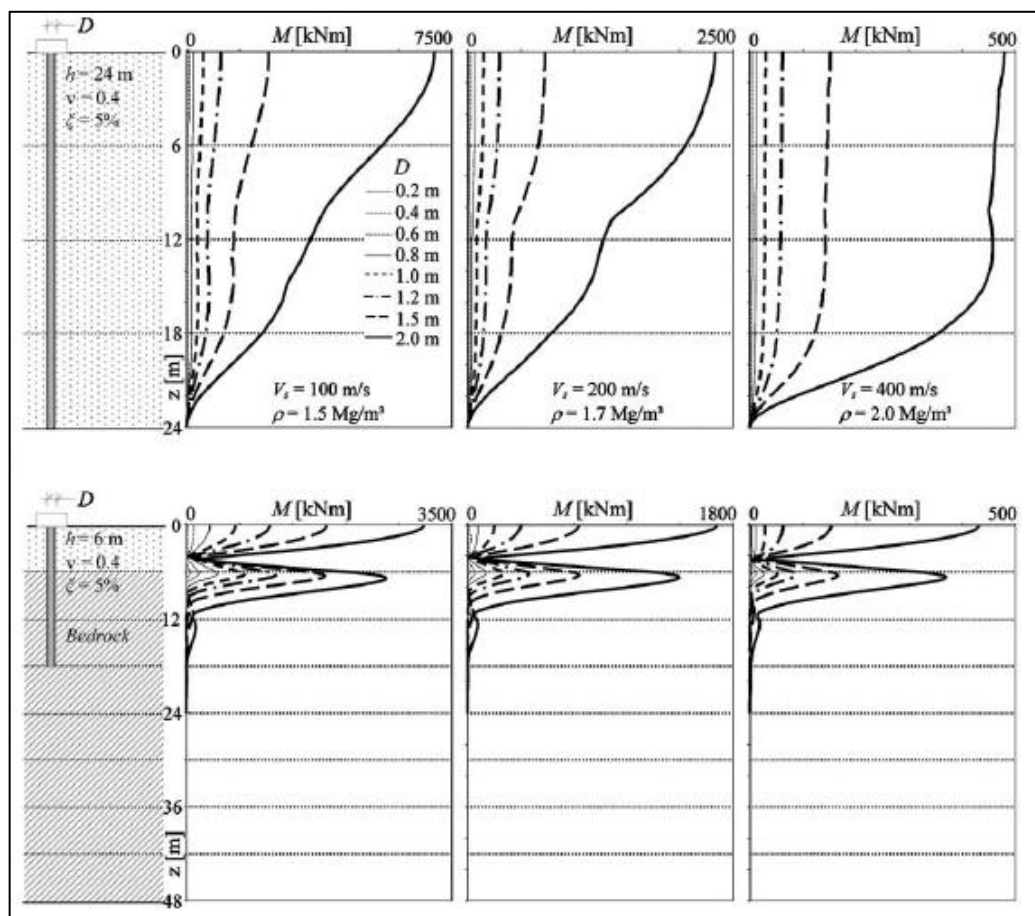
Figure 2.6. Bending moment diagrams (Dezi et al., 2010)

Additionally, since the peak bending moments were almost the same after a socket length of 3D, they have concluded that 3D socket length for the piles is enough for full restraint at pile tip. They obtained a considerable reduction in the peak bending moment (up to 50%) and smoother peaks located at upper elevations by using a smoother stiffness transition instead of sharp transition between the soil and bedrock. As a final conclusion, they have proposed new empirical design formulas for the end bearing piles to estimate the pile head bending moments and bending moments at layer interface.

Kardoğan and Onur (2018) performed a set of dynamic analysis to examine the dynamic behaviors of end bearing and friction piles. For the comparison purposes, a parametric study was performed for eight different pile models. The analyses were performed using Plaxis 2D and FLAC 2D software. The lengths and diameters of the piles were chosen as 25-30 m and 0.8-1.0m, respectively. The piles were assumed as free head piles which were constructed in a sandy soil. Axial load capacities of these piles were calculated and these capacities were used as vertical loads acting on the pile head. After the parametric study, they compared the displacements and bending moments of piles. The results obtained with Plaxis 2D and FLAC 2D were reasonably similar. According to the results of the analyses, piles having 100 cm diameter experienced higher bending moments compared to piles having 80 cm diameter. A similar scenario was observed for pile length, too. As the length of piles increased, bending moments also increased. Besides, since the piles were modeled as free head piles, they moved at the same rate with the ground. Therefore, they have concluded there were not significant changes in pile displacements. When Kocaeli earthquake was utilized as input signal in the analysis, bending moment and displacement values were higher than those observed in the analysis using Kobe earthquake. This situation was associated with the higher lateral loads caused by higher accelerations. In addition, for the case of axial load capacity calculation with the critical depth concept, an increase in axial load capacity led to a corresponding increase in bending moments and displacements. However, when each pile diameter and the earthquake record was evaluated separately, the results were close to each other.

Çimen and Osmanoğlu (2021) performed a study to examine piled raft foundations and compare seismic responses of them. Authors focused on analyzing seismic responses of various configurations of piled raft foundations specifically designed to solve the settlement issues encountered on a sand layer within Lefke, Cyprus. Firstly, a reinforced concrete building with 19 storey and 60.5 m height was modeled using the ETABS software. In the raft foundation case, calculations demonstrated that the maximum axial load coming from superstructure cannot be carried by the foundation safely due to the settlement problem. This situation has shown the necessity of piled foundation. Different configurations of piled foundation systems were designed incorporating the variations in diameters, lengths and numbers of piles. For comparison purposes, 18 different piled raft foundation systems were designed by using the variables mentioned above. Dynamic analyses of these foundation systems were conducted via Plaxis 2D. After the completion of analyses, a comprehensive comparison of the lateral deformation and settlements of these foundation systems is conducted. It has been observed that decreasing the pile diameter results in a linear decrease in the settlement and a nearly linear decrease in the lateral deformations. Analysis results showed also that the settlements and the lateral deformations decrease in an almost linear pattern if the pile length is increased and the number of piles is decreased while keeping the pile diameter constant. In addition, decreasing pile diameter and increasing number of piles led to decrease in the settlements for constant pile length. Finally, they have come up with the conclusion that increasing pile length in designed foundation systems is the most effective solution for mitigating the deformations induced by seismic action.

Yiğit et al. (2022) focused on pile-soil interaction of mono-piles and pile groups in their research. A parametric study was performed with FEM and dynamic behavior of these pile configurations were compared for different variables such as soil profile, earthquake record and pile properties (pile diameter, pile length, elasticity modulus etc.). The comparison of the pile behaviors was made utilizing a method called as Method-III in the national code Turkish Building Earthquake Code (TBDY-2018). Firstly, load capacities (lateral and vertical) of piles were calculated according to the formulations in the TBDY-2018 and American Petroleum Institute (API). After pile capacity calculations, site response analyses were carried out in DEEPSOIL software. The force-displacement curves for the piles were drawn which were used to model the soil as a spring in the

analyses. For the analysis model with the pile group, while the group efficiency factors for the pile groups were determined individually for each pile according to TBDY, FHWA suggests one group efficiency factor for all piles. ANSYS software was utilized for analyses and three different soil profiles were used for the models with single pile (homogeneous clay, homogeneous sand or layered soil profile). For the models with pile groups, a homogeneous clay soil profile was assumed. The parameters of the soils for the analyses were determined in accordance with ZE soil category defined in TBDY. The springs coming from force-displacement curves were applied to piles with 1 m spacing. The internal forces on the piles were computed in ANSYS software by applying the soil deformations in the 1D site response analyses to the p-y springs. According to results of analyses, increasing pile length, pile diameter, and elasticity modulus of piles gave rise to increase in the internal forces of piles (moments and shear forces). Since the spring constants of Q-Z curves were are higher in the sandy soils, smaller deformation values obtained in sandy soils. In the pile group analyses, while the internal forces acting on the piles were different depending on both the pile sequence and the direction of earthquake according to TBDY, they were the same for all of the piles according to FHWA method. In addition, the kinematic interaction effects increased in layered soil profiles.

Albusoda and Salem (2016) investigated the effect of pile spacing on dynamic behavior of piled foundations. A 25-storey building seated on medium dense sand was analyzed under dynamic forces. In the analysis, piles modeled with three different spacing (3D, 5D and 7D). The structural properties of the building, the soil profile and the parameters of the soils were determined according to a actual data and the soil was modeled with Mohr Coulomb model. The graphs representing the results of the analyses are presented in Figure 2.7 and Figure 2.8.
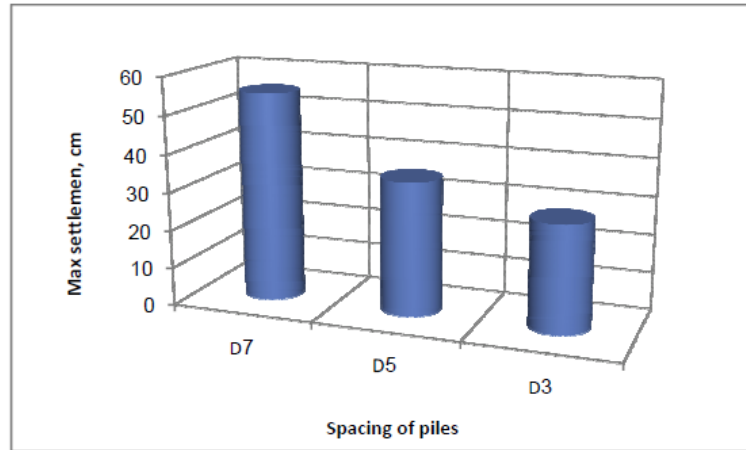
Figure 2.7. Effect of pile spacing on the total settlements of a raft foundation (Albusoda and Salem, 2016)
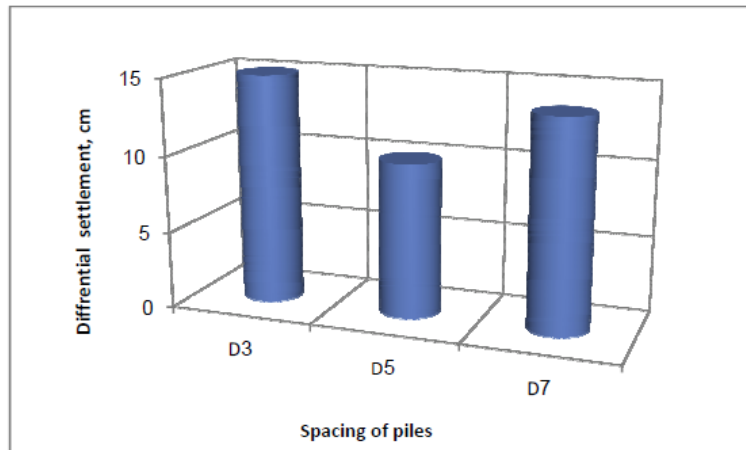
Figure 2.8. Effect of pile spacing on the differential settlements of a raft foundation (Albusoda and Salem, 2016)

At the end of the analyses, authors demonstrated that total settlements in the piled foundations with 5D and 7D pile spacing were 25% and 50% greater compared to the settlements of the piled foundation with 3D pile spacing, respectively. The minimum differential settlement was observed on the piled foundation with 5D pile spacing. The piles with 3D and 7D spacing gives 50% and 35% greater differential settlement than the piles with 5D spacing. They mentioned that the resistance to dishing effect was greater for the piles with 5D spacing since the piles were concentrated at the center of the raft and this situation led to a minimum differential settlement on the piles with 5D spacing.

Zein et al. (2021) conducted a comparison study to check reliability of plate elements for modeling the piles. A series of analyses were performed using variables as soil profile, the frequency of the earthquake and the spacing of the piles. Analyses were performed in Plaxis 2D and analysis models were comprised of 24 storey building resting on a piled foundation and 50 m thick soil profile with sandy soils having variable stiffnesses. Piles were modeled with a constant diameter of 0.5 m by using two different elements, plate and embedded beam row. For piles modeled by embedded beam row, four different spacings (1.0, 1.5, 2.0 and 2.5 m) were used. They have concluded that the plate element overestimates the internal forces of piles and gives inconsistent lateral displacement values for all soil types. In spite of the numerous variations in the parameters, the outcomes of the building response in dense sand exhibited an insignificant difference between the plate and embedded row. This implies that the utilization of the plate model could be securely implemented in dense sands for building response. Consequently, it has shown that the embedded beam row is a more reliable tool to model the piles for a real pile performance, especially for loose and medium dense sands. The plate model should not be implemented to model the piles due to its inaccurate and inconsistent results regardless of soil type. However, for the comparison of the structural behavior, the plate model can be implemented safely in dense sands.

Ordu and Özkan (2006) performed a dynamic analysis study to investigate the nonlinear behavior of piled foundations under dynamic forces. They carried out a comparison study for SSI analysis of a piled foundation system in two different soil profiles. Lucas 3D software was utilized for analyses. Analysis models were composed of a 1.5 * 1.5m square pillar which is resting on a 6.0 * 6.0 m square pile cap, 4 square reinforced concrete pile with L=18 m and two different soil profile. The height of the pillar was 6.0 m, pile cap thickness was 1.5 m, dimensions of square piles was 1.0 m and the spacing between them were 3.0 m. The soil profile was composed of loose sand, soft-moderate stiff clay and weathered rock layers. Two different soil profiles were used in the analysis, the difference between two analysis model was thickness of weathered rock layer. Layer thickness of weathered rocks in two analysis models were 1.5 m and 5.5 m, respectively. While piles in the first analysis model were floating piles, they were modeled as end bearing piles in the second analysis model. At the end of analysis, the lateral displacements of the piles, the bending moments and the shear forces acting on the piles

were compared. The results obtained from the study shows that lateral displacement, bending moment and shear force values acting on the piles under dynamic effects and the distribution of these internal forces depend on soil conditions. Displacement values acting on floating piles were greater than the ones acting on end bearing piles and internal force values were greater in the end bearing piles.

Shafiqu and Sa'ur (2017) examined the dynamic behavior of the piles in their study. In the study, the bending moments acting on a single pile at the interface of a two layered soil profile were compared with different studies in the literature. Analyses were performed with Plaxis 3D software. Five different soil profiles with variable upper layer thicknesses ($H_1 = 5, 10, 12, 15$ and 18 m) and two different soil layers having V_s values of 100 and 200 m/s were used in the analyses. In the analyses, diameter and length of piles 0.6 m and 20 m, respectively. Five different analyses were performed to determine bending moments at layer interface between two soils. Additionally, the 3D analysis model was modified to obtain a 2D model shape by changing the model dimension as 1 m in y-direction. The graph containing the bending moment comparisons from the analyses is presented in Figure 2.9.
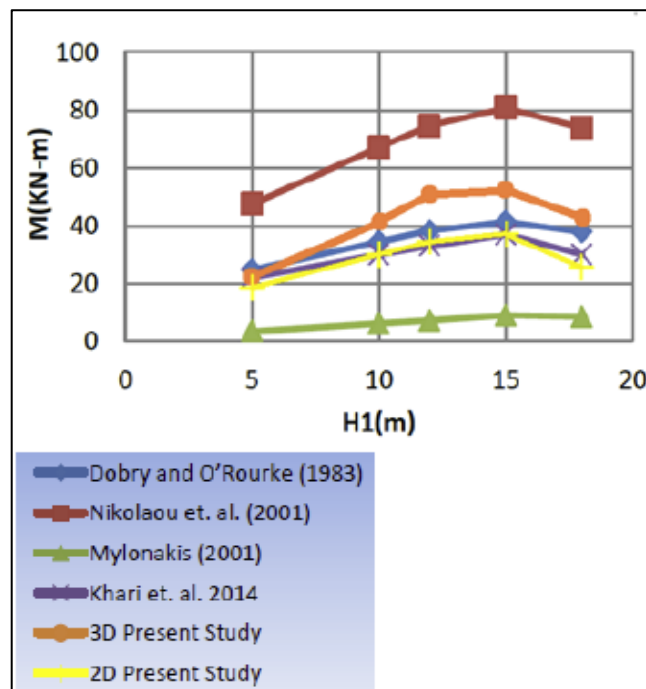
Figure 2.9. Comparison of pile bending moments in different studies (Shafiqu and Sa'ur, 2017)

23

The results of the analyses have revealed that an increased layer thickness of weaker soil generally resulted in an increase in bending moments, too. The 3D analysis results generally gave higher bending moments than the 2D analysis results calculated by Khari et al. (2014). This situation was considered due to the result of 3D modeling effect, which gives more realistic results. Analysis results of 2D model in presented study was very close to ones calculated by Khari et al. (2014). In addition to the study of Khari et al. (2014), 3D analysis results were compared with bending moments calculated with the simplified methods presented by different researchers in the literature. It has shown that the nonlinear soil behavior under dynamic behavior was not considered in the simplified methods.

3. DEFINITION OF THE PARAMETRIC STUDY

3.1. Introduction

This master's thesis study has focused on the comprehensive investigation of the dynamic behavior of different piled foundation systems subjected to varying soil and earthquake conditions. A comprehensive parametric study was conducted to examine the influence of various factors such as soil stiffness, earthquake PGA, pile diameter, pile spacing and pile length, on the internal forces acting on the piles. Plaxis 2D, which is a well-known finite element software for analyzing civil engineering problems, is utilized to perform the analyses in the scope of this thesis study. The details of the parametric study are presented in the following sections.

3.2. Variables in the Analyses

In this parametric study, dynamic analyses of piled foundations were performed using Plaxis 2D finite element software. Using three different input signals and various soil profiles, free field analyses were performed for each analysis model first. Then, different piled foundation configurations were analyzed with varying pile diameter, pile spacing and pile length.

3.2.1. Soil Profiles

Different soil profiles composed of loose sand, dense sand and rock, whose shear wave velocities (V_s) are 150 m/s, 300 m/s and 760 m/s, respectively, were used in the analyses. The soil profiles used in the analyses are explained below.

- 40 m thick layered soil profile with 20 m loose sand at the top (V_{s1} = 150 m/s) and 20 m dense sand at the bottom (V_{s2} = 300 m/s) of the soil profile

- 40 m thick layered soil profile with 20 m dense sand at the top (V_{s1} = 300 m/s) and 20 m loose sand at the bottom (V_{s2} = 150 m/s) of the soil profile

- 40 m thick layered soil profile with varying thicknesses of loose sand at the top (V_{s1} = 150 m/s) and dense sand at the bottom (V_{s2} = 300 m/s) of the soil profile. In this case, the thickness of each layer is determined according to pile length (L)

in order to evaluate the effect of pile length on the analysis results when the embedment length into the bottom layer is kept constant as 3 m. The thickness of the top layer, H_1, was assumed as (L-3) m and the thickness of the bottom layer, H_2, was assumed as (40-H_1) m.

-   40 m thick layered soil profile with varying thicknesses of dense sand at the top (V_{s1} = 300 m/s) and loose sand at the bottom (V_{s2} = 150 m/s) of the soil profile. Similar to the previous set of cases, the thickness of the top layer, H_1, was assumed as (L-3) m and the thickness of the bottom layer, H_2, was assumed as (40-H_1) m.

-   40 m thick layered soil profile with 20m loose sand at the top (V_{s1} = 150 m/s) and 20 m rock at the bottom (V_{s2} = 760 m/s) of the soil profile

3.2.2. Pile-Foundation Layouts

For the piled foundations, a 1.0 m thick foundation and pile groups with different properties are used. A uniform base pressure of 100 kPa is applied on the foundation. Three different pile diameters (D = 0.8, 1.0 and 1.2 m), three different pile spacings (s=3D, 4D and 6D) and pile lengths varying between 10.0-32.0 m are used for the analyses. Outer edges of peripheral piles are 0.5 m from the edge of the foundations. Pile-foundation layouts for various configurations of diameter and spacing are presented in Figure 3.1.
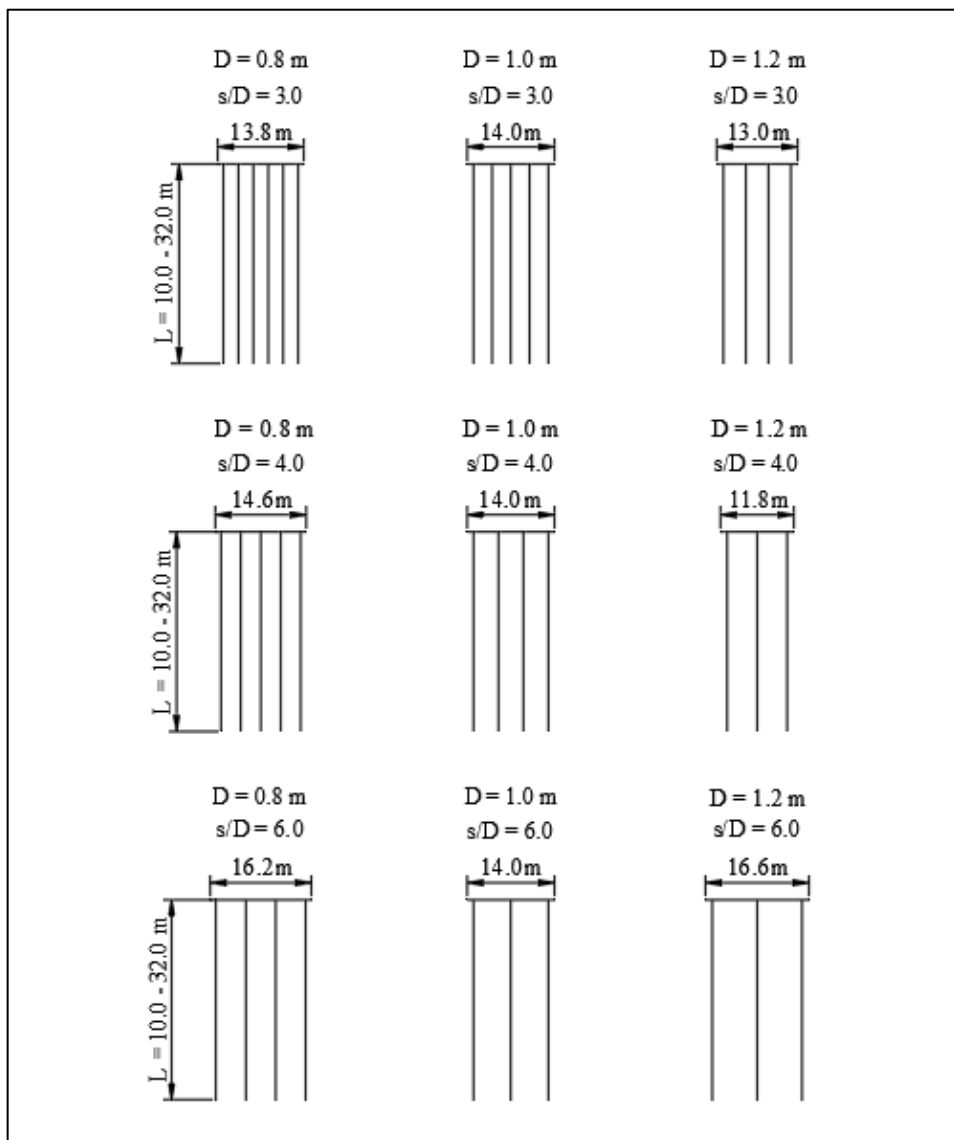
Figure 3.1. Pile foundation layouts used in the analyses

3.2.3. Input Signal

Three input signals, designated Earthquake-1, Earthquake-2 and Earthquake-3, with peak ground accelerations (PGA) of 0.8g, 0.4g and 0.2g, respectively, are used to examine the effect of earthquake PGA. Since soil profiles analyzed in this study do not belong to a specific site, the processes for selecting and scaling the ground motions recommended in various codes for actual sites are not implemented. Instead, a random earthquake record, Kobe (1995) earthquake, is selected and PGA scaling method is applied on the time history records of this earthquake to obtain three different input signals with different peak ground accelerations. Acceleration-time graphs of these input signals are provided in Figures 3.2 through 3.4.
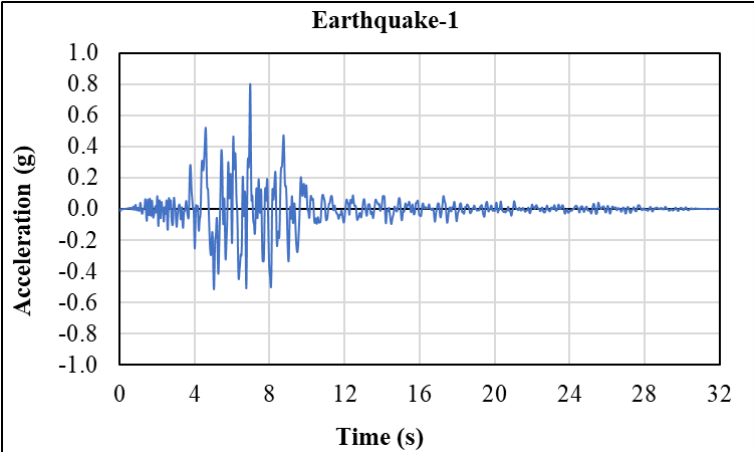
Figure 3.2. Acceleration-time graph of earthquake-1
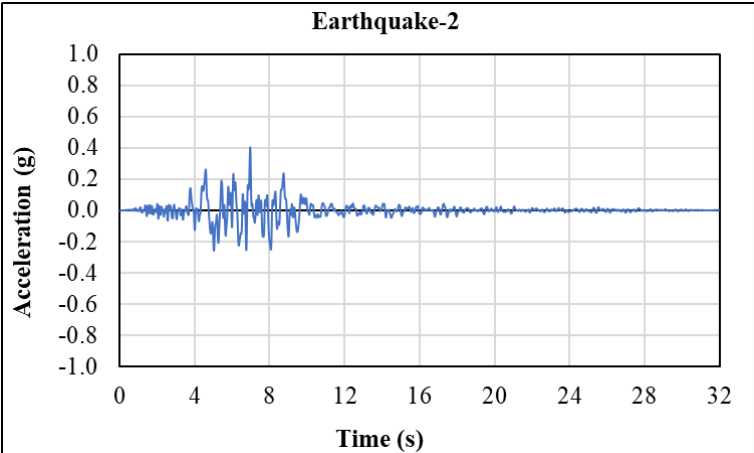
Figure 3.3. Acceleration-time graph of earthquake-2
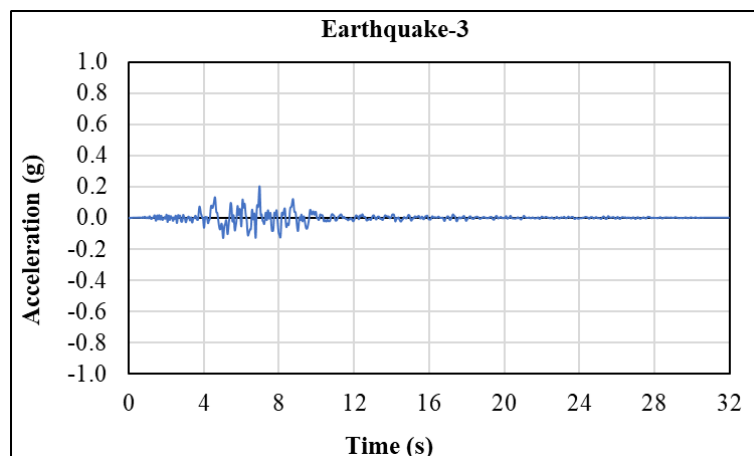
Figure 3.4. Acceleration-time graph of earthquake-3

3.2.4. Summary of the Parametric Study

A comprehensive investigation was performed by analyzing 114 different combinations (including free field analyses) of the variables mentioned in Tables 3.1 through 3.3.

Table 3.1. Analyzed Cases for Earthquake-1 (PGA = 0.8 g)

Pile Properties			Soil Profiles			
			$V_{s1} = 150$ m/s, $V_{s2} = 300$ m/s		$V_{s1} = 300$ m/s, $V_{s2} = 150$ m/s	
s(m)	L (m)	D (m)	$H_1=H_2=20$ m	$H_1=(L-3)$ m $H_2=(40-L_1)$ m	$H_1=H_2=20$ m	$H_1=(L-3)$ m $H_2=(40-L_1)$ m
3D	32	0.8	✓		✓	
		1.0	✓	✓	✓	✓
		1.2	✓		✓	
	30	1.0	✓		✓	
	28		✓	✓	✓	✓
	26		✓		✓	
	24		✓		✓	
	22		✓	✓	✓	✓
	20		✓	✓	✓	✓
	18		✓	✓	✓	✓
	14		✓		✓	
	10		✓		✓	
4D	32	0.8	✓		✓	
		1.0	✓		✓	
		1.2	✓		✓	
6D		0.8	✓		✓	
		1.0	✓		✓	
		1.2	✓		✓	

Table 3.2. Analyzed Cases for Earthquake-2 (PGA = 0.4 g)

Pile Properties			Soil Profiles		
s (m)	L (m)	D (m)	V_{s1} = 150 m/s, V_{s2} = 300 m/s, $H_1 = H_2$=20 m	V_{s1} = 300 m/s, V_{s2} = 150 m/s, $H_1 = H_2$=20 m	V_{s1} = 150 m/s, V_{s2} = 760 m/s, $H_1 = H_2$=20 m
3D	32	0.8	✓	✓	
		1.0	✓	✓	
		1.2	✓	✓	
	30	1.0	✓	✓	✓
	28		✓	✓	
	26		✓	✓	
	24		✓	✓	✓
	23				✓
	22		✓	✓	✓
	21				✓
	20		✓	✓	
	18		✓	✓	
	14		✓	✓	
	10		✓	✓	
4D	32	0.8			
		1.0	✓	✓	
		1.2			
6D		0.8			
		1.0	✓	✓	
		1.2			

Table 3.3. Analyzed Cases for Earthquake-3 (PGA = 0.2 g)

Pile Properties			Soil Profiles	
s (m)	L (m)	D (m)	V_{s1} = 150 m/s, V_{s2} = 300 m/s, $H_1 = H_2$=20 m	V_{s1} = 300 m/s, V_{s2} = 150 m/s, $H_1 = H_2$=20 m
3D	32	0.8	✓	✓
		1.0	✓	✓
		1.2	✓	✓
	30	1.0	✓	✓
	28		✓	✓
	26		✓	✓
	24		✓	✓
	22		✓	✓
	20		✓	✓
	18		✓	✓
	14		✓	✓
	10		✓	✓
4D	32	0.8		
		1.0	✓	✓
		1.2		
6D		0.8		
		1.0	✓	✓
		1.2		

3.3. Soil and Structural Element Properties

This study contains a set of analyses with different soil and piled foundation combinations. Soil profiles used in the analyses consist of different combinations of loose sand, dense sand and rock layers, whose shear wave velocities (V_s) are 150 m/s, 300 m/s and 760 m/s, respectively. Furthermore, pile groups with different diameters (0.8, 1.0 and 1.2 m), spacings (3D, 4D and 6D) and lengths (varying between 10.0-32.0 m) are used. In this section, geotechnical design parameters of soils are determined and the methods for the calculation of the load carrying capacities of the piles are explained.

3.3.1. Geotechnical Parameters for Sand Layers

Since the soil profiles used in the analyses does not belong to a real site, soil parameters are determined by using the correlations given in the literature.

There are lots of correlations using SPT-N_{60} blow count to determine the engineering properties of soils. Therefore, once the SPT-N_{60} blow counts are obtained, empirical correlations or relationships can be used to estimate various engineering parameters of the soil layers.

SPT-N_{60} values of the sand layers could be determined by using shear wave velocity (V_s) and the following correlations which were proposed by different researchers in literature.

Table 3.4. Correlations for V_s-SPT N_{60} relationship (Obrzud and Truty, 2018)

Researcher(s)	Correlation	SPT-N_{60}	
		Loose Sand (V_s = 150 m/s)	Dense Sand (V_s = 300 m/s)
Ohta et al. (1972)	$V_s = 87.2 * (N_{60})^{0.36}$	5	31
Imai (1977)	$V_s = 80.6 * (N_{60})^{0.331}$	7	53
Ohta and Goto (1978b)	$V_s = 88.4 * (N_{60})^{0.333}$	5	39
Imai and Tonouchi (1982)	$V_s = 87.8 * (N_{60})^{0.314}$	6	50
Sykora and Stokoe (1983)	$V_s = 100.5 * (N_{60})^{0.29}$	4	43
Lee (1990)	$V_s = 57.4 * (N_{60})^{0.49}$	7	29
Hasancebi and Ulusay (2007)	$V_s = 90.82 * (N_{60})^{0.319}$	5	42
Dikmen (2009)	$V_s = 73.0 * (N_{60})^{0.33}$	9	72

According to the correlations presented in the table below, SPT-N_{60} values of loose and dense sand layers could be taken as 6 and 44, respectively. Moreover, for the sake of simplicity, it is assumed that SPT-$N_{1,60}$ values are equal to SPT-N_{60} (i.e., overburden correction is ignored). After this point, these values will be used for the correlations based on SPT-N values.

Cohesion values for sand layers are taken as 0 since these layers are cohesionless soils. Approximate ranges for the internal friction angle (ϕ') and unit weight (γ) parameters for the sand layers proposed in the literature are provided in Table 3.5.

Table 3.5. Ranges of internal friction angle and unit weight for sands (after AASHTO, 2004 with 2006 Interims; FHWA, 2002c)

Description	Very loose	Loose	Medium dense	Dense	Very dense
SPT-$N_{1,60}$	0	4	10	30	50
ϕ' (°)	25-30	27-32	30-35	35-40	38-43
γ (kN/m^3)	11.0-15.7	14.1-18.1	17.3-20.4	18.8-22.0	20.4-23.6

Unit weights of loose and dense sand layers are determined as 17 kN/m^3 and 21 kN/m^3, respectively.

Furthermore, internal friction angles could also be found using the relationships suggested by Wolff (1986), Kulhawy and Mayne (1990) and Puri et al. (2018) in the geotechnical literature;

Table 3.6. Internal friction angle of sand layers

Researcher(s)	Correlation	Internal Friction Angle, ϕ' (°)	
		Loose Sand (SPT-$N_{1,60}$ = 6)	Dense Sand (SPT-$N_{1,60}$ = 44)
Wolff (1986)	$\phi' = 27.1 + 0.3 * N_{1,60} - 0.00054 * N_{1,60}^2$	29	39
Kulhawy and Mayne (1990)	$\phi' = 54 - 27.6034 * \exp(-0.014 * N_{1,60})$	29	39
Puri et al. (2018)	$\phi' = 0.3128 * N + 26$	28	40

Note: The N value in the correlation proposed by Puri et al. (2018) is taken as $N_{1,60}$.

Based on the approximate values and equations mentioned above, internal friction angles of loose and dense sand layers are selected as 29° and 39°, respectively.

Elasticity modulus of the sand layers are determined by using SPT-N blow-counts and the correlation which was proposed in literature by Kulhawy and Mayne (1990).

Table 3.7. Elasticity modulus of sand layers

Researcher(s)	Correlation	Elasticity Modulus, E (kPa)	
		Loose Sand (SPT-N_{60} = 6)	Dense Sand (SPT-N_{60} = 44)
Kulhawy and Mayne (1990)	$E = 1000 * N_{60}$	6000	44000

Taking into account the correlations presented above, geotechnical parameters for sand layers are summarized in Table 3.8.

Table 3.8. Geotechnical parameters for sand layers

Description	γ (kN/m³)	c' (kPa)	ϕ' (°)	E (kPa)
Loose Sand	17	0	29	6000
Dense Sand	21	0	39	44000

3.3.2. Geotechnical Parameters for Rock Unit

The rock unit used in the analysis is assumed as engineering rock with $V_s = 760$ m/s. Since the unit weight and shear strength parameters of the rock layer do not have a significant effect on the analysis results, parameters of this unit are selected randomly as presented in Table 3.9, for the sake of simplicity.

Table 3.9. Geotechnical design parameters for rock unit

Description	γ (kN/m³)	c' (kPa)	ϕ' (°)
Rock	25	50	30

3.3.3. Pile Capacity Calculations

Determination of the load carrying capacity of a pile is a critical component of pile design. This section will cover an overview for the vertical load capacity calculation of piles.

3.3.3.1 Vertical Load Capacity

Vertical pile capacity is comprised of two main components, the first one is skin friction (also known as side friction or shaft friction) and the second one is end bearing. Piles resist the load applied on the pile head through these resistance forces. A conceptual diagram illustrating the load transfer mechanism of a pile is provided in Figure 3.5.
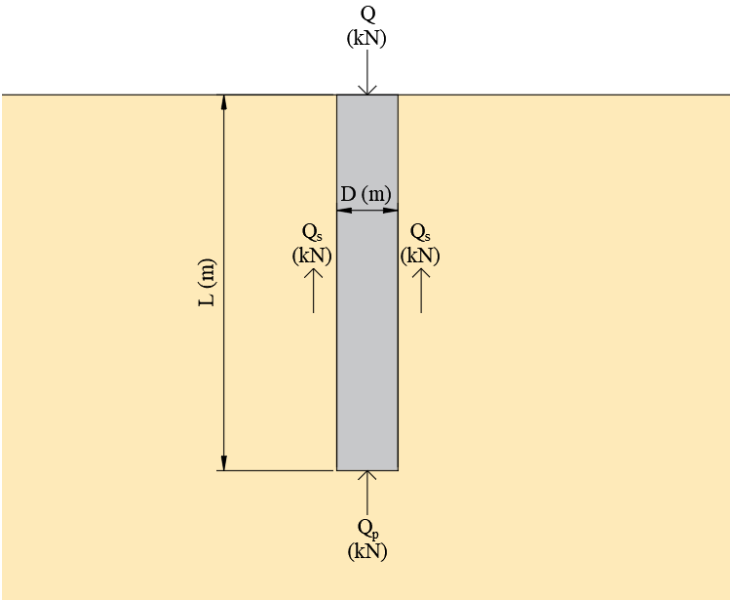
Figure 3.5. Load transfer mechanism of a pile (Das, 2010)

Ultimate load capacity depends on several factors such as properties of soil into which pile is embedded, installation method of pile and pile properties (diameter, length etc.).

The geotechnical literature encapsulates various methods for pile capacity calculations. Common methods utilized to calculate pile capacity are mentioned below.

- Static pile load tests
- Dynamic pile load tests
- Empirical relations based on different field tests
- Analytical methods
- Numerical methods

For the purpose of brevity, all of these methods will not be mentioned in this study. Only analytical methods will be implemented for the calculation of ultimate load capacity. The procedures for determining the skin friction and pile tip resistance are provided below.

Ultimate load capacity can be determined combining the skin friction and tip resistance, as indicated in Equation 3.1 proposed by Das (2010) presented below.

$$Q_u = Q_s + Q_p \tag{3.1}$$

where;

Q_u = Ultimate load capacity (kN)

Q_s = Skin friction (kN)

Q_p = Pile tip resistance (kN)

Skin Friction: The skin friction of a pile can be calculated by Equation 3.2.

$$Q_s = \Sigma q_{si} * A_{si} \tag{3.2}$$

where;

q_{si}: Unit skin friction in i^{th} layer (kPa)

A_{si}: Surface area of pile i^{th} layer (m^2)

The unit skin friction can be calculated using different techniques available in the literature, including α method (Tomlinson, 1957), λ method (Vijayvergiya and Focht, 1972) and β method (Burland, 1973). In this study, β method will be used for unit skin friction calculations of sand layers. In this approach, calculations are performed based on effective stresses (for drained conditions). The unit skin friction, which is generated between pile shaft and surrounding soil, can be calculated as follows:

$$q_s = \beta * \sigma_v' \tag{3.3}$$

$$\beta = K_s * tan\delta \tag{3.4}$$

where;

β: Friction coefficient (dimensionless)

K_s: Coefficient of earth pressure at rest (can be taken as 0.5 for bored piles in cohesionless soils (Birand et al., 2011))

δ: Soil-pile friction angle (for concrete piles, it is assumed 0.75 ϕ')

σ_v': Average vertical effective stress in the relevant layer (kPa)

ϕ': Internal friction angle of soil (°)

The unit skin friction of piles increases with depth in an almost linear manner up to a certain depth. After this depth, it remains constant. This specific concept is called as critical depth concept. A representative figure summarizing the critical depth concept is presented in Figure 3.6.
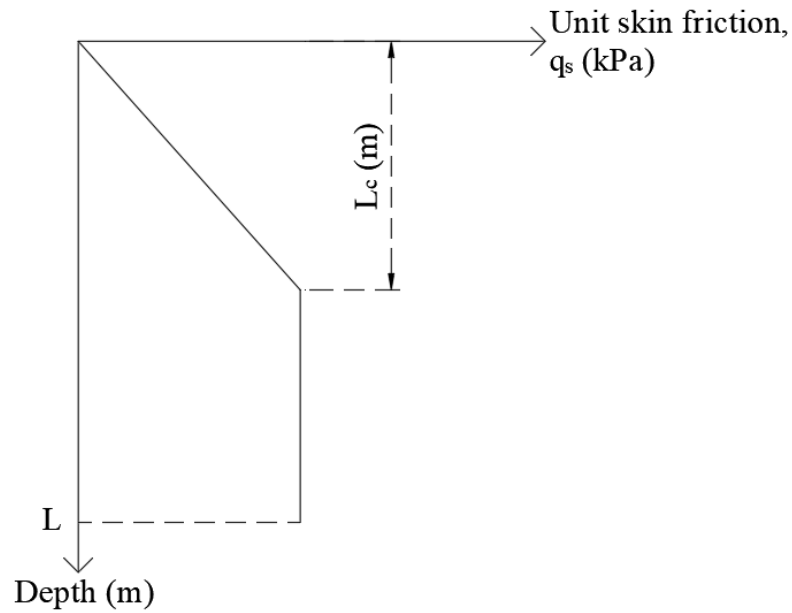
Figure 3.6. Critical depth concept (Das, 2010)

The critical depth, L_c, is usually accepted in a range between 10-20 times pile diameter (Fellenius and Altaee, 1995). In this study, critical depth is assumed as $L_c = 15D$ for sand layers.

Pile Tip Resistance: There are numerous methods for the calculation of pile tip resistance, which are proposed by different researchers such as Meyerhof (1976), Vesic (1977) and Coyle & Castello (1981), in the literature. In this study, Meyerhof's approach will be implemented. The tip resistance of a pile can be calculated by using Equation 3.5 and Equation 3.6.

$$Q_p = q_p * A_p \tag{3.5}$$

$$q_p = \sigma_v' * N_q \tag{3.6}$$

where;

q_p: Unit tip resistance (kPa)

A_p: Area of pile tip (m^2)

σ_v': Vertical effective stress at the pile tip (kPa)

N_q: Bearing capacity factor (dimensionless)

Bearing capacity factor, N_q, depends on different factors such as the type of pile and internal friction angle of soil. It can be determined by the charts, graphs and formulas provided in the literature. Bearing capacity factors, proposed by NAVFAC DM 7.2 (1984) are presented in Table 3.10.

Table 3.10. Bearing capacity factor values (NAVFAC DM 7.2, 1984)

ϕ' (°)	26	28	30	31	32	33	34	35	36	37	38	39	40
N_q for driven piles	10	15	21	24	29	35	42	50	62	77	86	120	145
N_q for bored piles	5	8	10	12	14	17	21	25	30	38	43	60	72

In this study, vertical load capacities of the piles in sand layers are determined by using the methods mentioned above. For the piles socketed to rock layers, the unit skin friction value in the rock unit is taken as 500 kPa according to typical skin friction values proposed by Arıoğlu and Yılmaz (2007). For the mobilization of the tip resistance, a displacement almost 10% of the pile diameter is required (Bowles, 1997). Due to the significant movement needed to mobilize the bearing resistance and the challenges in base cleaning, the bearing resistance is often neglected for rock socketed piles in current design methodologies (Sharudin et al., 2016). The vertical pile capacities used in the analyses are presented in Appendix B.

4. DYNAMIC FINITE ELEMENT MODELING

4.1. Introduction

The finite element method (FEM) is a well-known computational method for analyzing civil engineering problems. It is a method employed for obtaining approximate solutions to boundary value problems of differential equations. FEM's fundamental concept consists of discretizing the entire problem domain into finite number of elements with arbitrary shapes and sizes, interconnecting these elements with nodes and then, estimating the solutions by solving differential equations within each element.

Dynamic analyses in this thesis study were performed using Plaxis 2D finite element software, which is capable of analyzing various types of geotechnical engineering problems like settlement, excavation, slope stability, tunnels, dynamic analysis etc. This chapter focuses on the fundamental concepts of dynamic analysis and the details of the numerical analyses performed in the scope of this thesis study.

4.2. Important Aspects in Dynamic Analysis

Due to the intricate nature of nonlinear soil behavior and soil-pile interaction, there are some key components have to be carefully considered during the modeling process of dynamic analyses. These components are discussed in the following sections.

4.2.1. Element Types Used in the Analyses

Plaxis 2D offers different element types and constitutive soil models for modeling the structural elements and soils. It is quite important to select appropriate element types to perform a reliable analysis. A brief overview is provided on the element types used for modeling the soils and piles in this section.

4.2.1.1 Modeling of Soils

Soil medium can be modeled via 6-noded or 15-noded elements in Plaxis 2D. Both element types have their own advantages and disadvantages. Before starting the analyses, a set of analyses was performed for the comparison between the analyses utilizing 6-noded and 15-noded elements. It was seen that the results of the analyses using both element types were quite similar. Thus, due to their fast computational time and less memory requirement, 6-node triangular elements are used to model soil profiles under plane strain condition.

4.2.1.2 Modeling of Foundation and Piles

Foundations (pile caps) are modeled with plate elements, which are capable of simulating the behavior of foundations, walls, tunnels etc.

Modeling a pile in a two-dimensional environment is a difficult task since soil-pile interaction is inherently a three-dimensional problem. Plaxis 2D offers various element types for simulating the behavior of foundations and piles. In all of these methods, it is significantly important to be aware of that 2D finite element model assumes an infinite length in the third (out of plane) direction under plane strain conditions. Since the modeling of these elements in 2D is a representation of their actual behavior in 3D, adequate elements should be chosen to reflect 3D behavior as much as possible.

Piles can be modeled by plates, node to node anchors, volume elements and embedded beam rows in Plaxis 2D. Despite the benefits they offer, there are also drawbacks associated with them. Using the first three methods, piles are modeled as infinite walls in the out of plane direction, which means that they cannot represent the spacing between piles. While modeling the piles with plate and volume elements, interface elements are combined with these elements to consider soil-pile interaction, but they cannot represent the soil-pile interaction adequately since the soil meshes around the piles are separated. Accordingly, flowing of soil between and around the piles are neglected due to discontinuous mesh. Furthermore, using of volume piles result in higher number of elements and denser meshes which cause to high computational time and memory consumption. Even though node to node anchors allow the soil can flow independently

40

of the pile due to continuous soil mesh around the pile, but soil-pile interaction is not taken into account with this method.

The embedded beam row feature encapsulates the advantages of the aforementioned methods and provides a more accurate representation of the complex interaction between soil and pile. One of the most important advantages of this method is that it takes into account the spacing between piles in out of plane direction by taking the pile spacing as an input parameter, rather than modeling the pile as infinite wall. Besides, piles are modeled as separate elements by using special interfaces are implemented between the soil mesh and pile. Consequently, a continuous soil mesh is provided which allows the soil to flow around and between the piles. Furthermore, the reliability of the embedded beam row feature in Plaxis 2D is confirmed by a multitude of studies in the literature, which are mentioned in Section 1.1.

Consequently, taking into account the its advantages and the studies in the literature, it the embedded beam row feature is considered to be the most appropriate way for modeling the piles in Plaxis 2D. Therefore, piles are modeled as embedded beam rows in this study.

4.2.2. Dynamic Properties of Soils

4.2.2.1 Stiffness

The characteristics of the soil significantly influence the propagation of seismic waves. The primary concern in earthquake engineering is the shear stresses generated by the shear waves during earthquakes. Hence, the response of soil, usually characterized by the relationship between shear stress (τ) and shear strain (γ), is quite important under cyclic loading conditions (Ishiara, 1996). Stress-strain relation of soils exhibit hysteretic behavior under cyclic loading conditions such as earthquake. This hysteretic behavior is represented in Figure 4.1, which is proposed by (Jimenez, 2016).
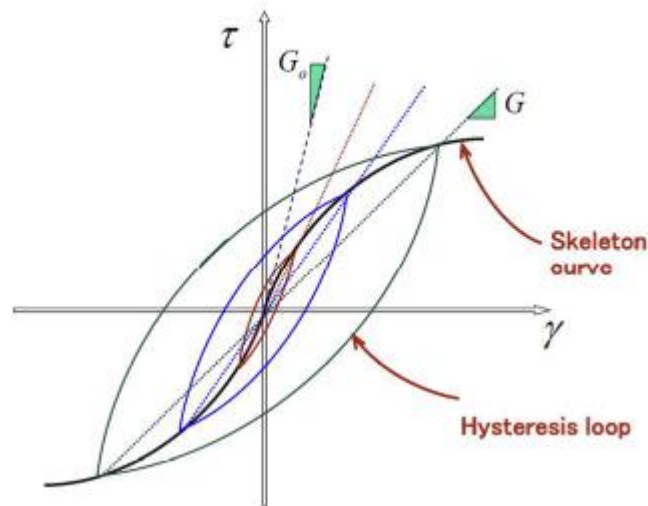
Figure 4.1. Stress-strain relation of soils under cyclic loading (Jimenez, 2016)

The stiffness of soil can be defined in two different ways under cyclic loadings: the first one is secant shear modulus (G_{sec}), which varies with the shear strain and the second one is maximum shear modulus (G_0), which is the maximum shear modulus representing the stiffness of the soil at very low strain levels (Kramer, 1996).

The secant shear modulus and maximum shear modulus can be determined by using Equation 4.1 and Equation 4.2, which are proposed by Kramer (1996).

$$G_{sec} = \frac{\tau}{\gamma} \qquad (4.1)$$

$$G_0 = V_s^2 * \rho \qquad (4.2)$$

Shear modulus of the soil is proportional to the shear strain (Kramer, 1996). To represent these variations, different researchers proposed modulus degradation and damping curves in the literature. Sample modulus degradation and damping curves proposed by Kavazanjian et al. (1997) for sand layers are presented in Figure 4.2.
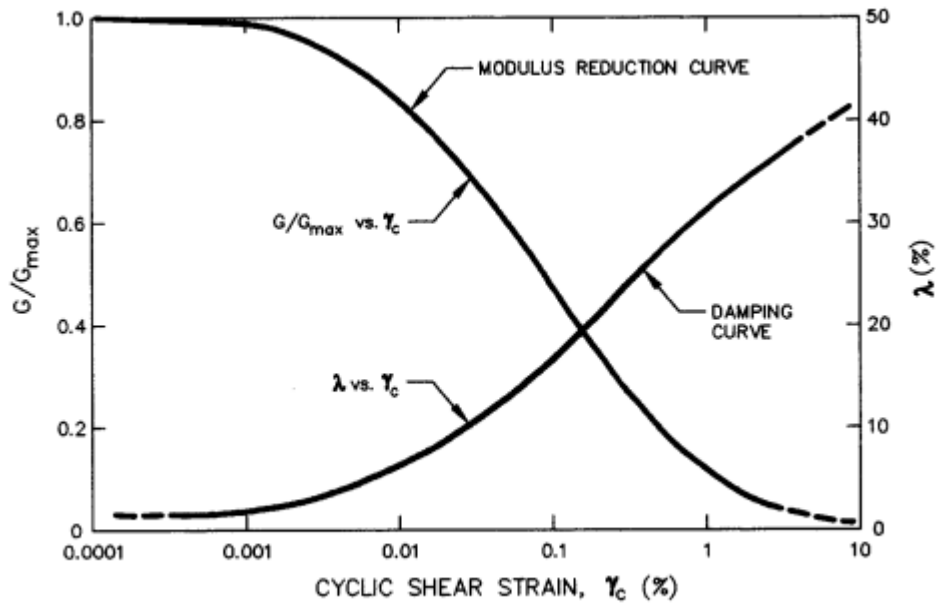
Figure 4.2. Modulus degradation and damping curves for sand layers (Kavazanjian et al., 1997)

4.2.2.2 Damping

Damping generally refers to the process of energy dissipation due to cyclic loading in a vibrating system, resulting in a decrease in the amplitude of oscillations. In Plaxis, energy dissipation due to cyclic loading can be defined by three types of damping, known as hysteretic, viscous and numerical damping (Plaxis 2D Reference Manual, 2022). An overview about these damping types is provided in the following paragraphs.

Hysteretic damping: Hysteretic damping can be defined as the ratio of the energy dissipated to the maximum strain energy stored during each cycle of the hysteresis loops (Darendeli, 2001). It is generated by the frictional loss within the soil and frequency independent. Graphical representation of the hysteretic damping is presented in Figure 4.3.
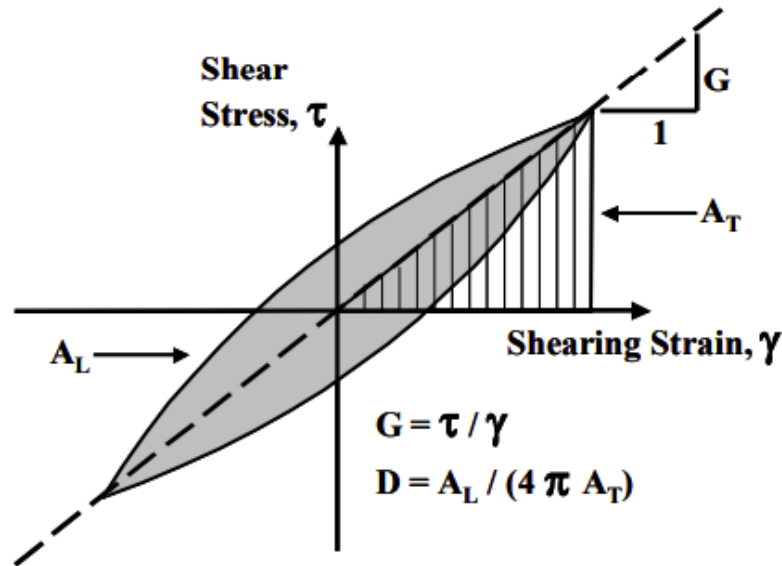
Figure 4.3. Determination of shear modulus and hysteretic damping ratio during a cyclic loading (Darendeli, 2001)

Contrarily to shear modulus, hysteretic damping is proportional to the shear strain (Kramer, 1996). To represent these variations, different researchers proposed modulus degradation and damping curves in the literature. A sample modulus reduction and damping curve proposed by Kavazanjian et al. (1997) for sand layers is presented in the Figure 4.2. Hysteretic damping can be added to dynamic analyses by using Hardening Soil with small strain stiffness constitutive soil model in Plaxis 2D. This constitutive soil model will be discussed in a detailed manner in section 4.2.3.

Viscous Damping: An alternative method for representing the energy dissipation is viscous damping. The main difference between viscous damping and hysteretic damping is that viscous damping is frequency dependent. In Plaxis, viscous damping can be applied in dynamic analyses by using Rayleigh damping. Rayleigh damping is described by a matrix incorporating certain proportions of mass and stiffness matrices (Plaxis 2D Reference Manual, 2022):

$$\underline{C} = \alpha_r * [\underline{M}] + \beta_r * [\underline{K}] \tag{4.3}$$

where;

C = Damping matrix

M = Mass matrix

K = Stiffness matrix

α_r, β_r: Rayleigh damping coefficients

The amount of damping is directly related to the mass and stiffness of each individual element. The damping ratio depends also on α_r and β_r. Having a higher α constant results in stronger damping of lower frequencies, while a higher β_r constant leads to stronger damping of higher frequencies.

Relation between the damping ratio and Rayleigh damping constants can be expressed by Equation (4.4) and Equation (4.5), presented in Plaxis 2D Reference Manual (2022).

$$a_r + \beta_r\omega^2 = 2\omega\xi \tag{4.4}$$

$$\omega = 2\pi f \tag{4.5}$$

where;

w: Angular frequency (rad / s)

f: Frequency (Hz)

ξ: Damping ratio

By solving the above equations for two distinct frequencies and damping ratios corresponds to them, Rayleigh damping constants (α_r and β_r) can be obtained.

$$a_r = 2\omega_1\omega_2 \frac{\omega_1\xi_2 - \omega_2\xi_1}{\omega_1^2 - \omega_2^2} \tag{4.6}$$

$$\beta_r = 2\frac{\omega_1\xi_1 - \omega_2\xi_2}{\omega_1^2 - \omega_2^2} \tag{4.7}$$

An example for Rayleigh damping parameters for a damping ratio of 8%, the first target frequency, $f_1 = 1.5$ Hz and the second target frequency, $f_2 = 8.0$ Hz is presented in Figure 4.4.
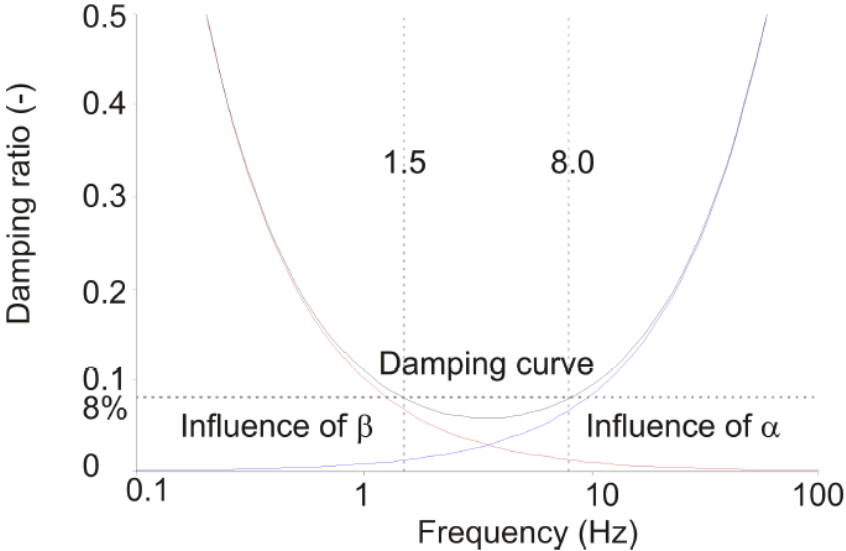
Figure 4.4. Rayleigh damping parameters (Plaxis 2D Reference Manual, 2022)

In engineering applications, Rayleigh damping ratio for soils typically ranges from 0.5% to 2% for both the first and second target frequencies (Kwaak, 2015). To determine target frequencies, there are different methods in the literature. Kwok et al. (2007) recommends to select the second target frequency as equal to five times f_1. Hudson et al. (1994) suggest to choose the first target frequency as equal to the natural frequency of soil profile. They suggest to determine the second target frequency by multiplying the first target frequency with the nearest odd integer greater than the ratio of the predominant frequency of earthquake to the natural frequency of soil (f_p / f_1). This approach is used in the analyses of this thesis study.

$$f_1 = \frac{V_s}{4H} \tag{4.8}$$

$$f_2 = odd\left(\frac{f_p}{f_1}\right) * f_1 \tag{4.9}$$

46

where;

H: Thickness of the soil profile

f_P: Predominant frequency of earthquake

Numerical Damping: In the numerical analysis, the method used for integrating the time plays a critical role in ensuring the stability and precision in the calculation process. There are two common time integration schemes, known as explicit integration and implicit integration. Although explicit method is very simple, it has the drawback that the calculation process is not strong and it has severe restrictions for time steps. Implicit integration method is a bit complex method, but it provides more accurate and stable solutions (Sluys, 1992)

Plaxis 2D implements the Newmark's implicit time integration scheme to solve the dynamic equations in the analyses. Using this method, the velocity and displacement at time t+Δt can be described using Equation 4.10, Equation 4.11 and Equation 4.12 (Plaxis 2D Scientific Manual, 2022).

$$u^{t+\Delta t} = u^t + \dot{u}^t \Delta t + \left(\left(\frac{1}{2} - \alpha \right) \ddot{u}^t + \alpha \ddot{u}^{t+\Delta t} \right) \Delta t^2 \qquad (4.10)$$

$$\dot{u}^{t+\Delta t} = \dot{u}^t + \left((1 - \beta) \ddot{u}^t + \beta \ddot{u}^{t+\Delta t} \right) \Delta t \qquad (4.11)$$

$$\beta \geq 0.5, \quad \alpha \geq \frac{1}{4} \left(\frac{1}{2} + \beta \right)^2 \qquad (4.12)$$

where;

u: Displacement

u̇: Velocity

ü: Acceleration

Δt: Time step

α, β: Numerical control parameters which determine the stability and accuracy of the time integration, should not be confused with the Rayleigh damping coefficients

In Plaxis 2D, the values of numerical control parameters (α and β) are adjusted to the lowest values possible to ensure a stable calculation without any numerical damping. for an unconditionally stable calculation and no extra numerical damping. These default values are implemented in the analyses of this study.

4.2.3. Constitutive Soil Models

Various material models can be implemented to describe the relationship between stress and strain. Plaxis 2D offers various constitutive models for accurately modeling the behavior of soil and structural elements. In the scope of this study, structural elements (piles and foundations), rock layers and sand layers are modeled by Linear Elastic, Mohr-Coulomb and Hardening Soil with small strain stiffness (HSsmall) model, respectively. In the following subsections, brief introductions of these constitutive soil models are provided.

4.2.3.1 Linear Elastic Model

Linear elastic model is one of the simplest models where stress is defined as linearly proportional to the strain. Graphical representation of stress-strain relationship of a linear elastic model is presented in Figure 4.5.
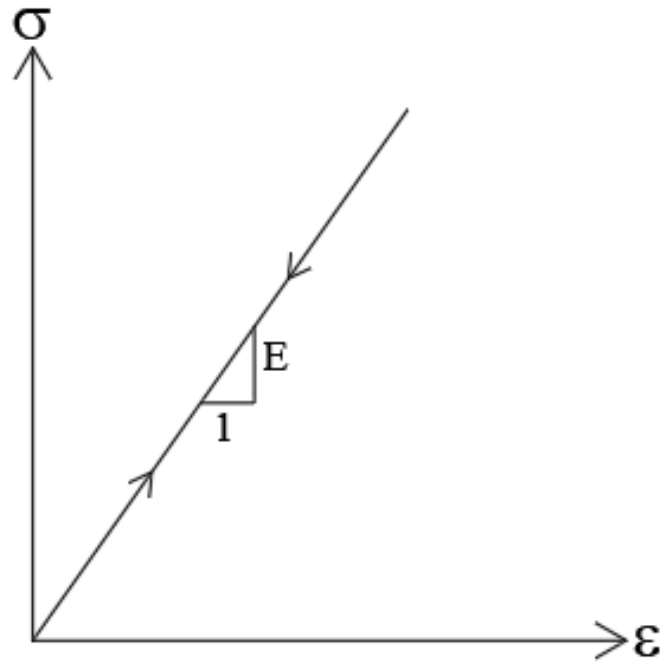
Figure 4.5. Stress-strain relationship for linear elastic materials

Linear elastic model describes the material behavior based on its elastic properties which are constant, (i.e., does not depend on strain level), like elastic modulus (E), shear modulus (G) and bulk modulus (K). Elastic modulus, bulk modulus and shear modulus of a linear elastic material can be determined using Equation 4.13, Equation 4.14 and Equation 4.15, respectively.

$$E = \frac{\sigma}{\varepsilon} \tag{4.13}$$

$$K = \frac{E}{3(1-v)} \tag{4.14}$$

$$G = \frac{E}{2(1+v)} \tag{4.15}$$

Input parameters of Linear elastic model for Plaxis 2D is provided in Table 4.1.

Table 4.1. Linear elastic model input parameters

Parameter	Description	Unit
γ	Unit weight	kN/m^3
E	Elastic modulus	kPa
ν	Poisson's ratio	-

This model can be used for representing the behavior of certain structural elements, as well as bedrock layers (Pinto, 2012). Since the stress-strain relation of soils is actually nonlinear and this model does not consider the stiffness reduction with increased strain, linear elastic model is only used for structural elements in the scope of this study.

4.2.3.2 Mohr-Coulomb Model

Contrarily to assumption of the linear elastic model, the response of soil to stress or strain is characterized by non-linear behavior. In addition, the stiffness of soil depends on various parameters like levels of stress and strain and path of stress (Plaxis 2D Material Models Manual, 2022). Although there are constitutive soil models including these concepts, Mohr-Coulomb model is a basic linear elastic perfectly plastic model which is frequently used for initial estimation of the soil behavior. The stress-strain relationship of the model shows linear behavior within the elastic region, which is characterized by Hooke's law. This elastic region extends up to failure point. Mohr-Coulomb failure criterion is used to predict the stress state at failure and it is assumed that the stress level stays constant in the plastic region. A sample stress-strain graph for linear elastic perfectly plastic materials is presented in Figure 4.6.
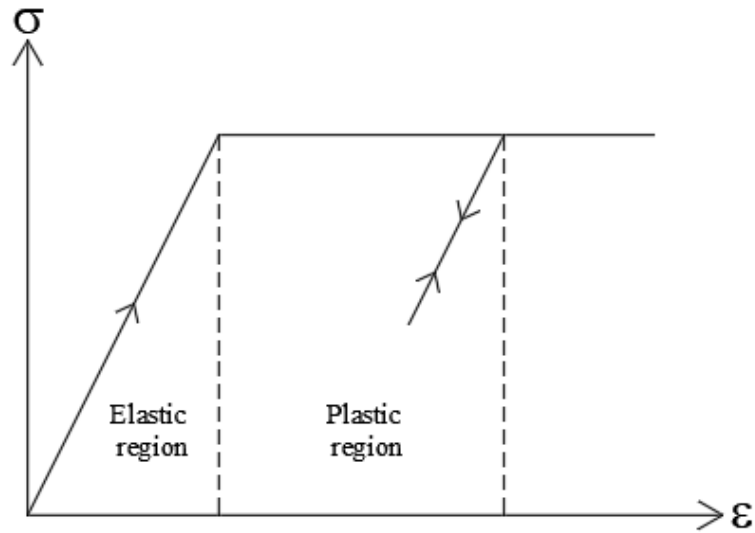
Figure 4.6. Stress-strain relationship for linear elastic perfectly plastic materials

The model operates on the assumption that the yield point for a specific material is reached when Mohr's circles intersect with the line representing the shear strength. The yielding point concept is represented in Figure 4.7.
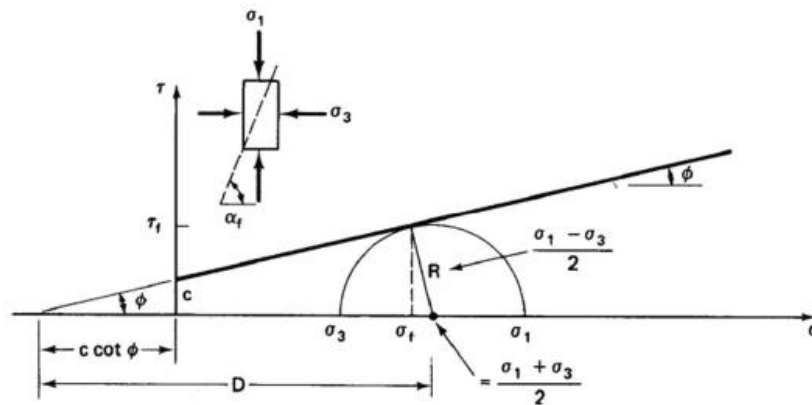
Figure 4.7. Mohr-Coulomb failure criterion (Labuz and Zang, 2012)

The straight line representing the shear strength is derived from the Mohr-Coulomb failure criterion and can be represented by Equation 4.16.

$$\tau_f = c + \sigma_f * \tan(\phi) \tag{4.16}$$

where;

τ_f: Shear strength

c: Cohesion

σ_f: Failure stress

ϕ: Internal friction angle

The yield condition of the model is based on the Coulomb's friction law. It comprises six yield functions when expressed based on principal stresses and these functions are represented by f. The yield surface, which is in the shape of a hexagonal cone in the principal stress space, for linear elastic perfectly plastic materials is obtained for the case of all yield functions is equal to zero (f=0) (Plaxis 2D Material Models Manual, 2022).
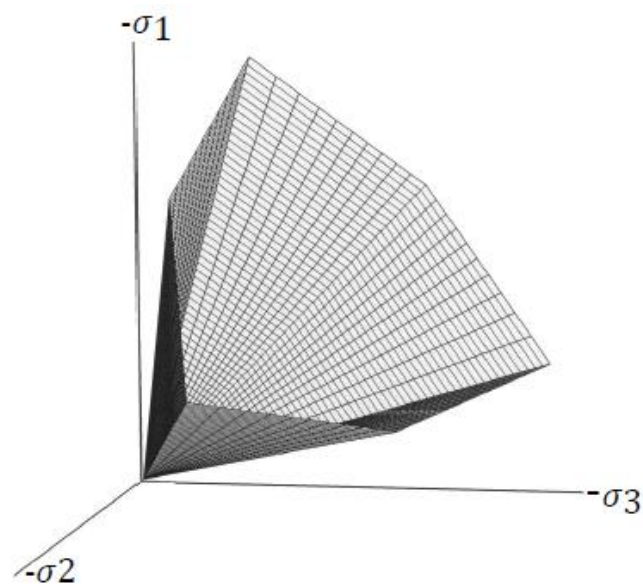
Figure 4.8. Mohr-Coulomb yield surface (Plaxis 2D Material Models Manual, 2022)

Input parameters of Mohr-Coulomb model for Plaxis 2D is provided in Table 4.2.

Table 4.2. Mohr-Coulomb model input parameters

Parameter	Description	Unit
γ	Unit weight	kN/m^3
E	Elastic modulus	kPa
ν	Poisson's ratio	-
G	Shear modulus (alternative stiffness parameter)	kPa
E_{oed}	Oedometric modulus (alternative stiffness parameter)	kPa
c'	Effective cohesion	kPa
ϕ'	Effective internal friction angle	°
ψ	Dilatancy angle	°
V_p	Primary wave velocity (Used to determine the stiffness according to wave velocities for the dynamic applications)	m/s
V_s	Shear wave velocity (Used to determine the stiffness according to wave velocities for the dynamic applications)	m/s

Mohr-Coulomb model is often used for initial estimation of the soil behavior. In the geotechnical engineering, it is one of the most commonly used constitutive soil models. This model can be used for dynamic applications, too. In dynamic analyses, stiffness parameters have to be defined carefully to ensure that the model predicts the seismic wave velocities accurately. Under cyclic loading conditions, plastic strains which can be generated in Mohr-Coulomb model, produces damping in dynamic calculations. But, it should be noted that these strains are only elastic strains, which means this model does not take into account the hysteretic damping in the soil. Rayleigh damping can be utilized to take into account the damping characteristics.

4.2.3.3 Hardening Soil with small strain Stiffness (HSsmall)

HSsmall model is a modified version of the Hardening Soil (HS) model, which was introduced by Schanz et al. (1999). Original HS model is enhanced with small-strain overlay model, proposed by Benz et al. (2006), to be able to take into account the small strain stiffness of soil.

Original HS model is based on the assumption of elastic material behavior during unloading and reloading. Yet, the range of strain in which soils behave completely elastic is quite small. Soil stiffness decreases in a nonlinear manner as the strain amplitude increases. Relationship between stiffness and strain is represented by a modulus reduction curve, which is created by plotting soil stiffness (G) as a logarithmic function of shear strain ($\gamma_{0.7}$) (Plaxis 2D Material Models Manual, 2022). A sample modulus reduction curve, including the strain ranges suitable for laboratory tests and particular shear strain ranges for the geotechnical structures, provided in Figure 4.9.
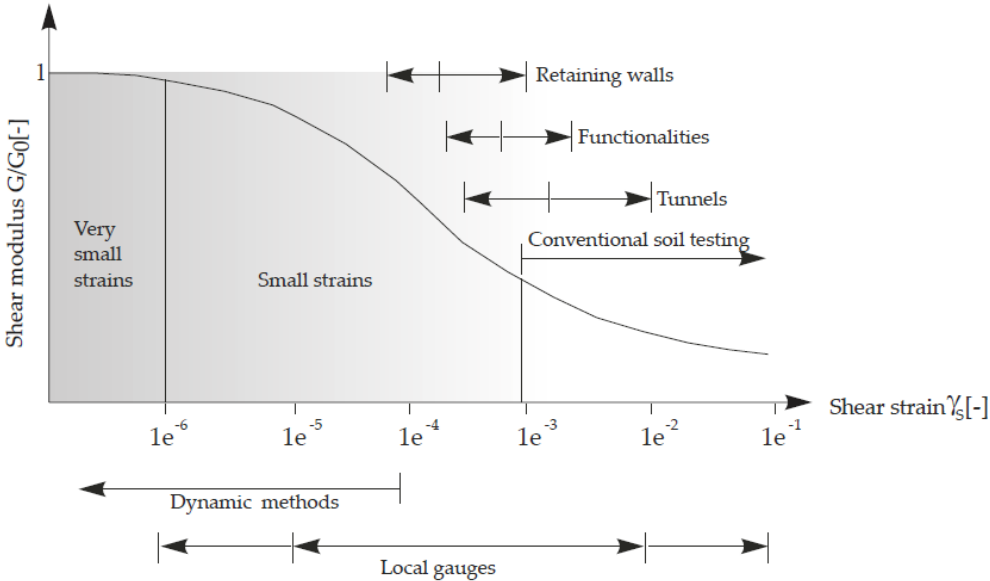
Figure 4.9. Sample modulus reduction curve (Plaxis 2D Material Models Manual, 2022)

The modulus reduction curve is developed as an improved form of the simple hyperbolic law introduced by Hardin and Drnevich (1972).

$$\frac{G_s}{G_0} = \frac{1}{1 + 0.385 \frac{\gamma}{\gamma_{0.7}}}$$

(4.17)

where;

G_s: Secant shear modulus

G_0: Maximum shear modulus

$\gamma_{0.7}$: Threshold shear strain, i.e., shear strain level at which $G_s / G_0 \approx 0.7$

Tangent shear modulus (G_t), which defines the stress-strain relations for all directions under multiaxial loading, can be computed by taking derivative of secant shear modulus with respect to shear strain (Plaxis 2D Material Models Manual, 2022). Tangent shear modulus can be calculated by using Equation 4.18.

$$G_t = \frac{G_0}{\left(1 + 0.385 \frac{\gamma}{\gamma_{0.7}}\right)^2}$$

(4.18)

The lower limit of the tangent shear stiffness modulus is defined by a certain value known as G_{ur} at a strain level called as the cut-off shear strain (Plaxis 2D Material Models Manual, 2022).

$$G_{ur} = \frac{E_{ur}}{2(1 + v_{ur})}$$

(4.19)

$$G_t = \frac{E_t}{2(1 + v_{ur})}$$

(4.20)

$$\gamma_{cut-off} = \frac{1}{0.385}\left(\sqrt{\frac{G_0}{G_{ur}}} - 1\right)\gamma_{0.7}$$

(4.21)

where;

G_{ur}: Unloading-reloading shear modulus

E_{ur}: Unloading-reloading elastic modulus

v_{ur}: Unloading-reloading Poisson's ratio

$\gamma_{(cut-off)}$: Cut-off shear strain

Input parameters of HSsmall for Plaxis 2D is provided in Table 4.3.

Table 4.3. HSsmall model input parameters

Parameter	Description	Unit
γ	Unit weight	(kN/m^3)
c'	Effective cohesion	(kPa)
ϕ'	Effective internal friction angle	(°)
ψ	Dilatancy angle	(°)
v_{ur}	Unloading-reloading Poisson's ratio	-
E_{50}^{ref}	Reference secant stiffness in standard drained triaxial test	(kPa)
E_{oed}^{ref}	Reference tangent stiffness for primary oedometer loading	(kPa)
E_{ur}^{ref}	Reference unloading / reloading stiffness (default $E_{ur}^{ref} = 3E_{50}^{ref}$)	(kPa)
m	Power for stress level dependency of stiffness	-
R_f	Failure ratio (default $R_f = 0.9$)	-
p_{ref}	Reference stress for stiffnesses (default $p_{ref} = 100$ kPa)	(kPa)
K_0^{nc}	K_0 value for normal consolidation (default $K_0^{nc} = 1 - \sin(\phi')$)	-
G_0^{ref}	Reference shear modulus at very small strains ($\gamma < 10^{-6}$)	(kPa)
$\gamma_{0.7}$	Threshold shear strain	-

The only differences between the parameters of original HS model and HSsmall model are the parameters G_0^{ref} and $\gamma_{0.7}$. Stiffness parameters of the model can be determined using the equations (4.22) through (4.26).

$$E_{50} = E_{50}^{ref} \left(\frac{c \cos(\phi') - \sigma'_3 \sin(\phi')}{c \cos(\phi') + p^{ref} sin(\o')} \right)^m \tag{4.22}$$

$$E_{oed} = E_{oed}^{ref} \left(\frac{c \cos(\phi') - \sigma'_1 \sin(\phi')}{c \cos(\phi') + p^{ref} \sin(\phi')} \right)^m \tag{4.23}$$

$$E_{ur} = E_{ur}^{ref} \left(\frac{c \cos(\phi') - \sigma'_3 \sin(\phi')}{c \cos(\phi') + p^{ref} \sin(\phi')} \right)^m \tag{4.24}$$

$$G_0 = G_0^{ref} \left(\frac{c \cos(\phi') - \sigma'_3 \sin(\phi')}{c \cos(\phi') + p^{ref} \sin(\phi')} \right)^m \tag{4.25}$$

$$\sigma'_1 = \frac{\sigma'_3}{K_0^{nc}} \tag{4.26}$$

where;

E_{50}: Secant stiffness in standard drained triaxial test

E_{50}^{ref}: Reference secant stiffness

E_{oed}: Tangent stiffness for primary oedometer loading

E_{oed}^{ref}: Reference tangent stiffness

E_{ur}: Unloading / reloading stiffness

E_{ur}^{ref}: Reference unloading-reloading stiffness

G_0: Shear modulus at very small strains ($\gamma < 10^{-6}$)

G_0^{ref}: Reference shear modulus at very small strains ($\gamma < 10^{-6}$)

σ'_3: Minor principal stress (confining pressure in a triaxial test (negative for compression))

σ'_1: Major principal stress (negative for compression)

The threshold shear strain, $\gamma_{0.7}$, parameter can be determined by using the different modulus degradation curves or equations proposed in the literature. In this study, the equation provided in Plaxis 2D Material Models Manual (2022) is used to determine the threshold shear strain.

$$\gamma_{0.7} = \frac{1}{9G_0}[2c'(1 + \cos{(2\phi')}) - \sigma_1'(1 + K_0)\sin{(2\phi')}] \tag{4.27}$$

Unlike Linear Elastic and Mohr-Coulomb models, the HSsmall model takes into account the hysteretic behavior of soil under cyclic loading conditions. The hysteretic behavior of this model generates damping. The amount of damping depends on the loading condition and strain level. Since this model takes into account the nonlinear soil behavior more accurately, HSsmall model is used to model the soil layers in this study.

4.2.4. Boundary Conditions

The primary objective of dynamic analysis is to accurately model the propagation of waves through soil layers. In order to avoid the reflection of seismic waves from the model boundaries, which leads to manipulations in the analysis results, it is essential to ensure that the model boundaries are sufficiently far away from the area of interest. Yet, placing the boundaries at a significant distance necessitates the incorporation of numerous additional elements, resulting in a substantial increase in both memory consumption and analysis time. Plaxis 2D offers special boundary conditions for dynamic analyses to counteract wave reflection and unwanted waves. These dynamic boundary conditions will be discussed in this section.

Viscous Boundaries: The viscous boundary condition, which has been proposed by Lysmer and Kuhlemeyer (1969), includes viscous dampers utilized in both x and y throughout at the boundary. These boundaries absorb the energy of outgoing waves and have the ability to eliminate reflected stresses generated by dynamic input. Viscous boundary conditions can be utilized for the analysis models that do not include structural components and the source of dynamic load is located inside the finite element mesh (Plaxis 2D Reference Manual, 2022).

Tied Degrees of Freedom: This particular boundary condition is appropriate only for lateral boundaries (x_{min} - x_{max}). Nodes located at the both sides of the model with the same elevation are connected and share the same vertical and horizontal movement in this boundary condition. This boundary condition can only be applied when the arrangement of nodes along the vertical boundaries of the model is identical, which means that the nodes on both the left and right boundaries should have the same elevation. A visual representation of tied degrees of freedom boundary condition is presented in Figure 4.10.

$$\Delta x_n^L, \Delta y_n^L \quad\bigcirc\!\!-\!\!\bigcirc\quad \Delta x_n^R, \Delta y_n^R$$

$$\Delta x_{n-1}^L, \Delta y_{n-1}^L \quad\bigcirc\!\!-\!\!\bigcirc\quad \Delta x_{n-1}^R, \Delta y_{n-1}^R$$

$$\Delta x_2^L, \Delta y_2^L \quad\bigcirc\!\!-\!\!\bigcirc\quad \Delta x_2^R, \Delta y_2^R$$

$$\Delta x_1^L, \Delta y_1^L \quad\bigcirc\!\!-\!\!\bigcirc\quad \Delta x_1^R, \Delta y_1^R$$
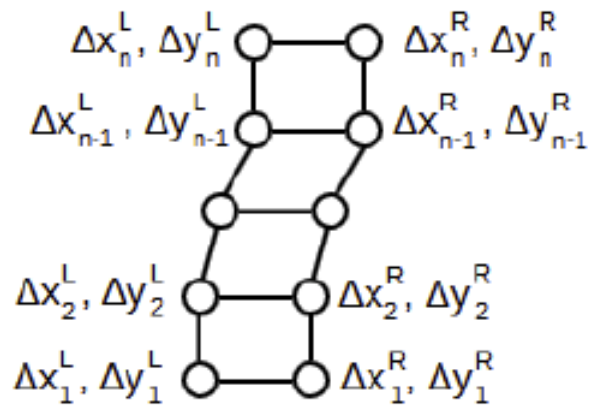
$$\Delta x_i^L = \Delta x_i^R \qquad \Delta y_i^L = \Delta y_i^R \qquad i = 1, 2, ...N$$

Figure 4.10. Visual representation of tied degrees of freedom boundary condition (Plaxis 2D Material Models Manual, 2022)

Tied degrees of freedom boundary condition is usually applied to perform site response analysis of 1D soil columns. When waves originate within the mesh or are reflected back into a model due to geometric irregularities or structural components, these waves cannot be successfully absorbed by these boundaries (Plaxis 2D Reference Manual, 2022).

Free Field Boundaries: The free field boundary condition, like tied degrees of freedom boundary condition, is suitable only for the lateral boundaries (x_{min} - x_{max}). It simulates the wave propagation to the far field by minimizing the reflections of the waves at model boundaries. Free field elements can be simulated on both ends of the main model geometry and they possess the same characteristics with the soil layers within the finite element mesh. At the lateral boundaries, two dashpots are added in each node, which are in the transverse and longitudinal directions, to absorb the waves which are reflected from the structures in the model. The visual representation of free field boundary condition is provided in Figure 4.11.
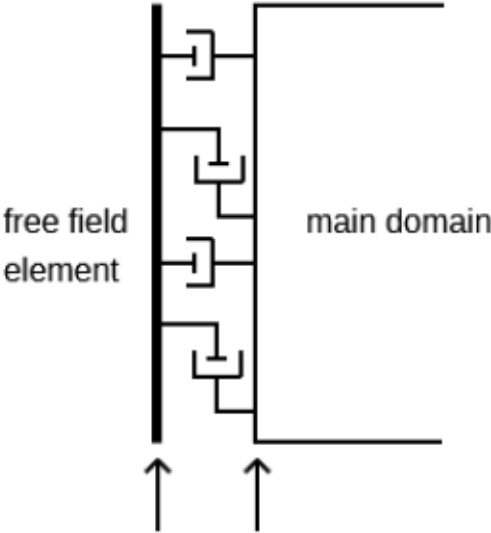
Figure 4.11. Visual representation of free field boundary condition (Plaxis 2D Material Models Manual, 2022)

Free field boundary condition should be applied on both of the lateral boundaries and is used together with the interface elements along the boundary. These interface elements should be placed inside the model. Furthermore, free field boundary conditions generally utilized for earthquake analyses, in which the seismic input motion is applied at the bottom boundary (Plaxis 2D Material Models Manual, 2022).

Compliant Base Boundary: The compliant base is a boundary condition, proposed by Joyner and Chen (1975), and composed of a viscous boundary and a prescribed displacement. This boundary condition is only applicable to the bottom boundary of the model. The main idea behind this boundary condition is modeling the propagation of towards the base of the model and minimizing the wave reflection from the bottom of the model. The input signal which consists of time history records of acceleration, velocity, or displacement is introduced at the base of the model and transferred to model as shear and normal forces. Furthermore, like free field boundaries, compliant base boundary also should be used with interface elements and these interface elements should be placed inside the model. For the input signal applied at the compliant base boundary, only the waves propagating in the upward direction have to be considered. Rock outcrop motions, which are obtained at the surface of rock layers, have both the upward and downward propagating waves. When a rock outcrop motion is used as input motion, by applying a factor of 0.5 to the prescribed displacement, only the upward propagating waves are applied to the model (Plaxis 2D Material Models Manual, 2022).

Boundary conditions used in the analyses performed in the scope of this study are presented in Figure 4.12.
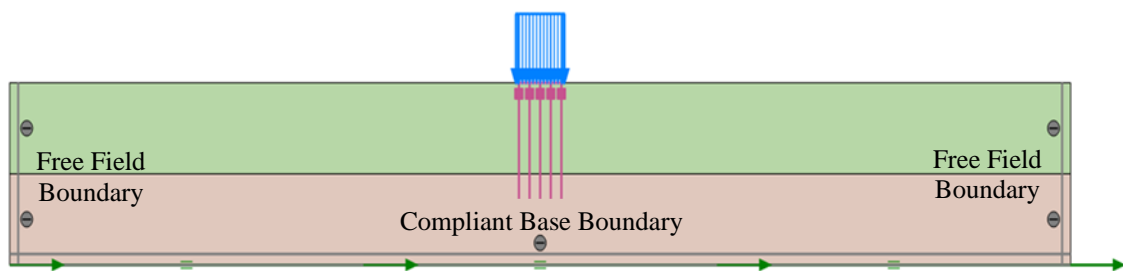
Figure 4.12. Boundary conditions in the analyses

4.2.5. Average Element Size and Time Step

In the dynamic analyses, it is important to consider the element size in the finite element mesh and the time step used for the calculations to make sure that wave propagation is accurately represented. Kuhlemeyer & Lysmer (1973) recommends using an average element size (AES) meeting the criterion presented below.

$$AES \leq \frac{\lambda}{8} = \frac{V_{s,min}}{8f_{max}} \qquad (4.28)$$

where;

λ: Wave length

$V_{s, min}$: Minimum shear wave velocity in the soil profile

f_{max}: Fundamental frequency of input signal

The time step is also quite important for the dynamic calculations. If a too large time step is chosen for the dynamic analyses, this situation can result in significant deviations in the solutions together with unreliable analysis results. The recommended time step for the dynamic analyses depends on the minimum element size in the finite element mesh and maximum shear wave velocity in the soil profile (Plaxis 2D Scientific Manual, 2022).

$$\Delta t_{max,recommended} = \frac{L_{min}}{V_{s,max}} \qquad (4.29)$$

Here, L_{min} is referred to the smallest distance among the three nodes within an element. The time step is determined in such a manner that the movement of a seismic wave in a single time step is limited to the smallest dimension of an element for 2nd order elements and half of an element for 4th order elements (Plaxis 2D Scientific Manual, 2022).

4.3. Analysis Procedures

The primary aim of this study is to investigate the effects of earthquake PGA, soil stiffness, pile diameter, pile spacing and pile length on the internal forces acting on the pile. A comprehensive parametric study was performed using the variables presented in the Section 3.2.4. Numerical analyses were performed using Plaxis 2D finite element software. The analysis procedures are explained in detail in the following sections.

4.3.1. Calibration of the Model Geometry

Model geometry was prepared in plane strain conditions. First of all, soil layers, foundation and piles were created. Foundation (pile cap) and piles were modeled by plate and embedded beam row features, respectively. A uniform line load of 100 kPa was applied to foundations by assuming a five-storey building at the top of foundations. After creating the soil layers and the structural elements, earthquake input signal was applied at the bottom of the model using prescribed displacement feature. Acceleration-time histories of Kobe (1995) earthquake were used as input signals for the analyses. After the creation of prescribed displacement, interface elements were added to the lateral and bottom boundaries to simulate the free field and compliant base boundary conditions.

As mentioned in the Section 3.2.1, the model height was selected as 40 m for all of the analysis cases. The width of the model was determined by an iterative calibration procedure. A set of sensitivity analyses was performed to determine the optimum model width to prevent the reflection of the seismic waves. The analysis results remained almost constant beyond a model width of 300 m. Thus, the model width was determined as 300 m for the numerical analyses. A sample model geometry is presented in Figure 4.13.
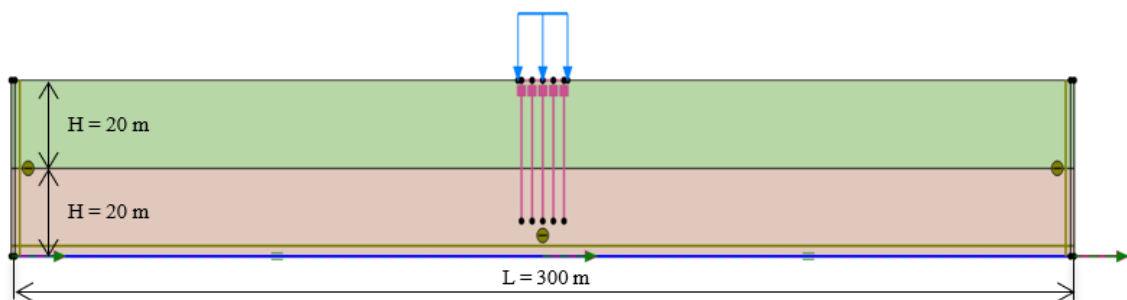
Figure 4.13. Sample model geometry

4.3.2. Creating the Finite Element Mesh

After creating the model geometry finite element mesh was generated for the analyses. Average element size for the finite element mesh was determined according to the equation proposed by Kuhlemeyer & Lysmer (1973). Fundamental frequency of the input signal (f_{max}) can be determined according to Fourier spectra in the dynamic multiplier menu, which is shown in Figure 4.14.
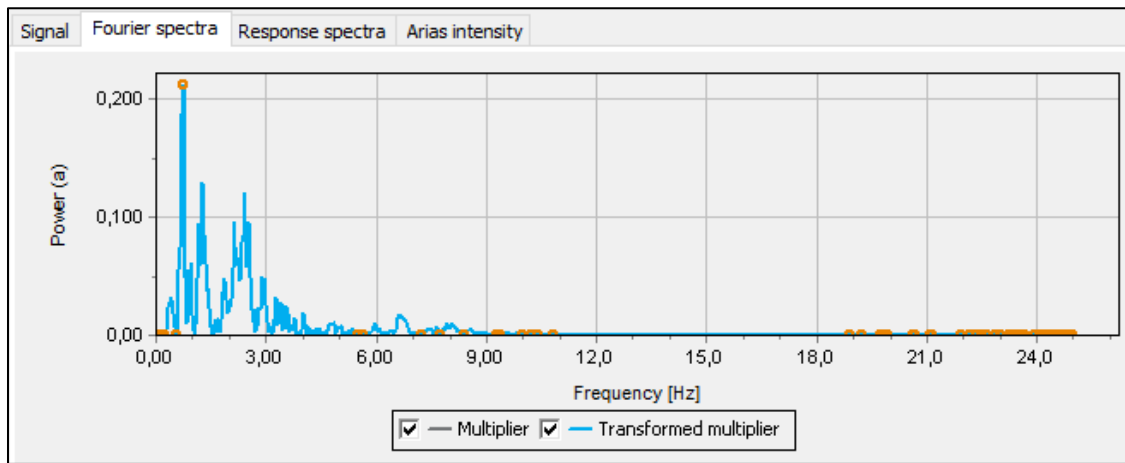
Figure 4.14. Fourier spectra of the input signal

To be on the safe side, the most critical situation was used to determine average element size. Minimum shear wave velocity ($V_{s, min}$) and the fundamental frequency of input signal were taken as 150 m/s and 8 Hz, respectively.

$$A.E.S. \leq \frac{V_{s,min}}{8f_{max}} = \frac{150}{8*8} = 2.3 \; m \qquad (4.30)$$

Average element size for the finite element mesh was taken as 2.1 m for the numerical analyses. The mesh information and sample mesh output from the analysis models are provided in Figure 4.15 and Figure 4.16.

Figure 4.15. Mesh information
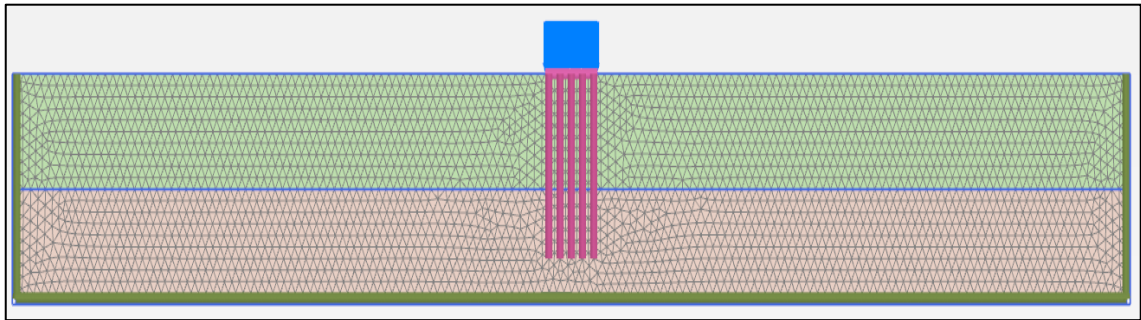
Figure 4.16. Sample mesh output

4.3.3. Defining the Model Parameters

The soil layers and rock layers were modeled by HSsmall and Mohr-Coulomb models, respectively. Although HSsmall model takes into account the hysteretic damping in the soil, a 0.5 % Rayleigh damping was added to account the damping in small strains. A 0.5% Rayleigh damping was considered for rock layers, too. The target frequencies for the Rayleigh damping were selected according to the method proposed by Hudson et al. (1994). Sample soil parameters for the analysis cases with (V_{s1} = 150 m/s, V_{s2} = 300 m/s, H_1 = H_2 = 20 m) and (V_{s1} = 150 m/s, V_{s2} = 760 m/s, H_1 = H_2 = 20 m) are presented in the Table 4.4 and Table 4.5, respectively. The remaining soil parameters are given in Appendix A.

Table 4.4. Parameters for the case with (V_{s1} = 150 m/s, V_{s2} = 300 m/s, H_1 = H_2 = 20 m)

Parameter	Loose Sand (V_{s1} = 150 m/s)	Dense Sand (V_{s2} = 300 m/s)	Unit
Material Model	HSsmall	HSsmall	-
Drainage type	Drained	Drained	-
γ_{sat}	17	21	kN/m^3
γ_{unsat}	17	21	kN/m^3
c'	0	0	kPa
ϕ'	29	39	°
ψ	0	9	°
E_{50}^{ref}	6580	26720	kPa
E_{oed}^{ref}	6580	26720	kPa
E_{ur}^{ref}	19740	80160	kPa
v_{ur}	0.2	0.2	-
m	0.7	0.7	-
p_{ref}	100	100	kPa
G_0^{ref}	41970	114800	kPa
$\gamma_{0.7}$	0.0006345	0.0004335	-

Table 4.5. Parameters for the case with (V_{s1} = 150 m/s, V_{s2} = 760 m/s, H_1 = H_2 = 20 m)

Parameter	Loose Sand (V_{s1} = 150 m/s)	Rock (V_{s2} = 760 m/s)	Unit
Material Model	HSsmall	Mohr-Coulomb	-
Drainage type	Drained	Drained	-
γ_{sat}	17	25	kN/m^3
γ_{unsat}	17	25	kN/m^3
c'	0	50	kPa
ϕ'	29	30	$^\circ$
ψ	0	0	$^\circ$
E'_{ref}	-	3800000	kPa
E_{50}^{ref}	6580	-	kPa
E_{oed}^{ref}	6580	-	kPa
E_{ur}^{ref}	19740	-	kPa
ν_{ur}	0.2	0.25	-
m	0.7	-	-
p_{ref}	100	-	kPa
G_0^{ref}	41970	-	kPa
$\gamma_{0.7}$	0.0006345	-	-

The foundations and piles were modeled using plate and embedded beam row features, respectively. For the parameters of these structural elements, Linear Elastic model was used. A 5% Rayleigh damping was assumed for the structural elements. Moreover, vertical load capacities of the piles were determined based on Section 3.3.3.1 and presented in the Appendix B. Sample parameters for the foundations and piles are presented in the Table 4.6 and Table 4.7.

Table 4.6. Sample parameters for foundations

Parameter	Foundation	Unit
Material Type	Plate	-
Material Model	Elastic	-
w	0	kN/m/m
EA	32000000	kN/m
EI	2667000	$kN*m^2/m$
v	0.2	-

Table 4.7. Sample parameters for piles

Parameter	Pile	Unit
Material Type	Embedded Beam Row	-
Material Model	Elastic	-
γ	24	kN/m^3
Predefined cross section type	Solid Circular Beam	-
D	1.0	m
s	3.0	m
A	0.7854	m^2
I	0.0491	m^4
E	32000000	kPa

4.3.4. Defining the Analysis Steps

After creating the model geometry, generation of the finite element mesh and defining the model parameters, phases of the analyses were created. Initial stresses were created in the initial phase using the K_o procedure. After the initial phase, a nil step was created for activating the structural elements and loads. Finally, dynamic analysis step was created. In this step, prescribed displacements and dynamic multipliers were activated and dynamic boundary conditions were defined. Free field and compliant base boundary conditions were chosen for the lateral boundaries and bottom boundary, respectively. Dynamic time interval of this phase was entered 31.97 s, which is the duration of input signal and then, the displacements were reset to zero. Finally, dynamic time steps of the analyses were defined in the numerical control parameters tab in the Phases menu.

In order to determine the dynamic time steps, recommended time step, proposed by Plaxis 2D Scientific Manual (2022), was calculated based on Equation (4.29) and required number of sub steps was calculated by dividing the time step of the input signal (0.01 s) by the recommended time step calculated according to Equation (4.29).

$$\Delta t_{max,recommended} = \frac{L_{min}}{V_{s,max}} = \frac{0.5}{300} = 0.00167 \; s$$

$$Required \; number \; of \; sub \; steps = \frac{Time \; step \; of \; input \; signal}{Recommended \; time \; step} = \frac{0.01}{0.00167} = 6.0$$

Phase information of a sample analysis case (V_{s1} = 150 m/s, V_{s2} =300 m/s) including the time interval and number of sub steps for dynamic analyses are presented in Figure 4.17.

General	
ID	Dynamic Analysis [Phase_2]
Start from phase	Phase-1
Calculation type	Dynamic
Loading type	Staged construction
Pore pressure calculation type	Use pressures from previous phase
Thermal calculation type	Ignore temperature
Dynamic time interval	31,97 s
Estimated end time	0,3700E-3 day
First step	
Last step	
Design approach	(None)
Special option	0
Deformation control parameters	
Ignore undr. behaviour (A,B)	☐
Reset displacements to zero	☑
Reset small strain	☑
Reset state variables	☐
Reset time	☐
Updated mesh	☐
Ignore suction	☑
Cavitation cut-off	☐
Cavitation stress	100,0 kN/m²
Numerical control parameters	
Max cores to use	256
Max number of steps stored	3197
Use compression for result files	☐
Use default iter parameters	☐
Max steps	3197
Time step determination	Manual
Number of sub steps	6

Figure 4.17. Phase information

After defining the analysis steps, dynamic analyses were conducted for various scenarios outlined in Section 3.2.4, and parametric study was finalized taking the analysis outputs. The analysis outputs containing the accelerations in the soil and the internal forces acting on the piles were obtained using the Plaxis 2D output software and then, these data were arranged in the MS Excel software and presented in the graphical format. Sample graphs containing the analysis results are presented in Figure 4.18 and Figure 4.19.
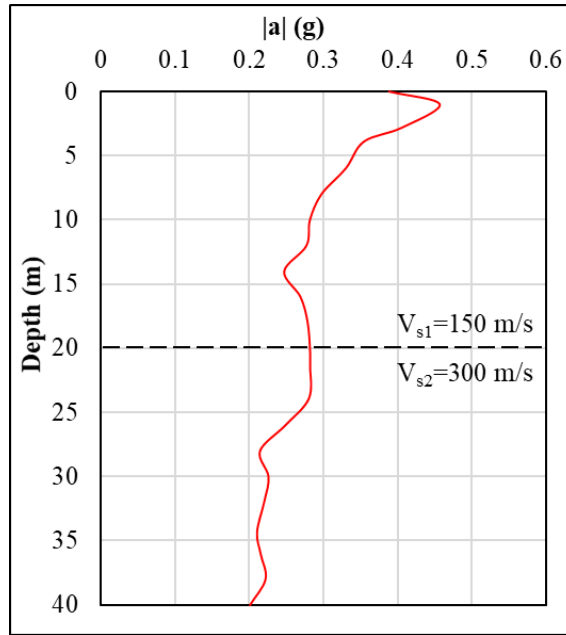
Figure 4.18. Sample acceleration-depth graph for soils
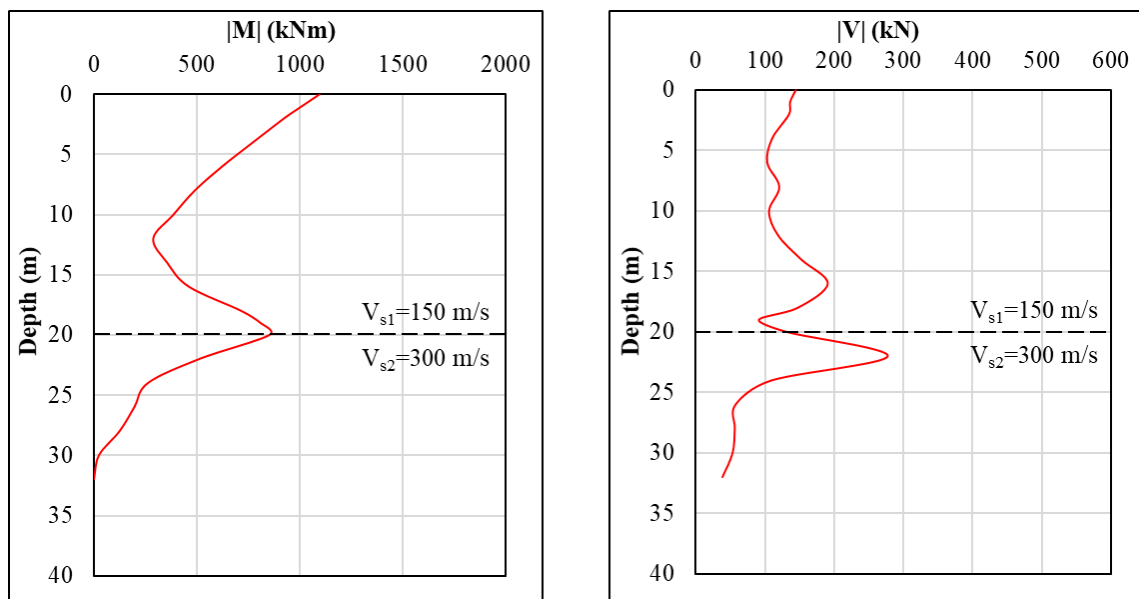
Figure 4.19. Sample internal force diagrams for piles

5. RESULTS AND INTERPRETATION

A total of 114 analyses (107 kinematic interaction and 7 free field analyses) were carried out in the scope of the parametric study using the variables presented in Section 3.2. In order to investigate the influence of various parameters such as pile diameter, pile spacing, pile length, soil stiffness and earthquake accelerations, the acceleration values in the soil layers and the internal forces acting on the piles (bending moments and shear forces) were compared in graphical format. For comparison purposes, acceleration-depth, bending moment-depth and shear force-depth graphs are provided. The acceleration graphs for each analysis case were generated by using the acceleration data from different depths of soils at the center of the model geometry. The bending moment and shear force diagrams present the distribution of the maximum absolute bending moment and shear force values over time domain, at different depths along the pile (i.e., envelopes of bending moments and shear forces). Moreover, the data for the presented diagrams were taken from the outer piles, which are the piles experiencing the highest levels of internal forces.

This chapter presents the results of the analyses performed in the scope of the parametric study. Additionally, comprehensive discussions of how different variables affect the analysis results are also provided in each section.

5.1. Influence of the Pile Diameter

To investigate the influence of the pile diameter, six analyses were conducted for each of three input signals. In two different soil profiles, piles with three different diameters (0.8 m, 1.0 m and 1.2 m) were analyzed. In all cases, the spacings and lengths of the piles were kept constant as 3D and 32.0 m, respectively. The results of these analyses are presented in the following sections.

5.1.1. Accelerations

The graphs containing the accelerations in the soil layers are presented in Figure 5.1 through Figure 5.3. The accelerations in the free field analyses and kinematic interaction analyses are presented together for each soil profile.
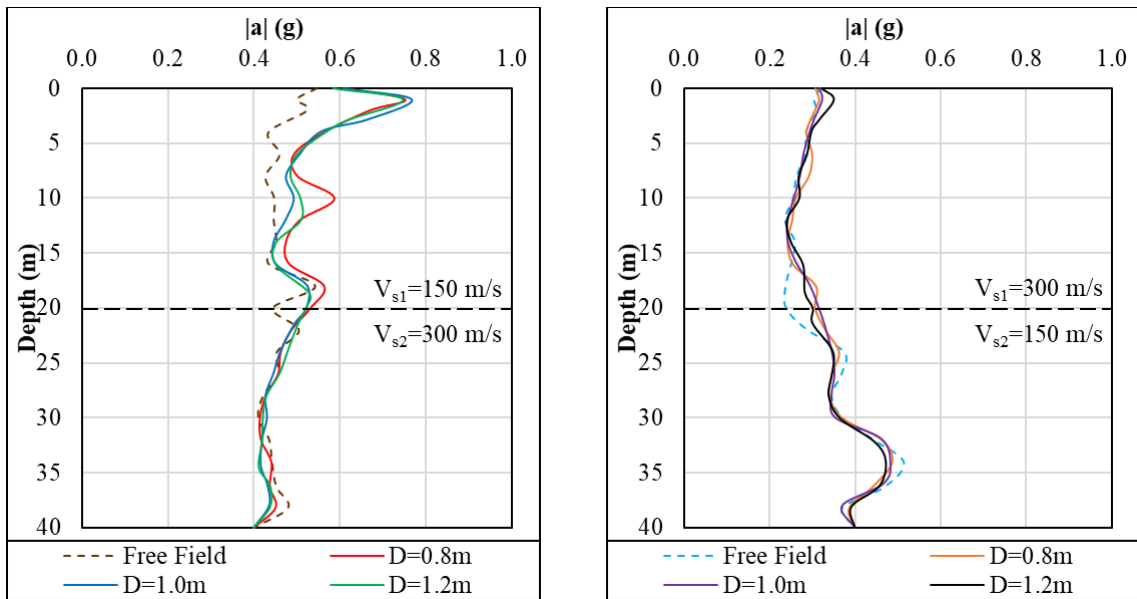
Figure 5.1. Influence of the pile diameter on the soil accelerations (earthquake-1)
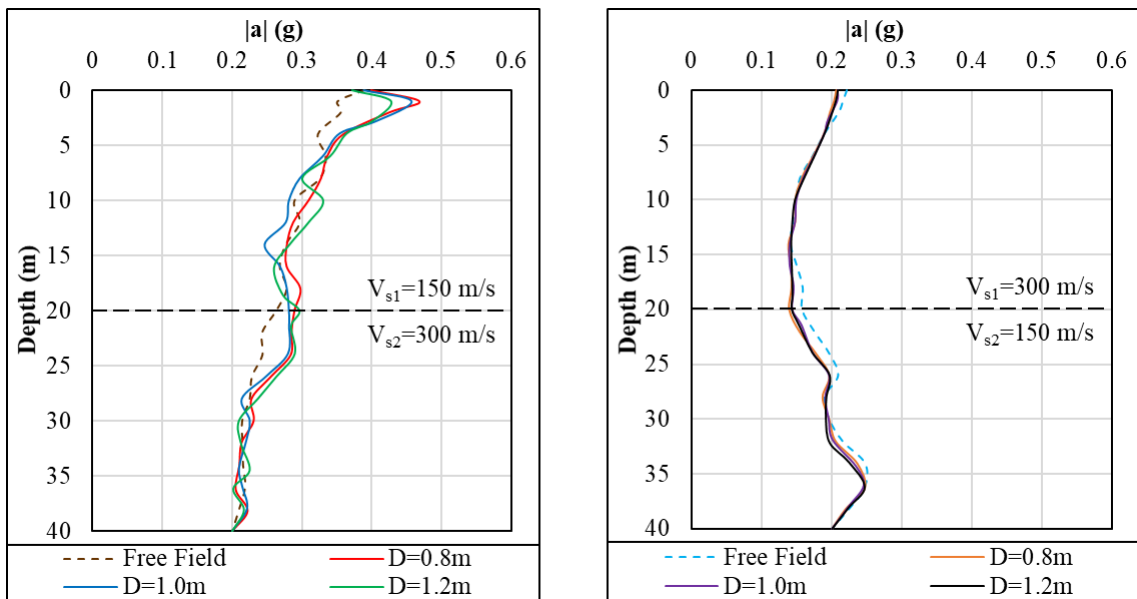
Figure 5.2. Influence of the pile diameter on the soil accelerations (earthquake-2)
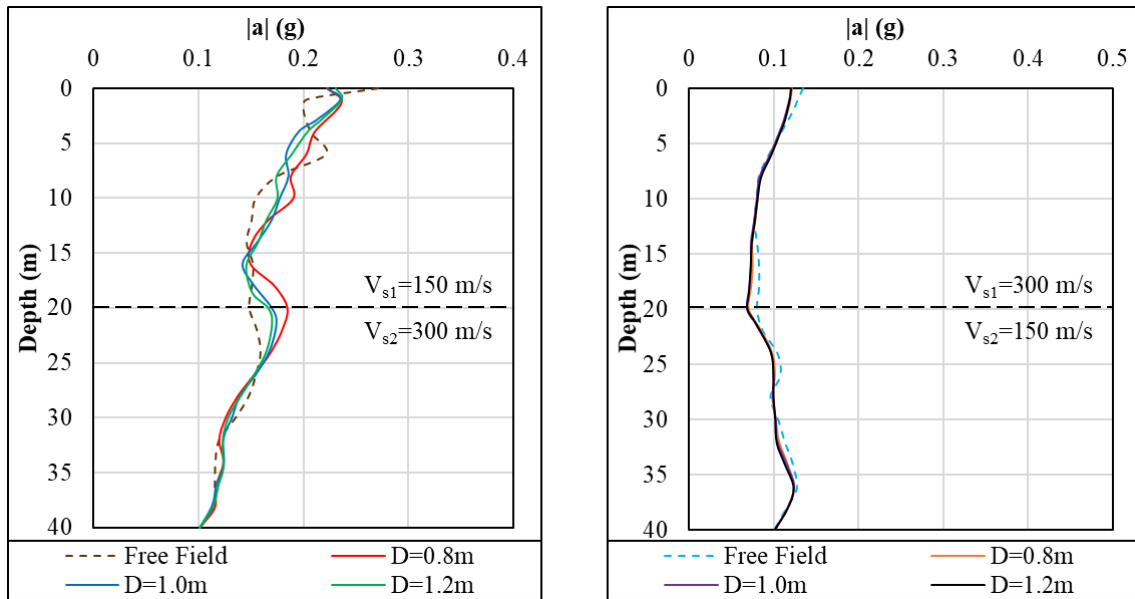
Figure 5.3. Influence of the pile diameter on the soil accelerations (earthquake-3)

As can be seen from the graphs presented above, the accelerations in the kinematic analyses did not change significantly with increasing pile diameter, there were only little fluctuations.

In the analyses with Earthquake-1 and Earthquake-2 input signals: It was observed that for the soil profile having loose sand layer at the top (V_{s1} = 150 m/s), in the kinematic analyses, the accelerations near the pile head were found to be greater than the accelerations at the same depths in the free field analysis. The reasons for this situation can be considered as wave reflection and soil stiffness. Since the loose sand layer amplified the accelerations more than the dense sand layer, the first soil profile was exposed to higher wave reflections and higher accelerations near the pile head. In addition, the stiffness of the soil directly affects the deformations under seismic loading. Since the loose sand layer showed more deformations, this situation also led to higher wave reflections and higher accelerations near the pile head.

In the analyses with Earthquake-3 input signals: Accelerations in the kinematic analyses and free field analysis showed a good agreement except little fluctuations for all analysis cases. Since this input signal has a smaller PGA than the other input signals, the effects of kinematic interaction were also smaller.

74

5.1.2. Bending Moments

The bending moment diagrams for each soil profile and each pile diameter are presented in Figure 5.4 through Figure 5.6.
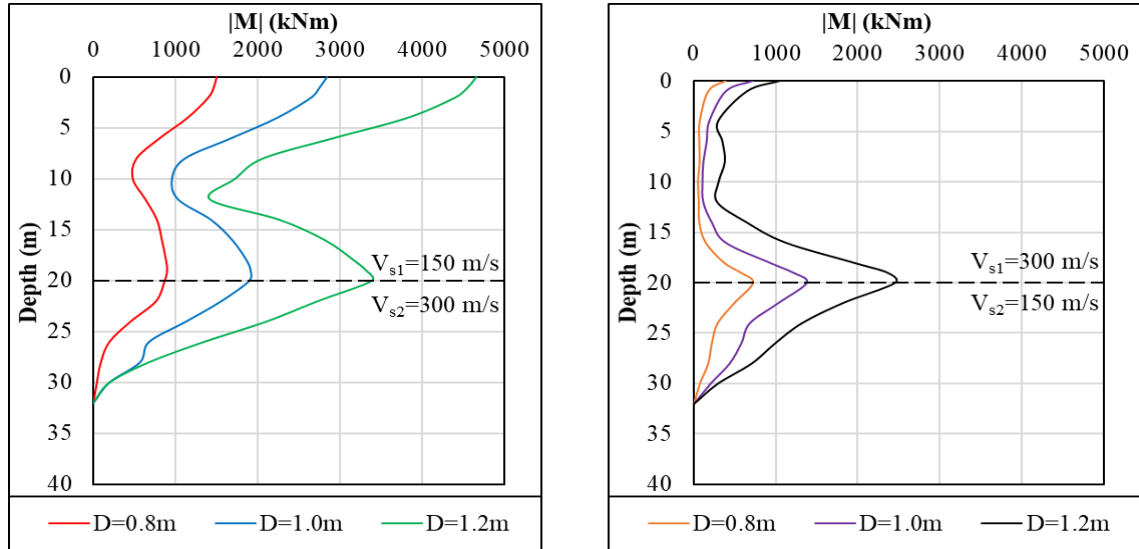
Figure 5.4. Influence of the pile diameter on the bending moments (earthquake-1)
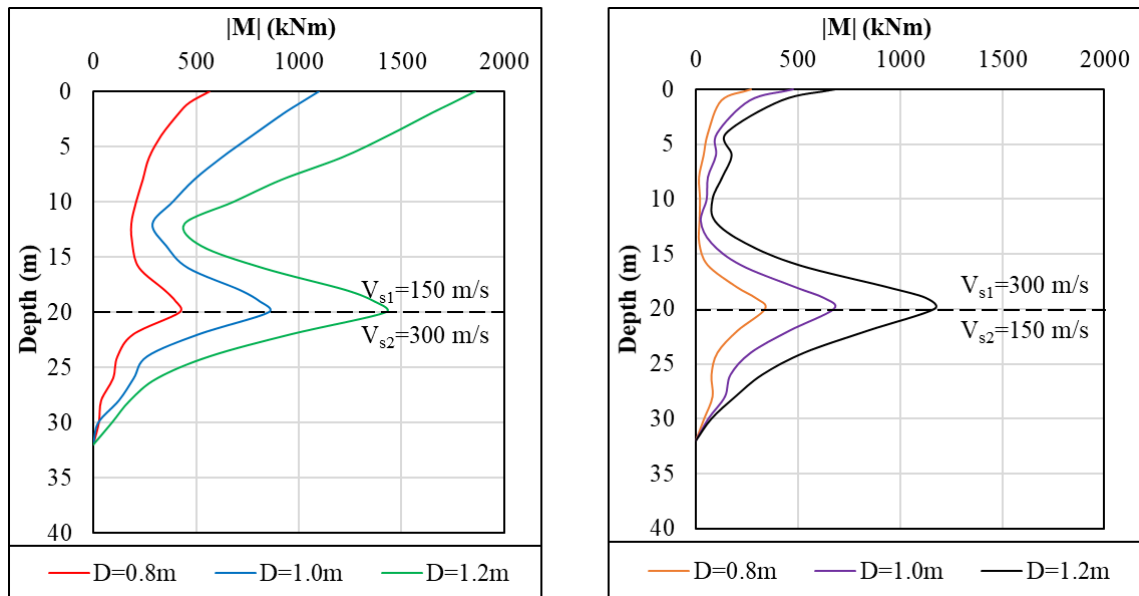
Figure 5.5. Influence of the pile diameter on the bending moments (earthquake-2)
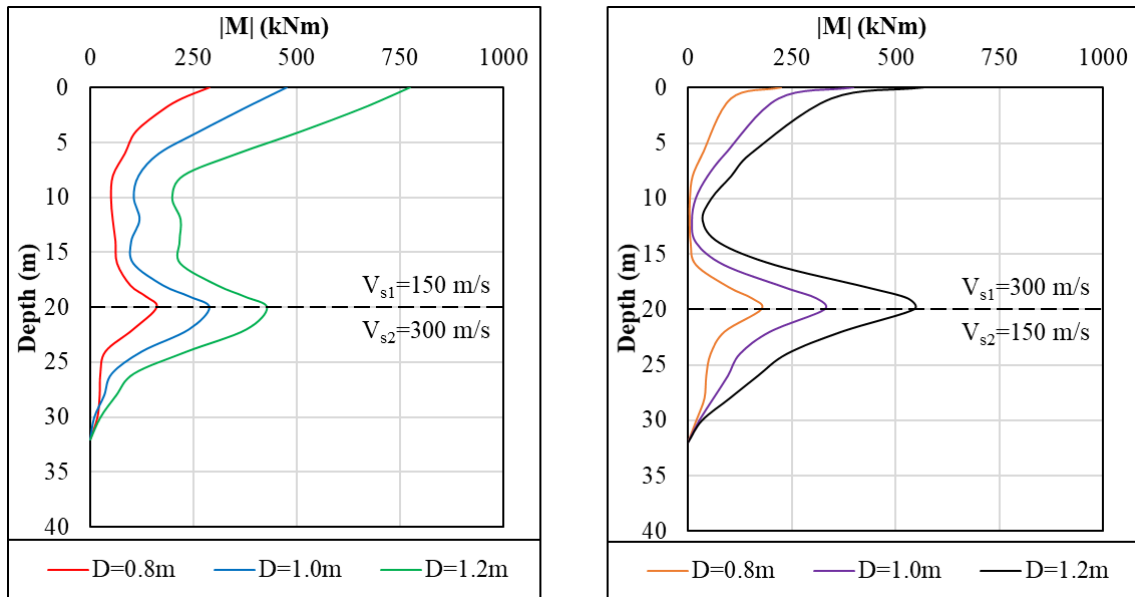
Figure 5.6. Influence of the pile diameter on the bending moments (earthquake-3)

As can be seen in the graphs presented above, the bending moment diagrams are characterized by double peaks in each graph. In both of the soil profiles, these peak values occurred at the pile head and the layer interface. These peak values can be attributed to the restraint exerted by the pile cap on the pile head and the stiffness difference between the layers.

Based on the analysis results, it is evident that the pile diameter has a significant effect on the bending moments acting on the piles. It was observed that the bending moments increased with increasing pile diameter.

In the first soil profile (V_{s1} = 150 m/s, V_{s2} = 300 m/s), between the diameters of 0.8 m and 1.0 m, the bending moments at the pile head increased by 89%, 94% and 64% for earthquake-1, 2 and 3 input signals, respectively. The bending moments at the layer interface increased by 118%, 103% and 79%, respectively for each input signals. Between the diameters of 1.0 m and 1.2 m, the bending moments at the pile head increased by 64%, 70% and 63% for earthquake-1, 2 and 3 input signals, respectively. The bending moments at the layer interface increased by 79%, 67% and 49%, respectively for each input signals.

76

In the second soil profile ($V_{s1} = 300$ m/s, $V_{s2} = 150$ m/s), between the diameters of 0.8 m and 1.0 m, the bending moments at the pile head exhibited increases of 87%, 76% and 77% for earthquake-1, 2 and 3 input signals, respectively. The bending moments at the layer interface increased by 92%, 99% and 86%, respectively for each input signals. Between the diameters of 1.0 m and 1.2 m, the bending moments at the pile head increased by 45%, 42% and 43% for earthquake-1, 2 and 3 input signals, respectively. The bending moments at the layer interface increased by 78%, 72% and 66%, respectively for each input signals.

These increases in the bending moments can result from different reasons. The first reason is increase in the flexural rigidity. Pile with a larger diameter has greater flexural rigidity. This increased flexural rigidity means that pile resists bending more effectively, potentially leading to higher bending moments. The second reason is increased interaction area between the pile and soil. A larger diameter pile has a greater contact area with the soil. This greater contact area results in greater soil-pile interaction forces which also lead to increase in bending moments.

In summary, the pile diameter has a direct and significant influence on the kinematic bending moments acting on a pile. Larger diameters generally lead to higher bending moments due to increased flexural rigidity and greater soil-pile interaction forces. This relationship should be carefully considered in the context of overall pile design to ensure structural integrity and safety against seismic effects.

5.1.3. Normalized Bending Moments

In addition to bending moment diagrams, normalized bending moment diagrams were generated to be able to see the difference when the effects of the material stiffness (E), geometric properties (inertia) and spacing on the bending moments were excluded. For a straightforward comparison of bending moments across different piled foundation systems, regardless of variations in material properties, cross-sectional geometry, or spacing, bending moments were normalized as $\dfrac{M \times s}{EI}$.

where;

M: Bending moment (kNm)

s: Pile spacing (m)

EI: Flexural rigidity (kNm^2)

Normalized bending moment diagrams for each soil profile and each pile diameter are presented in Figure 5.7 through Figure 5.9.
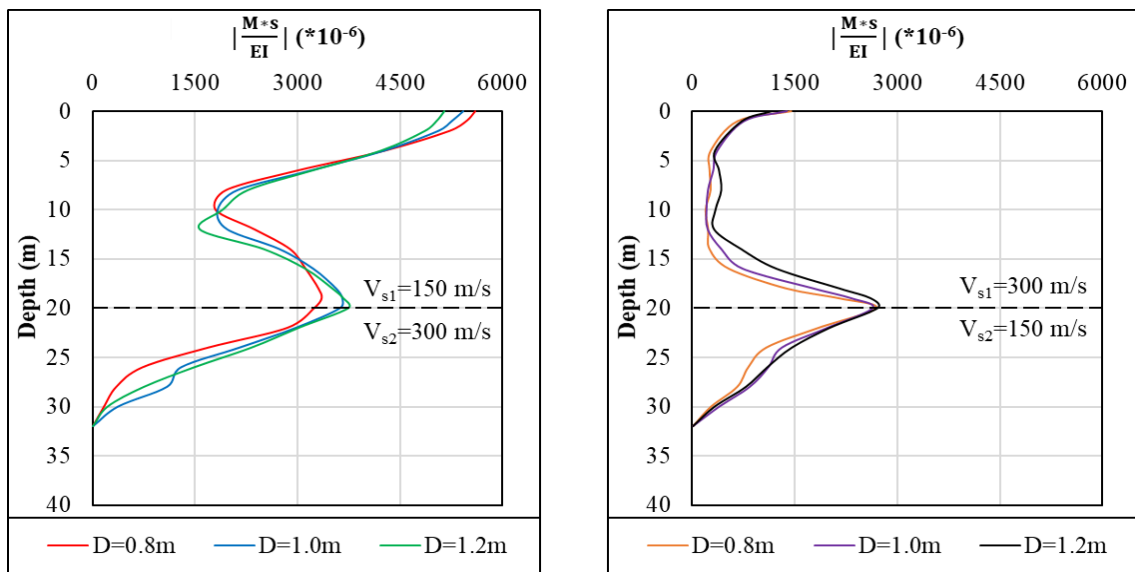
Figure 5.7. Normalized bending moment diagrams (earthquake-1)
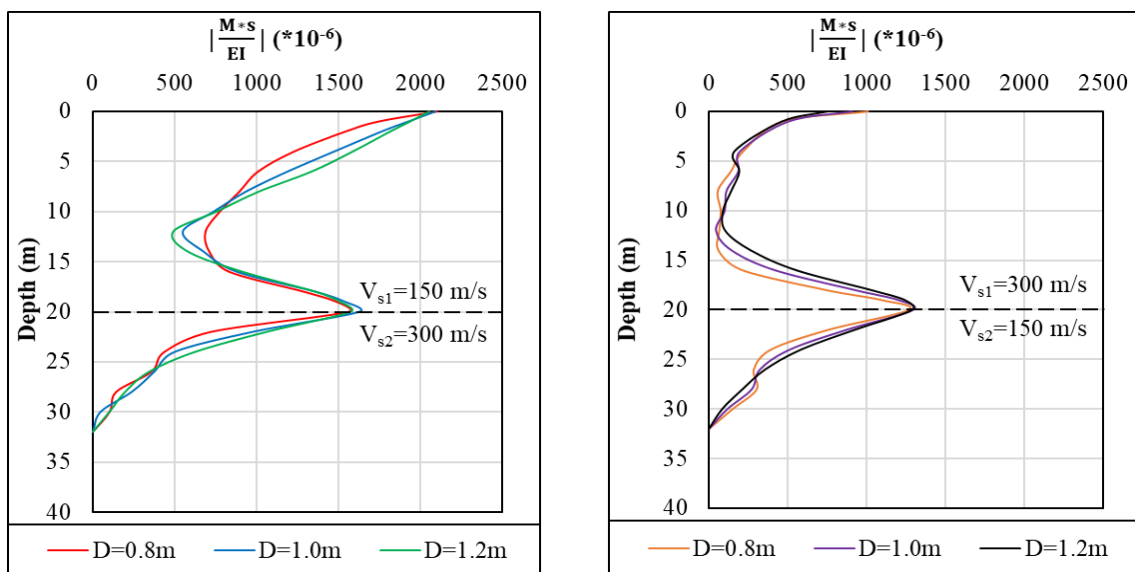
Figure 5.8. Normalized bending moment diagrams (earthquake-2)
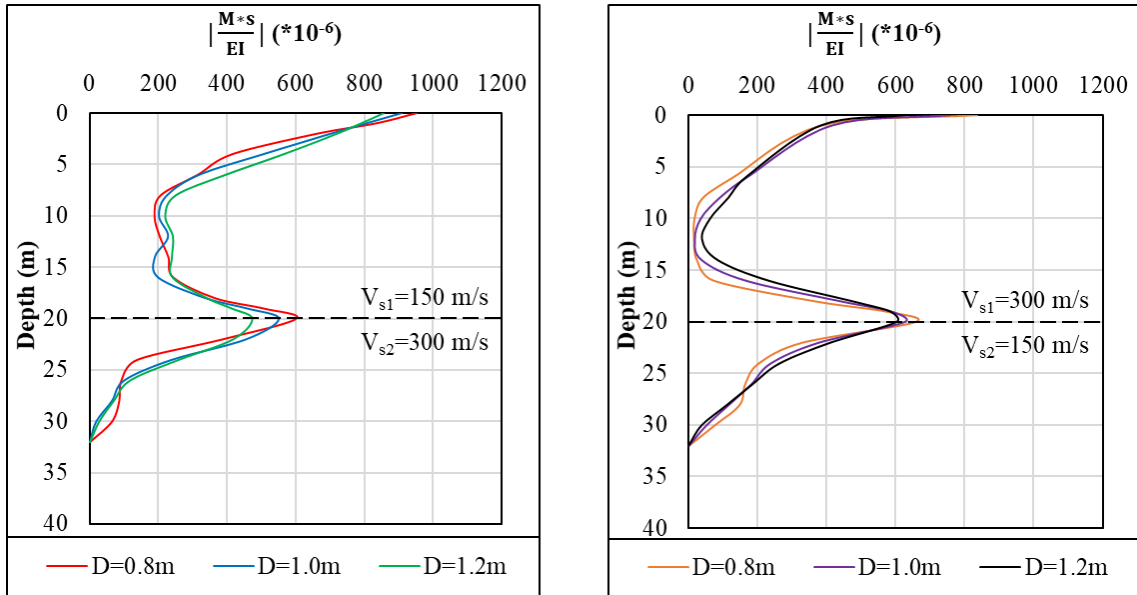
Figure 5.9. Normalized bending moment diagrams (earthquake-3)

According to normalized bending moment diagrams provided above, it can be said that normalized bending moments did not change significantly for different pile diameters in each soil profiles. The magnitudes were quite similar when the effects of the material stiffness (E), geometric properties (inertia) and spacing were excluded.

5.1.4. Shear Forces

The shear force diagrams for each soil profile and each pile diameter are presented in Figure 5.10 through Figure 5.12.

Figure 5.10. Influence of the pile diameter on the shear forces (earthquake-1)

Figure 5.11. Influence of the pile diameter on the shear forces (earthquake-2)

Figure 5.12. Influence of the pile diameter on the shear forces (earthquake-3)

As can be seen in the graphs presented above, in the first soil profile, whose upper layer is loose sand (V_{s1} = 150 m/s), the shear force distribution on the piles showed different behavior for each input signal. During earthquake-1, the peak values of the shear forces were obtained at the pile shaft within the loose sand layer or near the layer interface. During earthquake-2, the shear force at the pile head remained almost constant or increased slightly in the loose sand layer and a peak occurred near the layer interface.

During earthquake-3, the shear force has shown a peak at the pile head, slightly decreased in the loose sand layer and then, a peak occurred again near the layer interface.

On the other hand, in the second soil profile, whose upper layer is dense sand (V_{s1} = 300 m/s), the distribution of the shear forces showed similar behavior for each input signal. For all of the input signals, the peak values of the shear forces occurred at the pile head and near the layer interface.

Moreover, it was observed that the shear forces at the pile head started to exceed the shear force at the layer interface with decreasing earthquake PGA in both soil profiles. This situation can be considered due to less kinematic interaction at the layer interface, with decreasing earthquake PGA.

The variations in the distribution of the shear forces in soil profile having loose sand at the top can be considered due to the variations of the displacement distributions in the loose sand layer with different levels of accelerations. Since this layer amplifies the accelerations more than the dense sand layer, variations in the soil displacements are also more in this layer. Sample graphs containing the maximum displacement distributions at different depths of the soil layers for each input signal are presented in Figure 5.13.
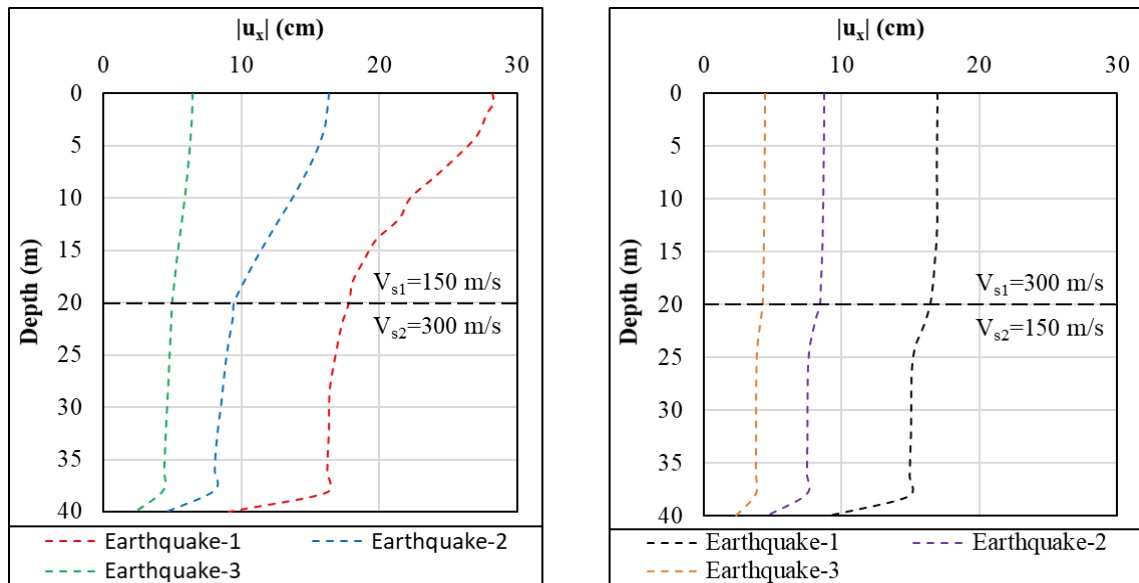
Figure 5.13. Variations of the maximum soil displacements over time domain, at each depth

As can be seen in Figure 5.13, both magnitude and distribution of the soil displacements in the soil profile having loose sand layer at the top (V_{s1} = 150 m/s) vary significantly with different levels of accelerations. Conversely, in the soil profile having dense sand at the top (V_{s1} = 300 m/s), while the magnitudes of the displacements change with different levels of accelerations, distribution of the soil displacements are similar for each input signal.

Based on the analysis results, it can be said that the pile diameter has a significant effect on the shear forces acting on the piles. It was observed that the shear forces increased with increasing pile diameter. Since the distribution of the shear forces varies with the soil profiles and earthquake records, only the maximum values will be compared for the sake of brevity.

In the first soil profile (V_{s1} = 150 m/s, V_{s2} = 300 m/s), between the diameters of 0.8 m and 1.0 m, the maximum shear forces increased by 69%, 69% and 21% for earthquake-1, 2 and 3 input signals, respectively. Between the diameters of 1.0 m and 1.2 m, the maximum shear forces increased by 52%, 46% and 27% for earthquake-1, 2 and 3 input signals, respectively.

In the second soil profile (V_{s1} = 300 m/s, V_{s2} = 150 m/s), between the diameters of 0.8 m and 1.0 m, the maximum shear forces increased by 66%, 41% and 44% for earthquake-1, 2 and 3 input signals, respectively. Between the diameters of 1.0 m and 1.2 m, the maximum shear forces increased by 40%, 20% and 22% for earthquake-1, 2 and 3 input signals, respectively.

These increases in the shear forces can be explained by the increased flexural rigidity and increased interaction forces acting on the pile, as mentioned for the bending moment. These effects should be taken into account in design process.

5.1.5. Normalized Shear Forces

In addition to shear force diagrams, normalized shear force diagrams were generated to be able to see the difference when the effects of the pile cross sectional area on the shear forces were excluded. For this purpose, shear forces were normalized as $\frac{V}{A}$.

where;

V: Shear force (kN)

A: Cross sectional area (m^2)

Normalized shear force diagrams for each soil profile and each pile diameter are presented in Figure 5.14 through Figure 5.16.
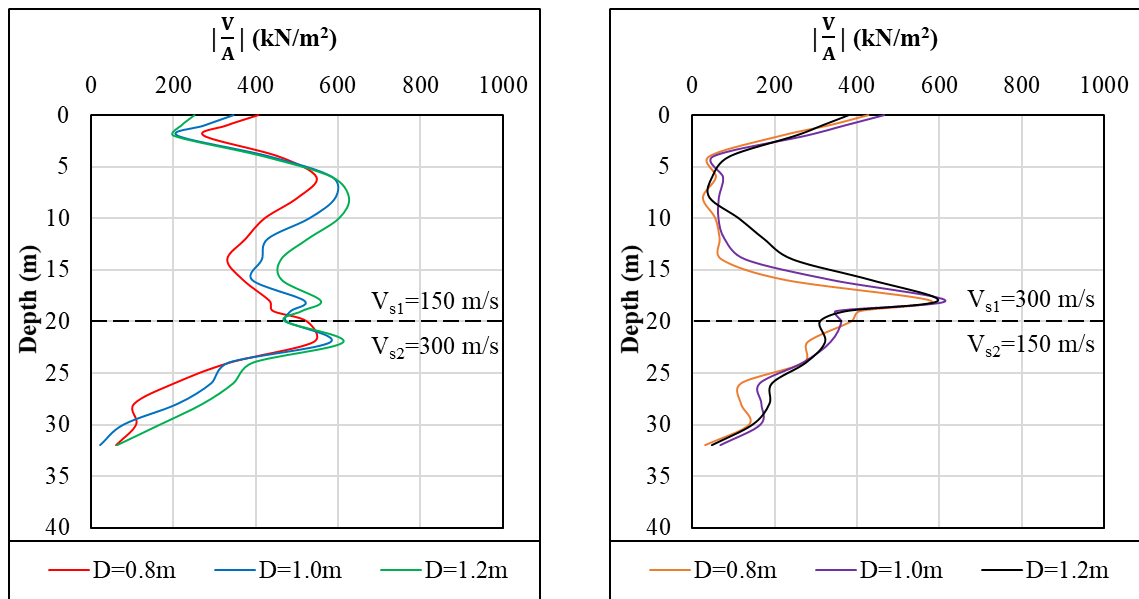
Figure 5.14. Normalized shear force diagrams (earthquake-1)
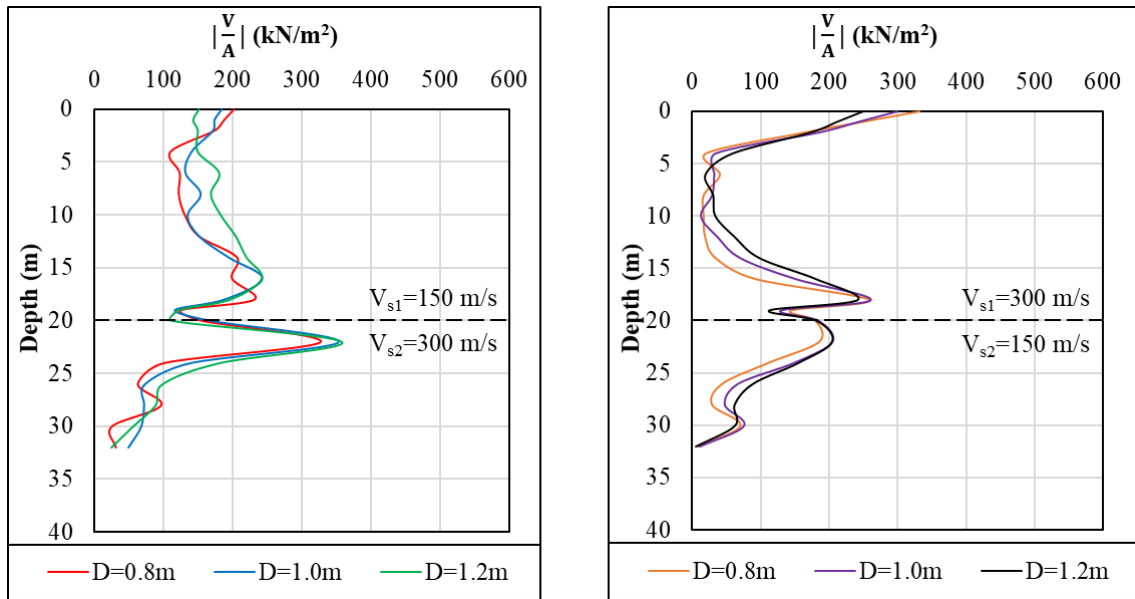
Figure 5.15. Normalized shear force diagrams (earthquake-2)
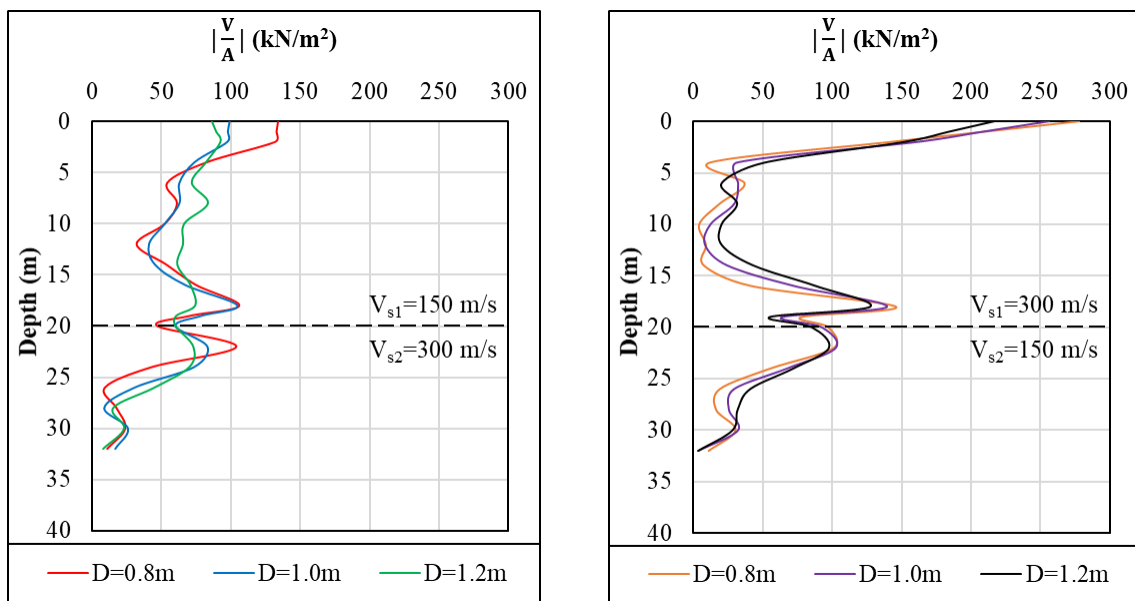
Figure 5.16. Normalized shear force diagrams (earthquake-3)

According to normalized shear force diagrams provided above, it can be said that normalized shear forces did not change significantly for different pile diameters in each soil profiles. The magnitudes were quite similar when the effects of pile cross sectional area were excluded.

5.2. Influence of the Pile Spacing

To examine the influence of the pile spacing, eighteen analyses were performed for earthquake-1 and six analyses were performed for both of the earthquake-2 and 3. In two different soil profiles, piles with three different pile spacings (3D, 4D and 6D) were analyzed. For the first input signal (earthquake-1), these analyses were carried out for three different pile diameters (0.8 m, 1.0 m and 1.2 m) by keeping the pile length constant at 32.0 m. Besides, for the other two input signals, pile diameter was also kept constant at 1.0 m, as well as the pile length (32.0 m). The results of these analyses are presented in the following sections.

5.2.1. Accelerations

The graphs containing the accelerations in the soil layers are presented in Figure 5.17 through Figure 5.21. The accelerations in the free field analyses and kinematic interaction analyses are presented together for each soil profile.
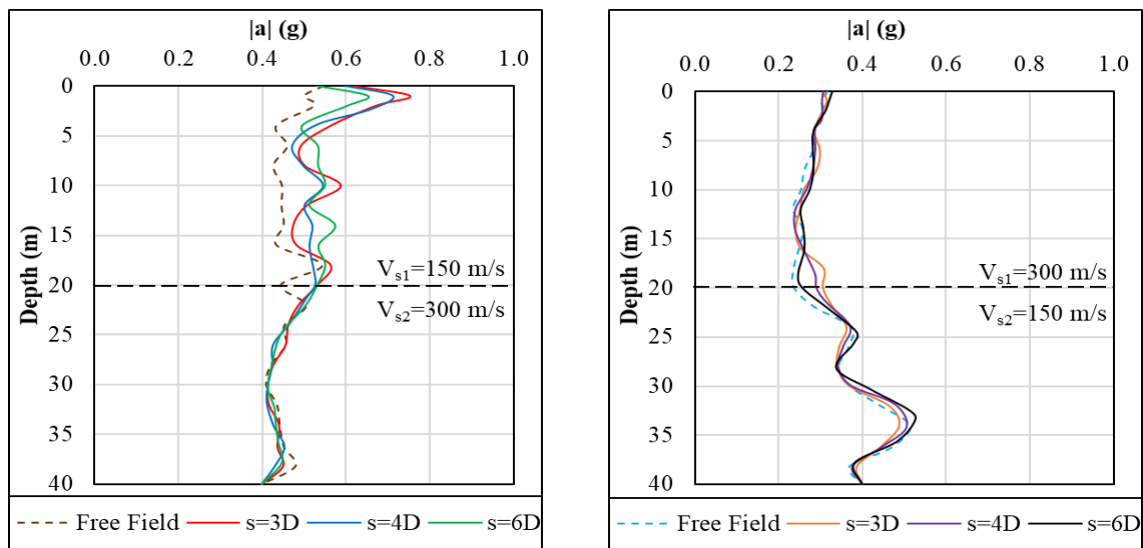
Figure 5.17. Influence of the pile spacing on the soil accelerations (earthquake-1, D = 0.8 m)
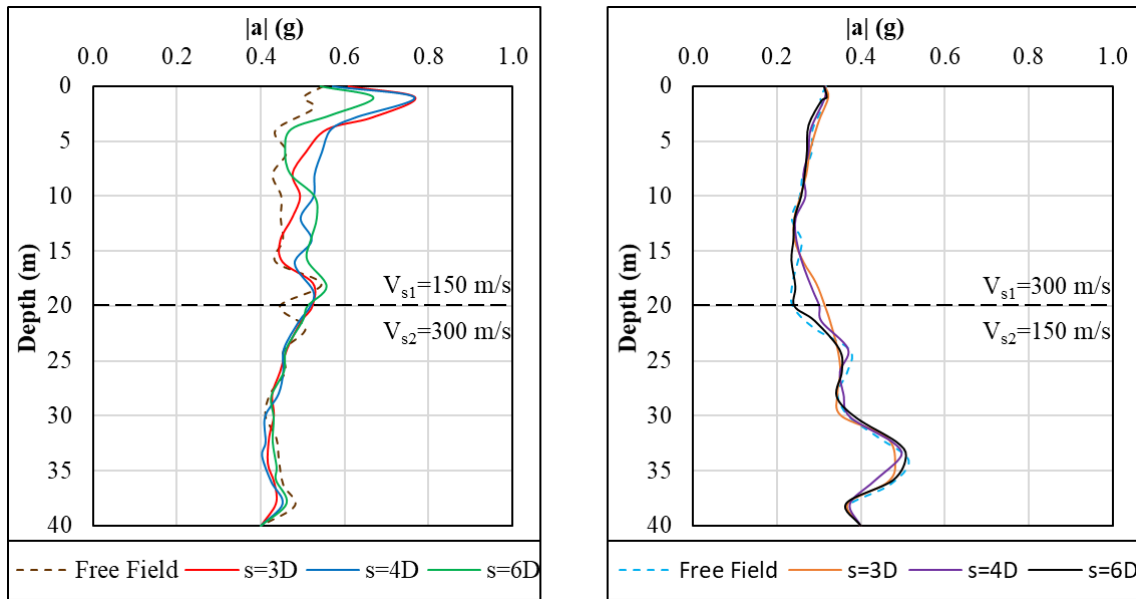
Figure 5.18. Influence of the pile spacing on the soil accelerations (earthquake-1, D = 1.0 m)
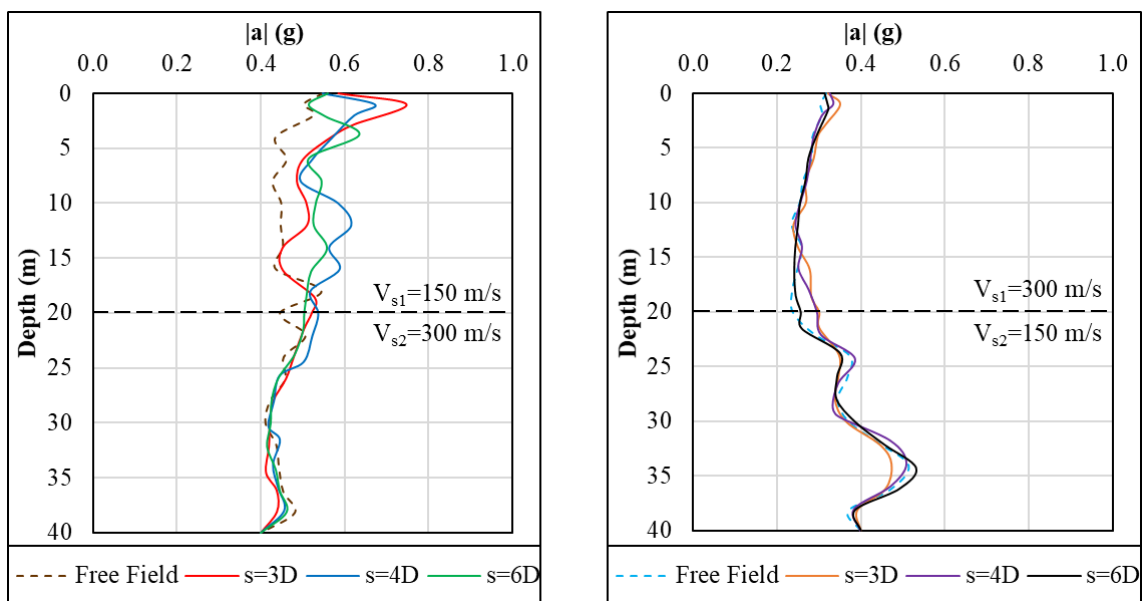
Figure 5.19. Influence of the pile spacing on the soil accelerations (earthquake-1, D = 1.2 m)
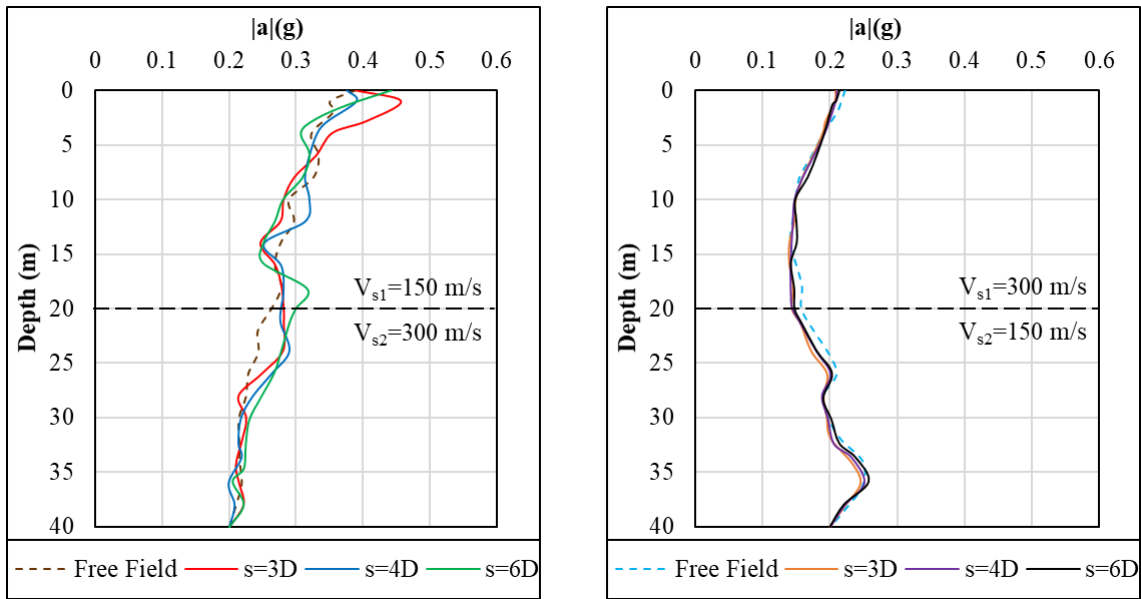
Figure 5.20. Influence of the pile spacing on the soil accelerations (earthquake-2)
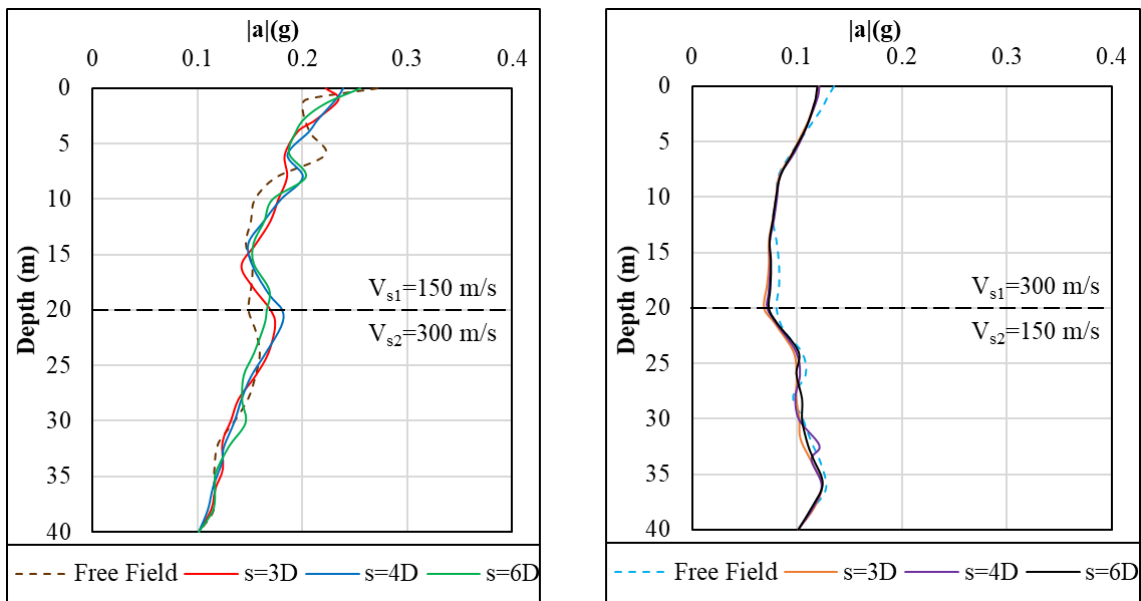
Figure 5.21. Influence of the pile spacing on the soil accelerations (earthquake-3)

According to the graphs presented above, the soil accelerations in the kinematic analyses did not change significantly with increasing pile spacing, there were only little fluctuations.

In the analyses with Earthquake-1 and Earthquake-2 input signals: It was observed that for the soil profile having loose sand layer at the top (V_{s1} = 150 m/s), in the kinematic analyses, the accelerations near the pile head were found to be greater than the accelerations at the same depths in the free field analysis. The reasons for this situation were explained in Section 5.1.1.

In the analyses with Earthquake-3 input signals: Accelerations in the kinematic analyses and free field analysis showed a good agreement except little fluctuations for all analysis cases. Since this input signal has a smaller PGA than the other input signals, the effects of kinematic interaction were also smaller.

5.2.2. Bending Moments

The bending moment diagrams for each soil profile and each pile spacing are presented in Figure 5.22 through Figure 5.26.
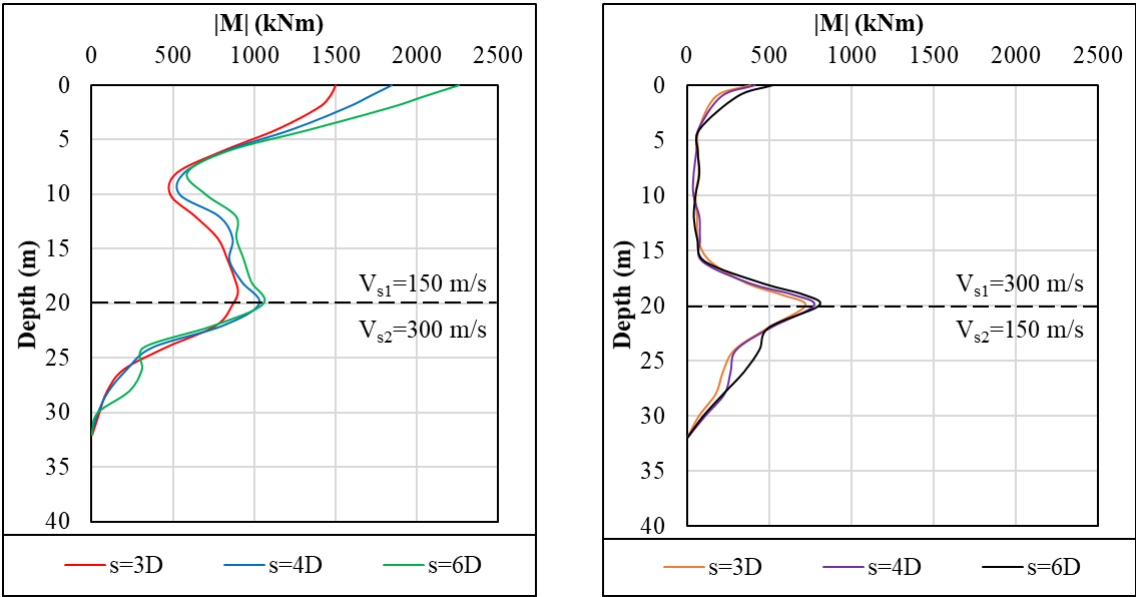
Figure 5.22. Influence of the pile spacing on the bending moments (earthquake-1, D = 0.8 m)
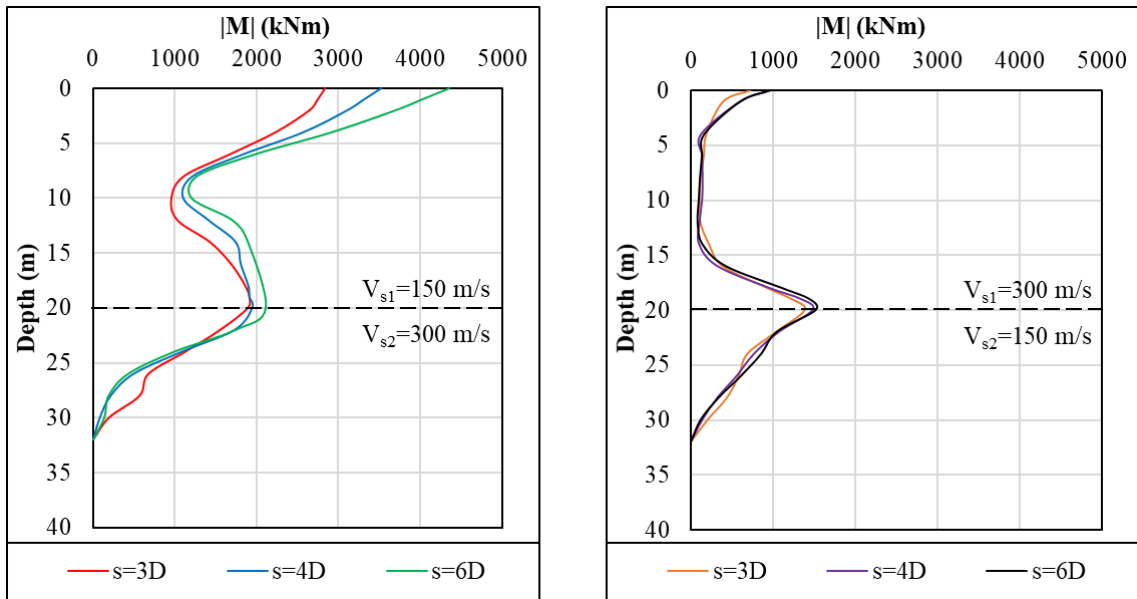
Figure 5.23. Influence of the pile spacing on the bending moments (earthquake-1, D = 1.0 m)
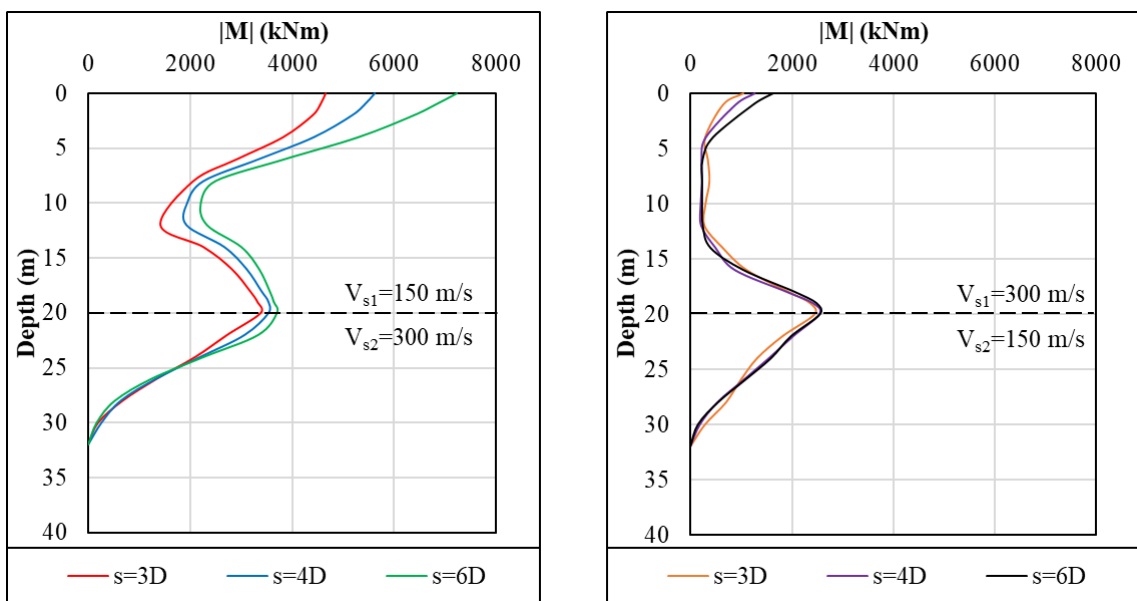
Figure 5.24. Influence of the pile spacing on the bending moments (earthquake-1, D = 1.2 m)
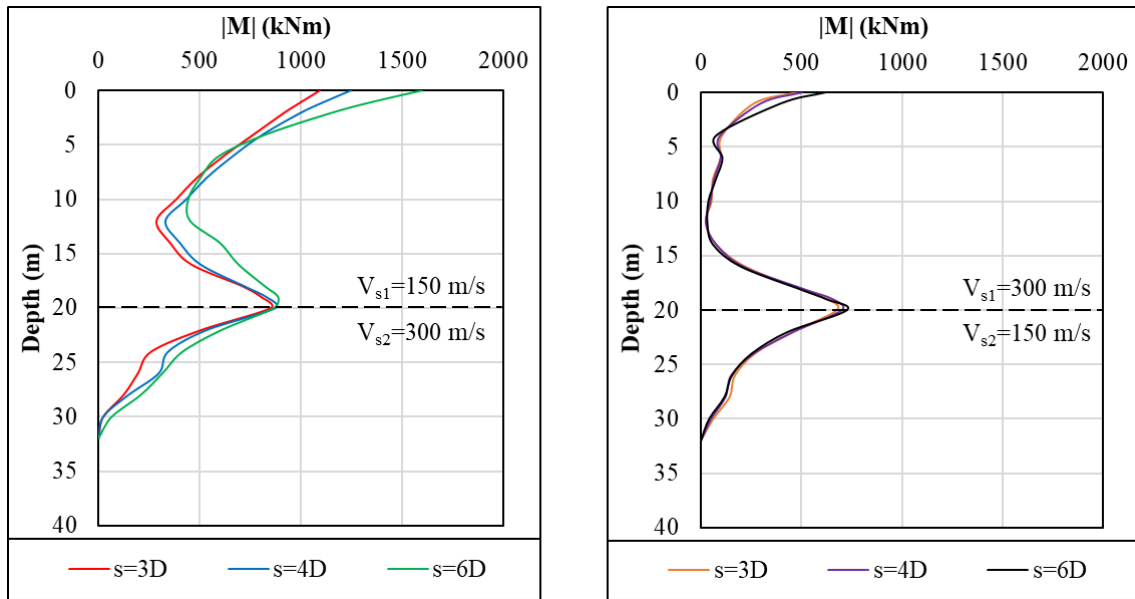
Figure 5.25. Influence of the pile spacing on the bending moments (earthquake-2)
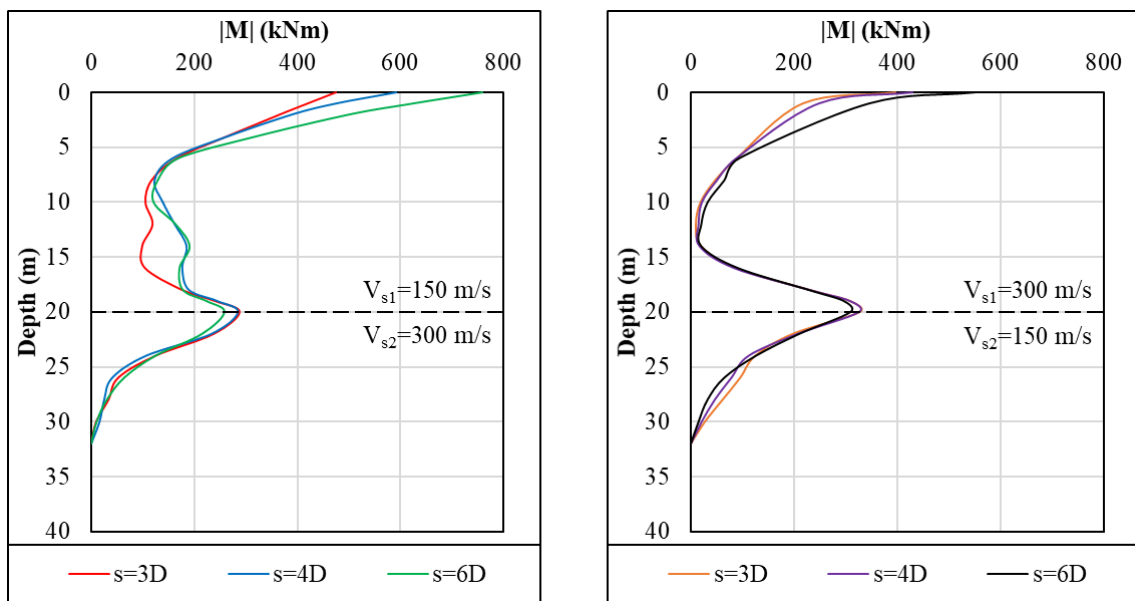
Figure 5.26. Influence of the pile spacing on the bending moments (earthquake-3)

According to the bending moment diagrams provided above, it was observed that the bending moments acting on the pile increased as the pile spacing increased. However, the influence of the pile spacing is not as significant as the pile diameter.

90

In both soil profiles, the bending moments at the pile head generally increased by an average rate of almost 20% between the spacings of 3D-4D and 4D-6D for all input signals. Additionally, the rate of increase of bending moments at the layer interfaces is generally negligible, i.e., less than 10%. The increase in the bending moments can be attributed to the increased interaction between the soils and piles, as a result of the increase in soil volume affecting each pile.

5.2.3. Shear Forces

The shear force diagrams for each soil profile and each pile spacing are presented in the Figure 5.27 through Figure 5.31.
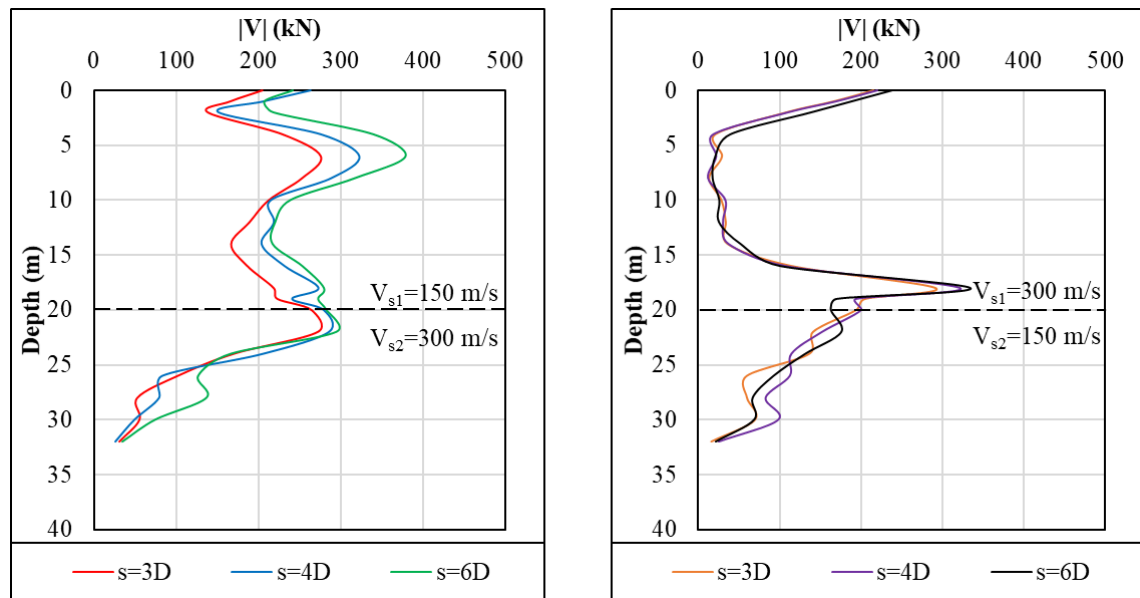
Figure 5.27. Influence of the pile spacing on the shear forces (earthquake-1, D = 0.8 m)
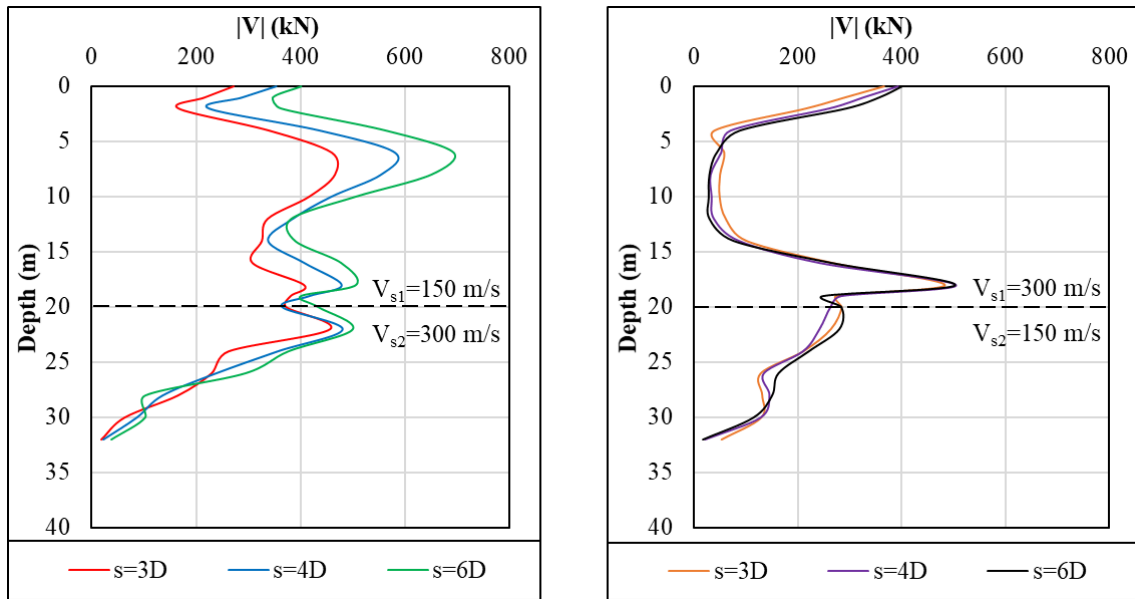
Figure 5.28. Influence of the pile spacing on the shear forces (earthquake-1, D = 1.0 m)
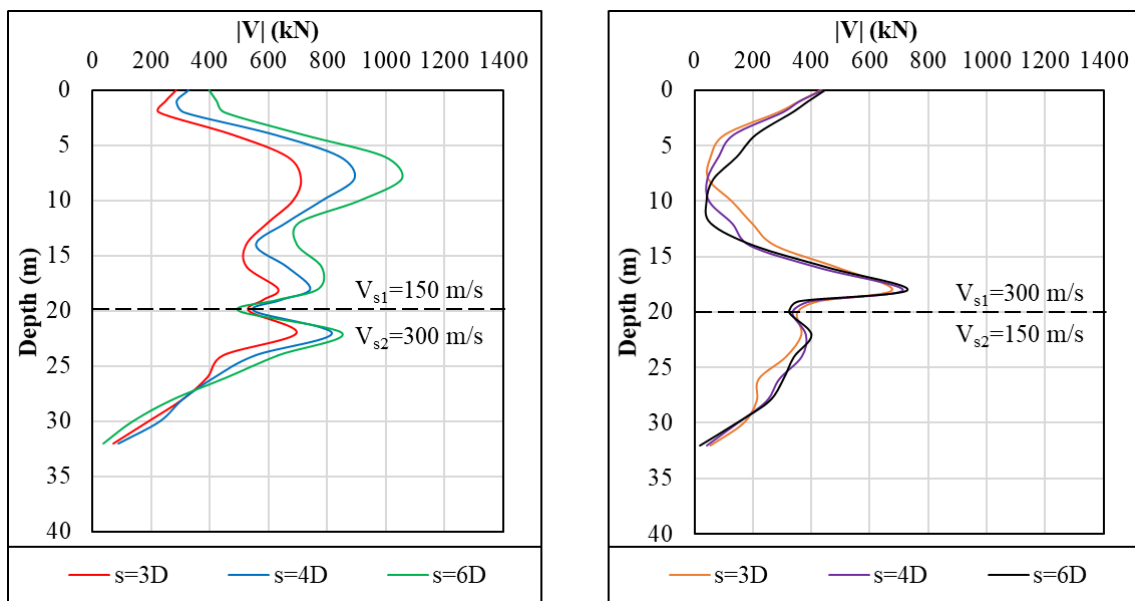
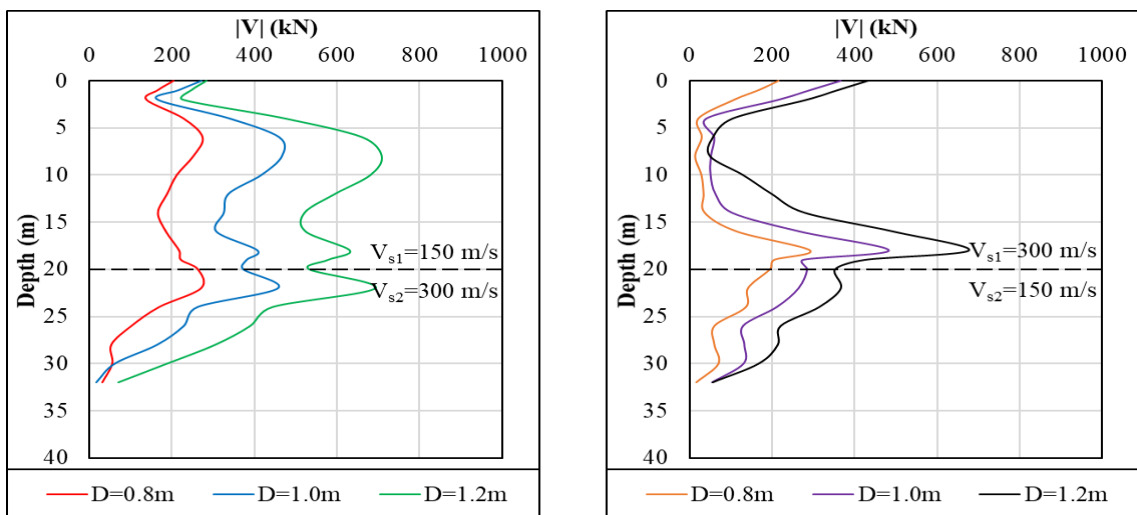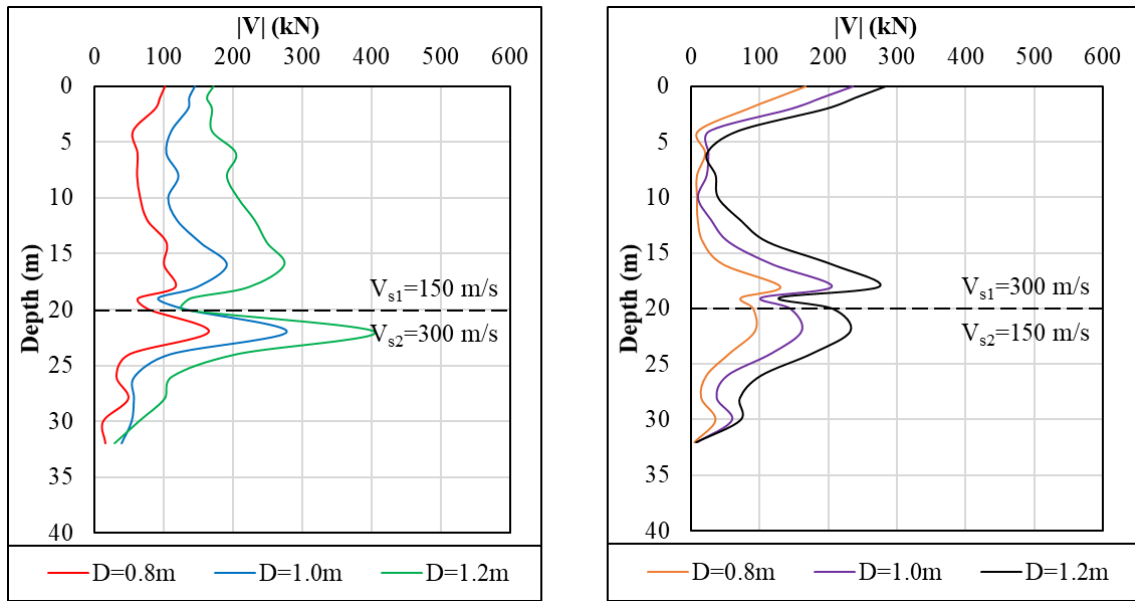Figure 5.29. Influence of the pile spacing on the shear forces (earthquake-1, D = 1.2 m)
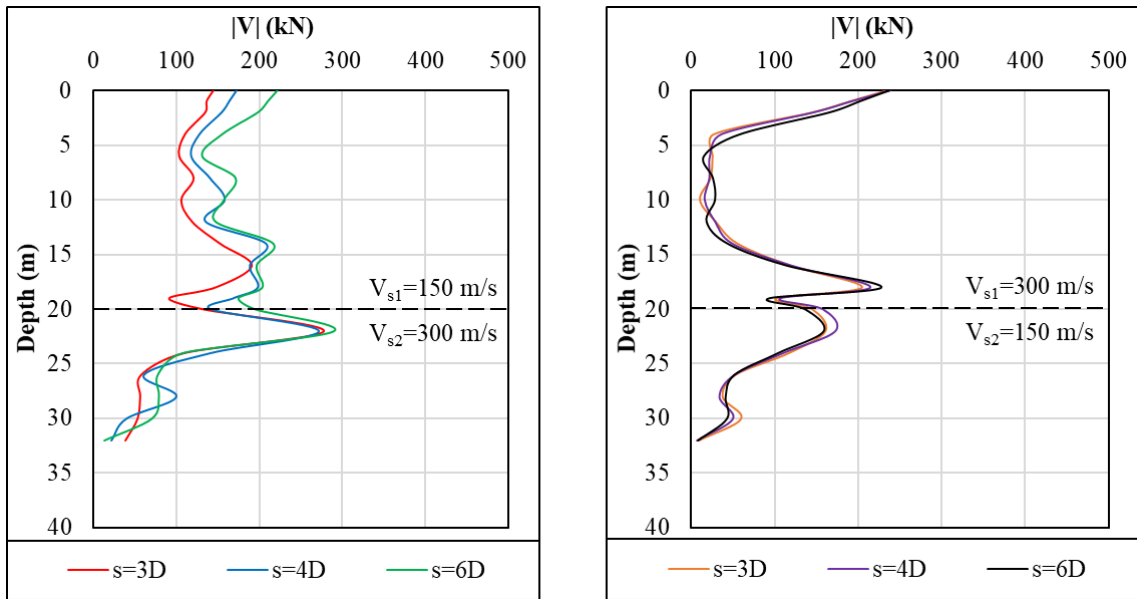
Figure 5.30. Influence of the pile spacing on the shear forces (earthquake-2)

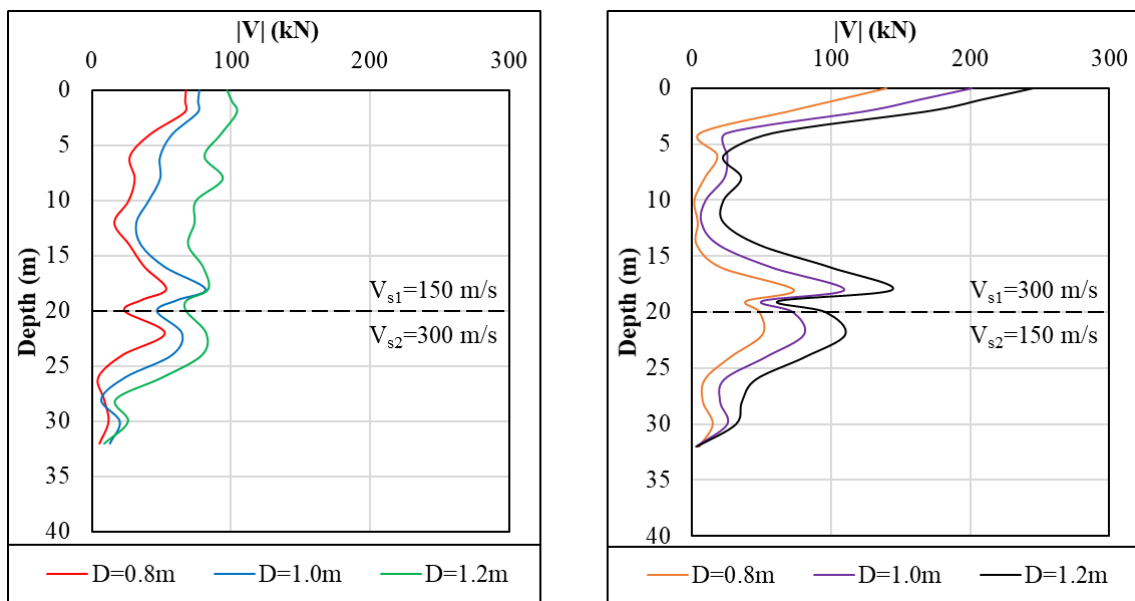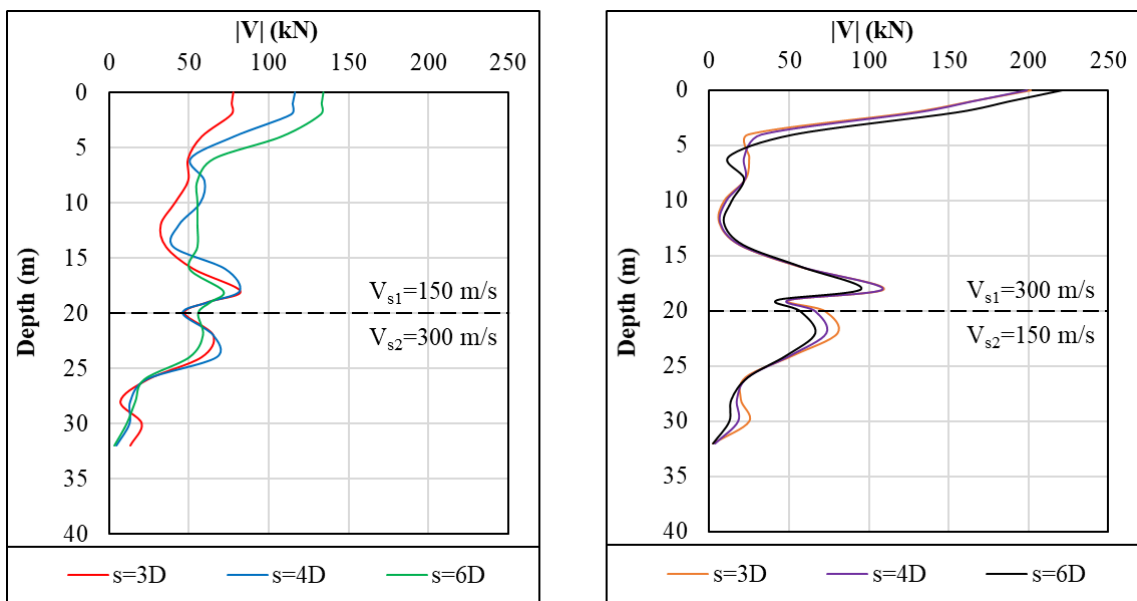Figure 5.31. Influence of the pile spacing on the shear forces (earthquake-3)

According to the shear force diagrams provided above, it has been observed that the shear force acting on the pile generally increased as the pile spacing increased. However, the influence of the pile spacing on the shear forces is not as significant as the pile diameter.

Since the distribution of the shear forces varies with the soil profiles and earthquake records, the maximum values will be compared for the sake of brevity. In the first soil profile (V_{s1} = 150 m/s, V_{s2} = 300 m/s), the maximum shear forces generally increased by an average rate of 20% between the spacings of 3D-4D and 4D-6D for all input signals. In the second soil profile (V_{s1} = 300 m/s, V_{s2} = 150 m/s), the rate of increase of the maximum shear forces is generally negligible, i.e., less than 10% for all input signals. The increase in the shear forces can also be attributed to the increased interaction between the soil and piles, resulted from the increase in the soil volume surrounding the piles.

5.3. Influence of the Pile Length

Since the kinematic analyses require too much time and computer memory, the primary aim of this study is to provide a sample guide for designers to be able to make predictions about the effects of pile length on the design processes of large-scale projects. To achieve this goal, detailed analyses were performed. To investigate the influence of the pile diameter: 30, 25 and 20 analyses were performed for the input signals of earthquake-1, 2 and 3 respectively. The piles with varying lengths between 10.0-32.0 m were analyzed in different layered soil profiles. In all of the analysis cases, the diameters and spacings of the piles were kept constant as 1.0 m and 3D, respectively. The results of the aforementioned analysis cases are presented in the following sections. For the sake of clarity, the results of the analyses were presented separately for each input signal due to the presence of distinct analysis cases in each input signal.

5.3.1. Earthquake-1

For the first input signal (earthquake-1), 30 analyses were performed to investigate the influence of the pile length on the analysis results. Layered soil profiles composed of loose sand (V_s = 150 m/s) and dense sand (V_s = 300 m/s) layers were used in two different combinations. In these soil profiles, piles with both varying and constant embedment length into the bottom layer were analyzed. For the case of varying pile embedment length into the bottom layer, ten different pile lengths ranging from 10.0 to 32.0 m were analyzed in the soil layers having an identical thickness of 20.0 m (H_1 = H_2 = 20.0 m). For the case of piles with constant 3.0 m embedment length into the bottom layer, five different pile

lengths varying between 18.0 – 32.0 m were used and the layer thicknesses were determined according to the pile length ($H_1 = (L - 3)$ m, $H_2 = (40 – H_1)$ m).

5.3.1.1. Accelerations

The graphs containing the accelerations in the soil layers are presented in Figure 5.32 and Figure 5.33. The accelerations in the free field analyses and kinematic interaction analyses are presented together for each soil profile.
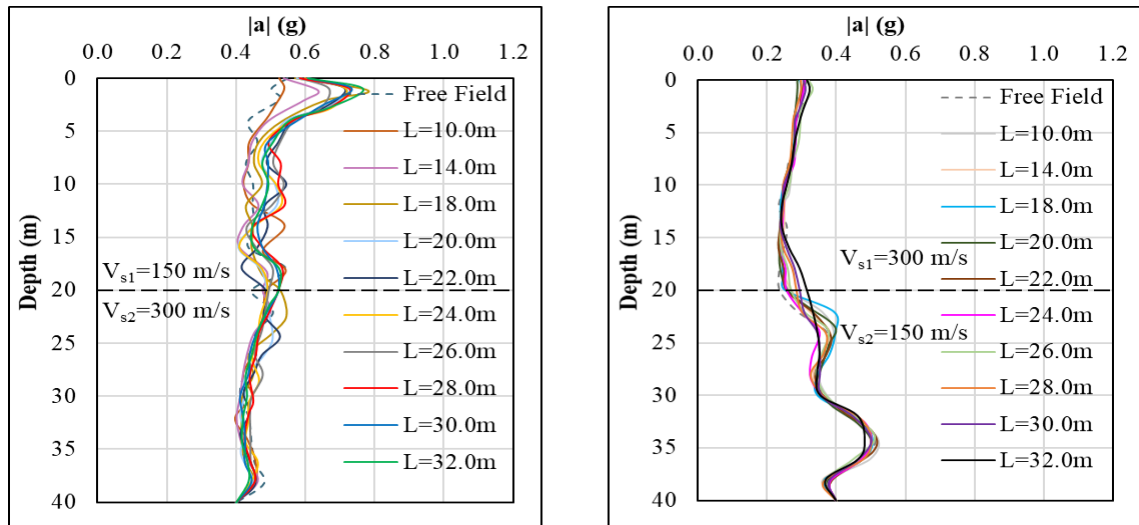
Figure 5.32. Influence of the pile length on the accelerations (varying pile embedment length into the bottom layer)
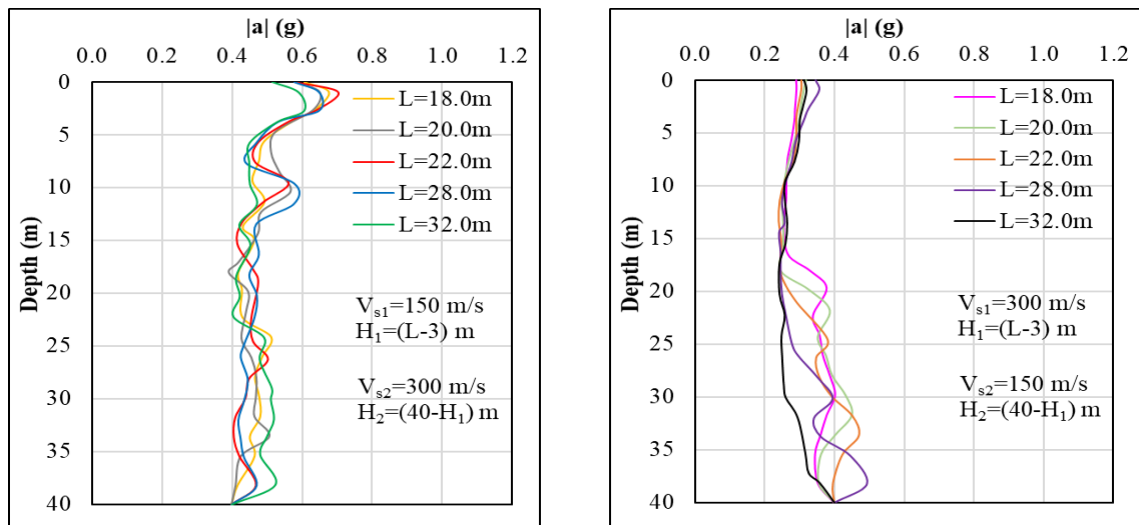
Figure 5.33. Influence of the pile length on the accelerations (constant 3.0 m pile embedment length into the bottom layer)

As can be seen in the acceleration graphs, the soil accelerations in the kinematic analyses did not change significantly with increasing pile length, there were only little fluctuations.

It can be stated that for the soil profiles having loose sand layer at the top (V_{s1} = 150 m/s), in the kinematic analyses, the accelerations near the pile head were found to be greater than the accelerations at the same depths in the free field analysis. The reasons for this situation were explained in Section 5.1.1.

Furthermore, it can be said that the fluctuations in the acceleration values were a bit more in the bottom layers of both soil profiles in the case of constant 3.0 m pile embedment length. This situation resulted from the changes in the thicknesses of soil layers.

5.3.1.2. Bending Moments

The bending moment diagrams for each soil profile and each pile length are presented in Figure 5.34 and Figure 5.35.

Figure 5.34. Influence of the pile length on the bending moments (varying pile embedment length into the bottom layer)
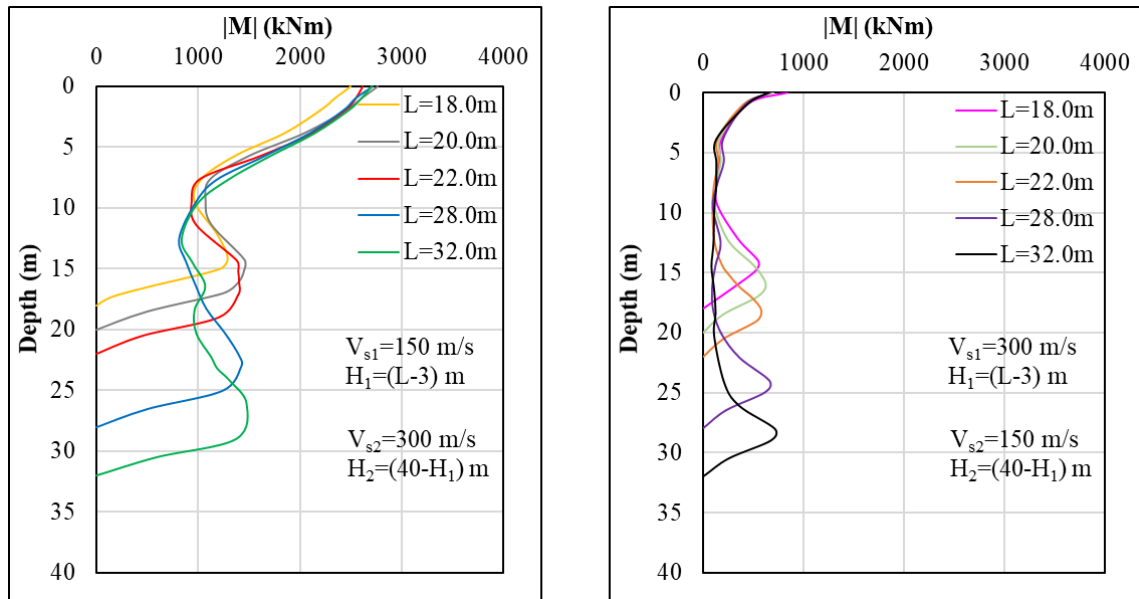
Figure 5.35. Influence of the pile length on the bending moments (constant 3 m pile embedment length into the bottom layer)

The interpretations of the analysis results for different analysis cases are presented in the following paragraphs.

Varying pile embedment length into the bottom layer: It was observed that the bending moments at the pile head and layer interface increased up to a certain pile length and then, remained almost constant. In the first soil profile (V_{s1} = 150 m/s, V_{s2} = 300 m/s), a small decrease was observed in the pile head bending moments of piles with length of 24.0 m. This is most probably due to a numerical error. The variations in the bending moments at the pile head and layer interface for each pile length can be seen more clearly in Figure 5.36.

Figure 5.36. Bending moment variations at the pile head and layer interface for each pile length (a) $V_{s1} = 150$ m/s, $V_{s2} = 300$ m/s, b) $V_{s1} = 300$ m/s, $V_{s2} = 150$ m/s)

For the first soil profile ($V_{s1} = 150$ m/s, $V_{s2} = 300$ m/s), it can be stated that the increases in the bending moments at the pile head and layer interface are negligible (i.e., less than 10%) after 2D and 6D embedment lengths into the bottom layer, respectively. If the design is performed according to maximum bending moments, it can be stated that performing analyses up to 2D embedment length is sufficient for this soil profile. On the other hand, if the local increases in the bending moment along the pile length is also considered in the design for reinforcements, it can be said that the bending moments along the pile remains almost constant after 6D embedment length.

For the second soil profile ($V_{s1} = 300$ m/s, $V_{s2} = 150$ m/s), it can be said that the increase in the bending moments at the pile head is negligible (i.e., less than 10%) after 18.0 m pile length. On the other hand, the increase in the bending moments at layer interface is negligible after 8D embedment length into the bottom layer. Since the maximum bending moments occurred at the layer interface, it can be said that the bending moments along the pile remains almost constant after 8D embedment length for this soil profile.

Constant 3.0 m pile embedment length into the bottom layer: For the case of constant 3.0 m embedment length into the bottom layer, while the bending moments near the layer interface generally showed slight increases (i.e., less than 10%) with the increasing pile length for both of the soil profiles, the bending moments at the pile head remained almost constant.

5.3.1.3. Shear Forces

The shear force diagrams for each soil profile and each pile length are presented in Figure 5.37 and Figure 5.38.

Figure 5.37. Influence of the pile length on the shear forces (varying pile embedment length into the bottom layer)
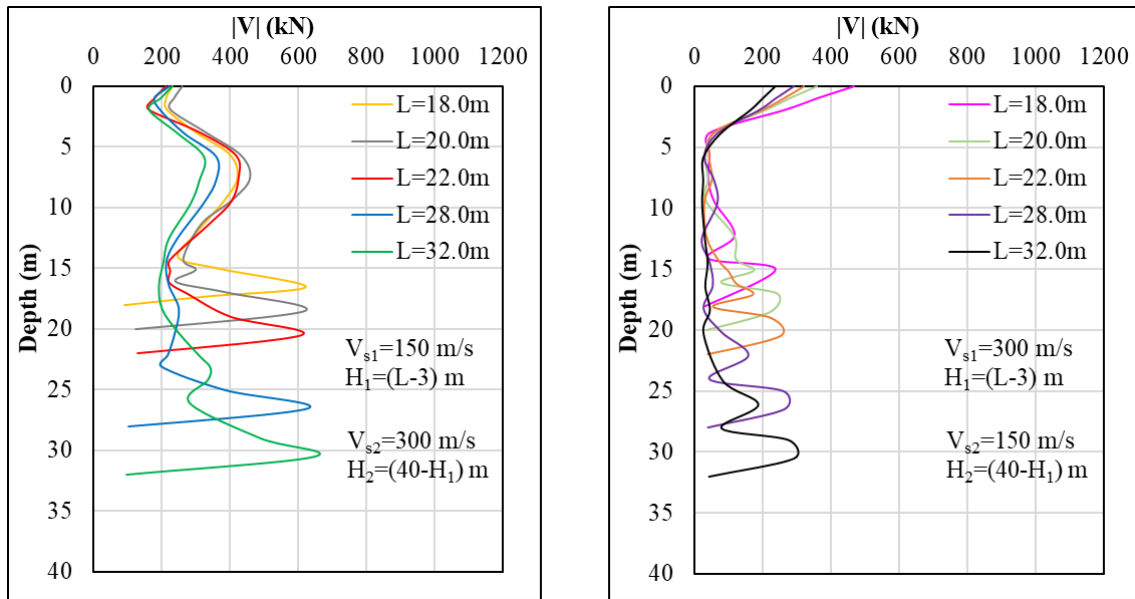
Figure 5.38. Influence of the pile length on the shear forces (constant 3 m pile embedment length into the bottom layer)

The interpretations of the analysis results for different analysis cases are presented in the following paragraphs.

Varying pile embedment length into the bottom layer: The variations in the maximum shear forces, shear forces at the pile head and shear forces at the layer interface can be seen more clearly in Figure 5.39.
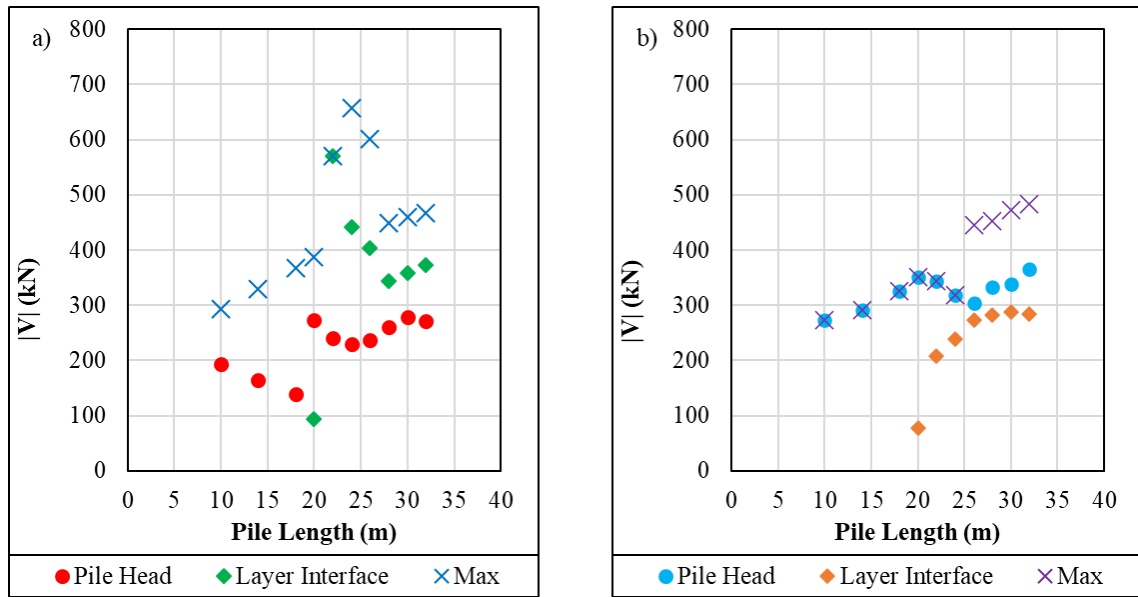
Figure 5.39. Variations of maximum shear forces and shear forces at the pile head and layer interface for each pile length (a) V_{s1} = 150 m/s, V_{s2} = 300 m/s, b) V_{s1} = 300 m/s, V_{s2} = 150 m/s)

In the first soil profile (V_{s1} = 150 m/s, V_{s2} = 300 m/s), the shear forces at the pile head decreased with increasing pile length until 18.0 m pile length. When the pile reached the layer interface (20.0 m pile length), the shear forces at the pile head showed a sudden increase and remained almost constant after this length, except little fluctuations. The shear forces at the layer interface showed a dramatic increase when the pile started to be embedded into the bottom layer. Then, decreased with the increasing pile length up to 8D embedment length and remained almost constant after this embedment length. Furthermore, the maximum shear forces generally increased with increasing pile length, especially after the pile started to be embedded into the bottom layer and then, decreased with the increasing pile length up to 8D embedment length and remained almost constant after this embedment length. To sum up, although the shear forces did not show a uniform increase or decrease with increasing pile length, it can be said that the fluctuations in the shear force values are negligible after 8D embedment length.

In the second soil profile ($V_{s1} = 300$ m/s, $V_{s2} = 150$ m/s), the shear forces at the pile head increased with increasing pile length until the pile reached the layer interface (20.0 m pile length). After this length, they slightly decreased with increasing shear force at the layer interface and then, showed slight increases. In spite of the fluctuations, it can be said that the shear forces at the pile head did not change significantly after 20.0 m pile length. Furthermore, the maximum shear forces generally increased with increasing pile length until the pile reached the layer interface (20.0 m pile length). After this length, they slightly decreased with increasing shear force at the layer interface and showed an immediate increase in 26.0 m pile length. After this length, both the maximum shear forces and the shear forces at layer interface did not change significantly. To sum up, although the shear forces did not show a uniform increase or decrease with increasing pile length, it can be said that the fluctuations in the shear force values are negligible after 6D embedment length.

Layered soil profiles and constant 3 m pile embedment length into the bottom layer:
For the case of constant 3 m embedment length into the bottom layer, the shear forces near the layer interface slightly increased with increasing pile length. On the other hand, it was observed that while the shear forces at the pile head did not change significantly in the first soil profile ($V_{s1} = 150$ m/s, $V_{s2} = 300$ m/s), they decreased with increasing pile length in the second soil profile ($V_{s1} = 300$ m/s, $V_{s2} = 150$ m/s).

5.3.2. Earthquake-2

For the second input signal (earthquake-2), twenty-five analyses were performed in three different layered soil profiles. In these soil profiles, loose sand ($V_s = 150$ m/s), dense sand ($V_s = 300$ m/s) and rock ($V_s = 760$ m/s) layers were used in different combinations. In these soil profiles, twelve different pile length ranging from 10.0 to 32.0 m were analyzed in the soil layers having an identical thickness of 20.0 m. The results of these analyses are presented in the following sections.

5.3.2.1. Accelerations

The graphs containing the accelerations in the soil layers are presented in Figure 5.40. The accelerations in the free field analyses and kinematic interaction analyses are presented together for each soil profile.
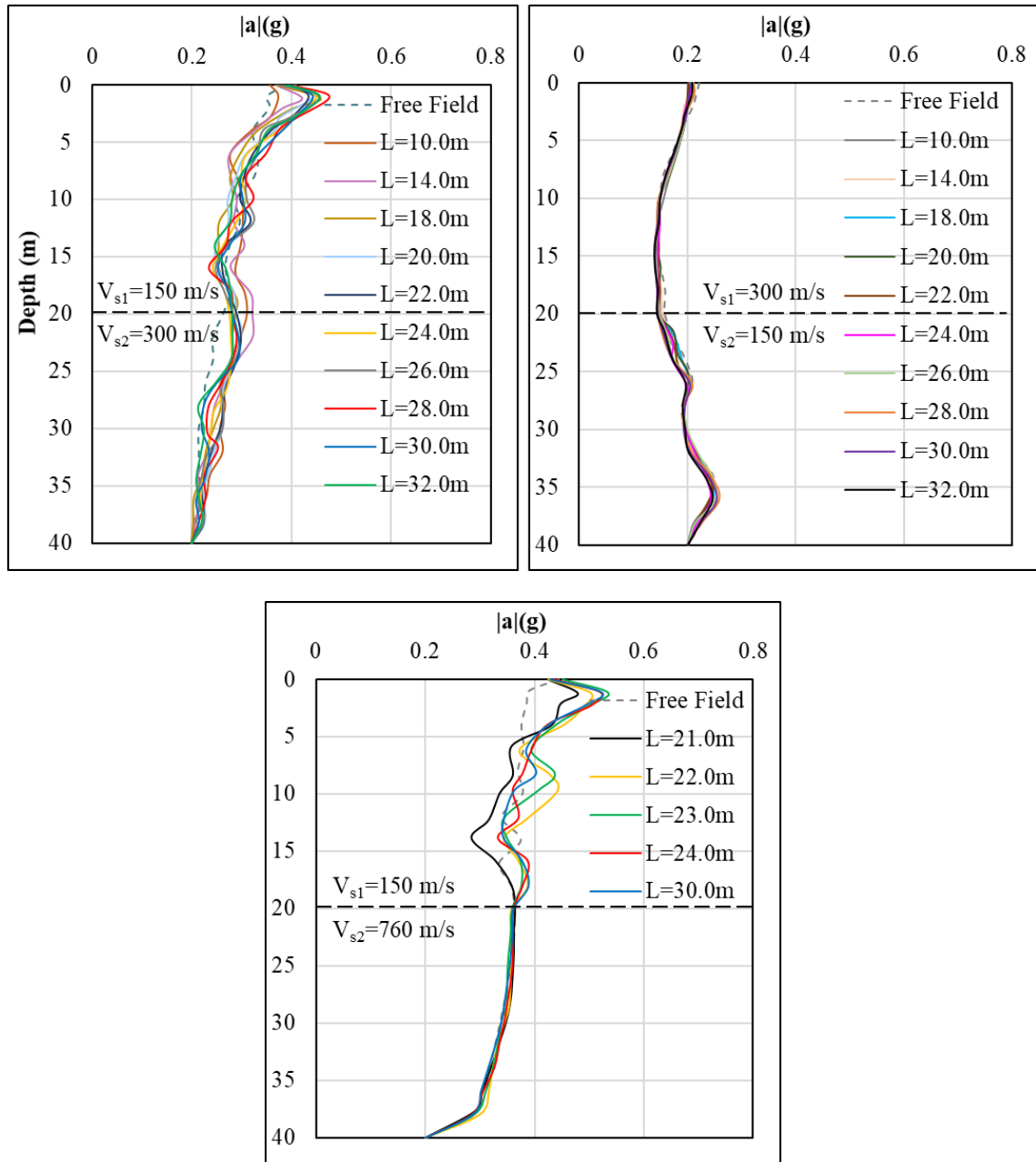
Figure 5.40. Influence of the pile length on the accelerations

As can be seen in the acceleration graphs, the soil accelerations in the kinematic analyses did not change significantly with increasing pile length, there were only little fluctuations.

103

Moreover, it can be stated that for the soil profiles having loose sand layer at the top (V_{s1} = 150 m/s), in the kinematic analyses, the accelerations near the pile head were found to be greater than the accelerations at the same depths in the free field analysis. The reasons for this situation were explained in Section 5.1.1.

5.3.2.2. Bending Moments

The bending moment diagrams for each soil profile and each pile length are presented in Figure 5.41.
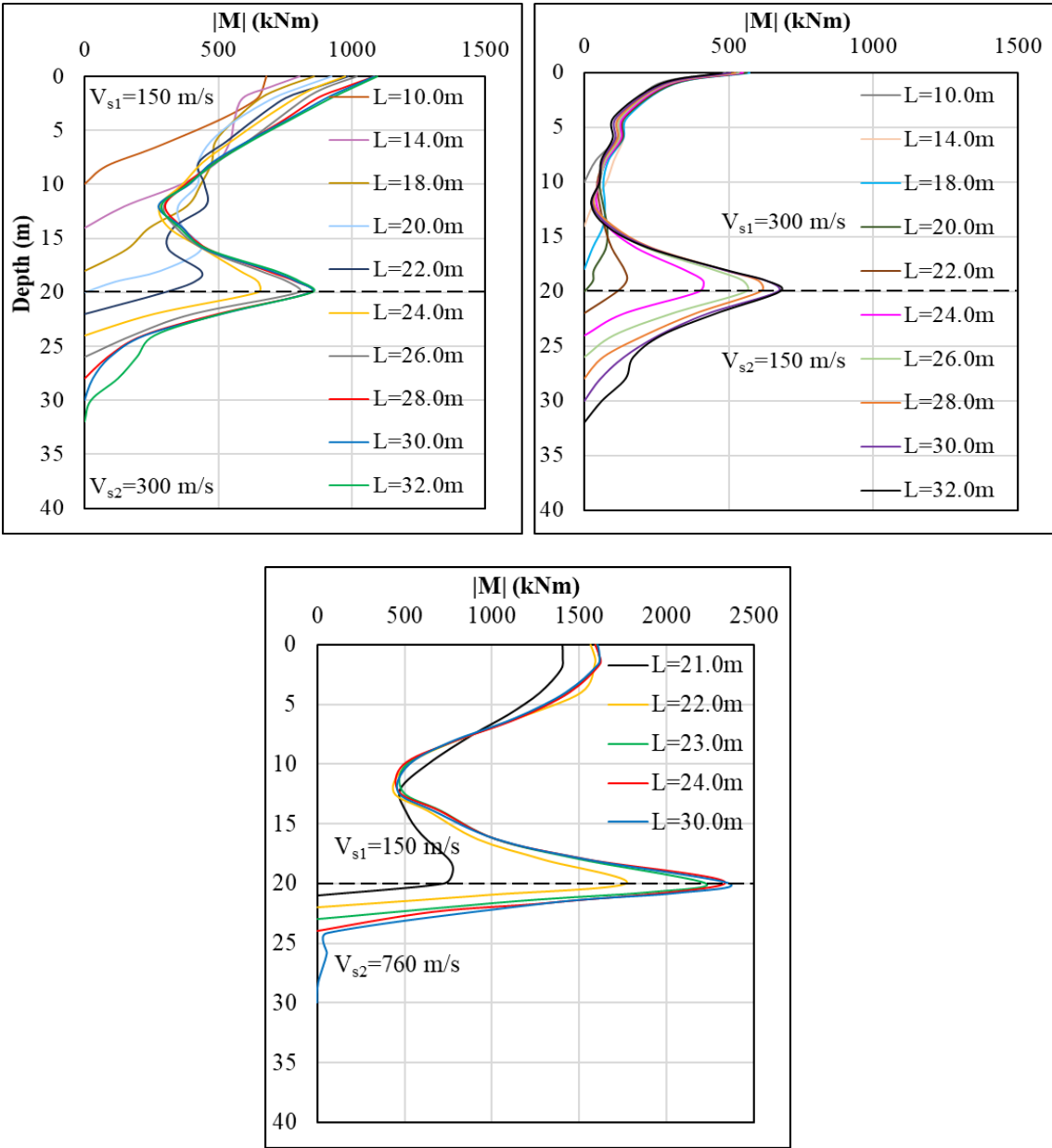
Figure 5.41. Influence of the pile length on the bending moments

The variations in the bending moments at the pile head and layer interface for each pile length can be seen more clearly in Figure 5.42.
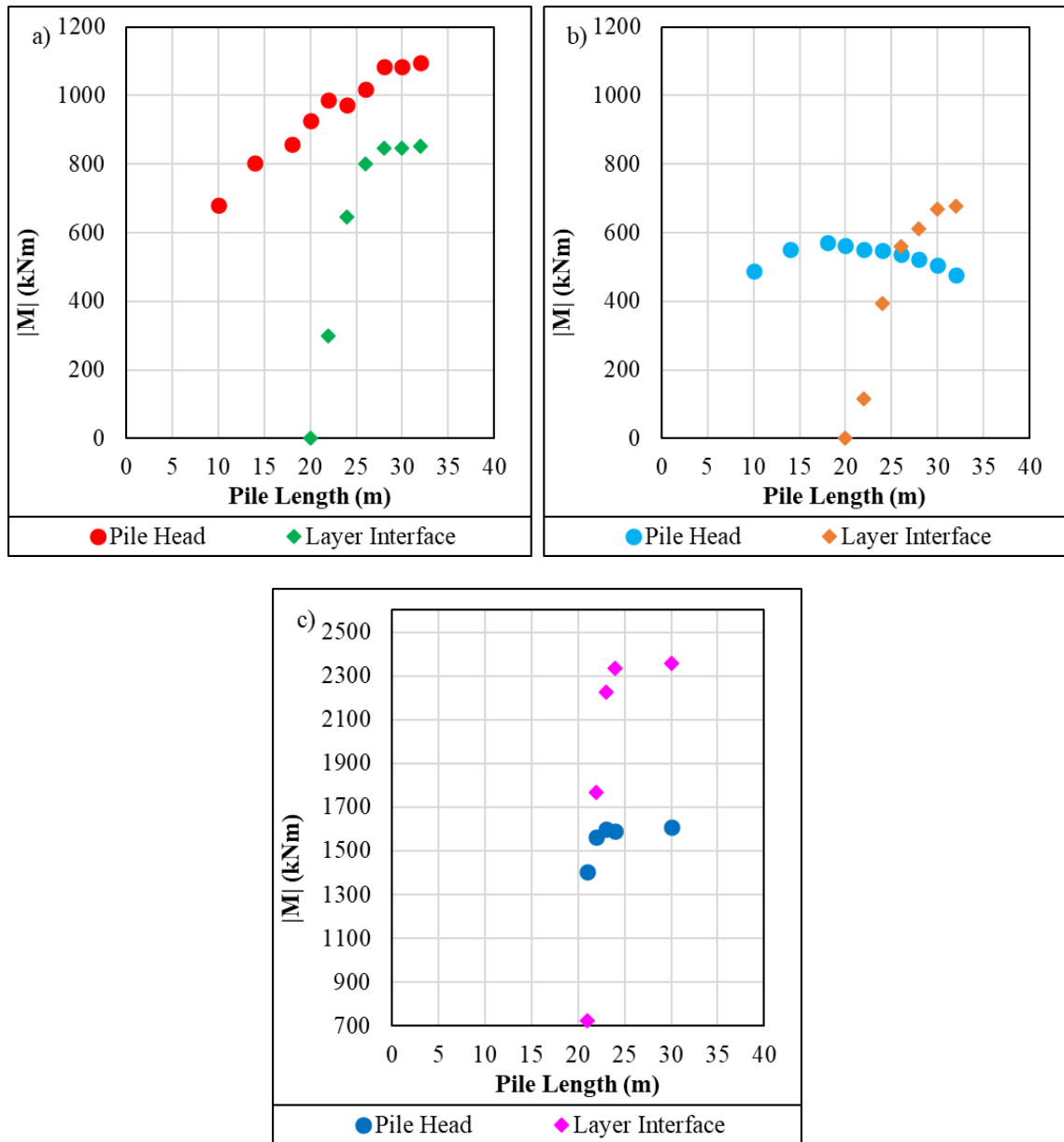
Figure 5.42. Bending moment variations at the pile head and layer interface for each pile length (a) $V_{s1} = 150$ m/s, $V_{s2} = 300$ m/s, b) $V_{s1} = 300$ m/s, $V_{s2} = 150$ m/s, c) $V_{s1} = 150$ m/s, $V_{s2} = 760$ m/s)

It was observed that in the first soil profile (V_{s1}=150 m/s, V_{s2}=300 m/s), the bending moments at the pile head and layer interface increased up to 26.0 m pile length and then, remained almost constant. On the other hand, in the second soil profile (V_{s1}=300 m/s, V_{s2}=150 m/s), the bending moments at the pile head increased up to 20.0 m pile length and then, slightly decreased with the increasing bending moments at the layer interface. In the third soil profile (V_{s1}=150 m/s, V_{s2}=760 m/s), the bending moments at the pile head increased between the pile lengths of 21.0 & 22.0 m and it remained almost constant after 22.0 m. Additionally, it can be seen that the bending moments at the layer interface increased with increasing pile lengths in all three soil profiles. Nonetheless, these changes in the bending moments became negligible after certain pile lengths. It can be concluded that the bending moment increases in the first, second and third soil profiles are negligible (i.e., less than 10%) after 6D, 8D and 3D embedment length into the bottom layer, respectively.

5.3.2.3. Shear Forces

The shear force diagrams for each soil profile and each pile spacing are presented in Figure 5.43.

106
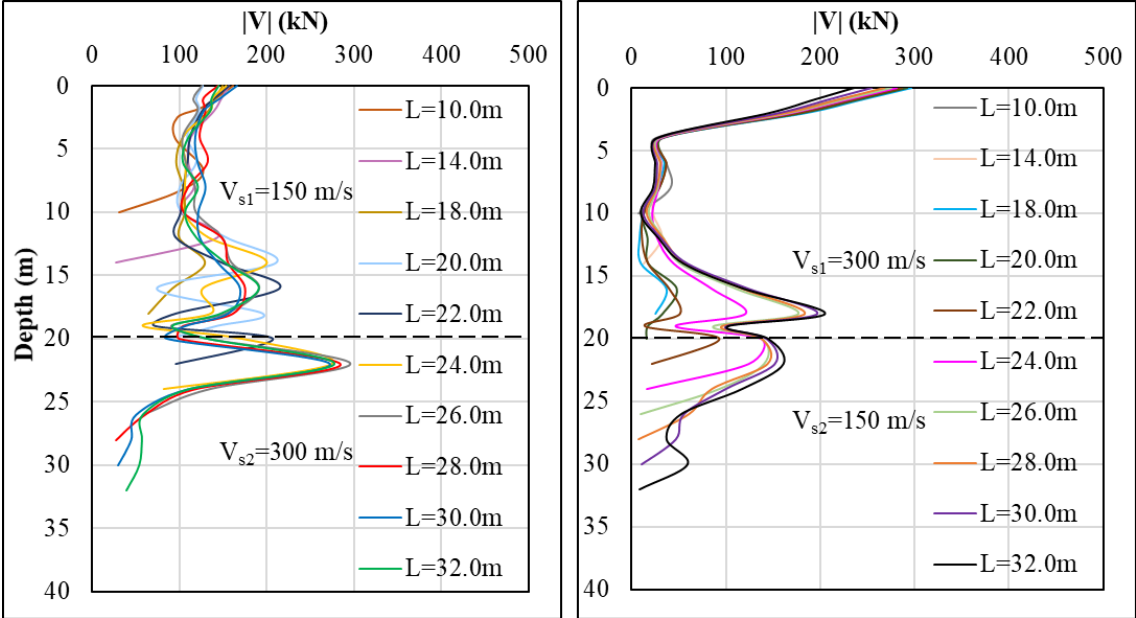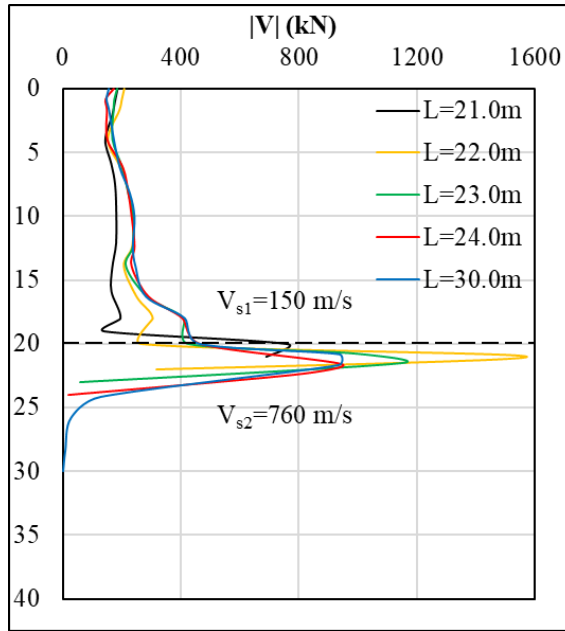
Figure 5.43. Influence of the pile length on the shear forces

The variations in the maximum shear forces and the shear forces at the pile head and layer interface for different pile lengths can be seen more clearly in Figure 5.44. Since the maximum shear forces occurred at the pile head in the second soil profile, they were not shown separately in the graphs.
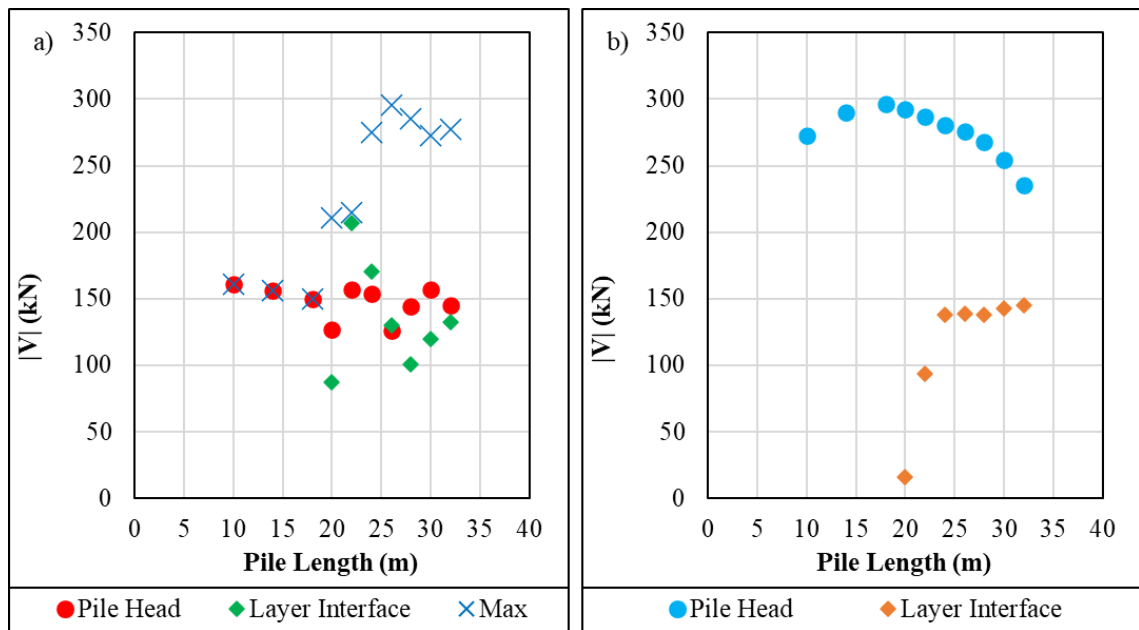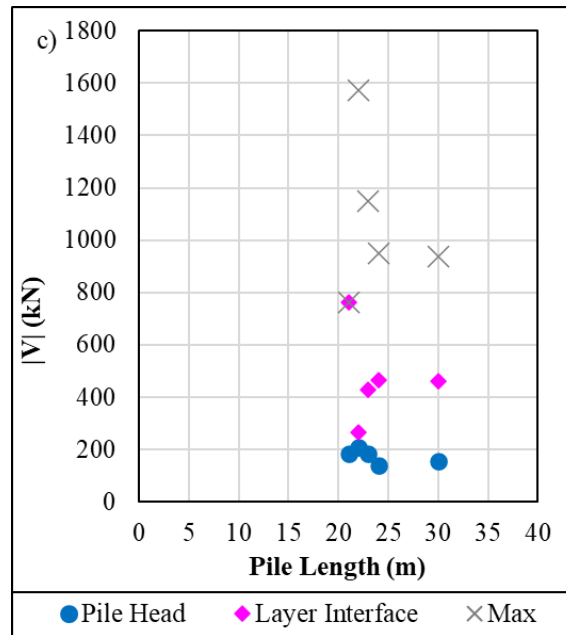
Figure 5.44. Variations of maximum shear forces and shear forces at the pile head and layer interface for each pile length (a) $V_{s1} = 150$ m/s, $V_{s2} = 300$ m/s, b) $V_{s1} = 300$ m/s, $V_{s2} = 150$ m/s, c) $V_{s1} = 150$ m/s, $V_{s2} = 760$ m/s)

It was observed that in the first soil profile ($V_{s1}=150$ m/s, $V_{s2}=300$ m/s), there were fluctuations in the shear force values. The shear forces at the pile head remained almost constant except little fluctuations. Furthermore, although the maximum shear forces and the shear forces at the layer interface did not show a uniform increase or decrease with increasing pile length, it can be said that the fluctuations are negligible after 4D embedment length into the bottom layer.

In the second soil profile ($V_{s1} = 300$ m/s, $V_{s2} = 150$ m/s), it was observed that the shear forces at the layer interface generally increased as the pile length increased up to a certain pile length. After 4D embedment length into the bottom layer, the shear forces at the layer interface remained almost constant. On the other hand, it was observed that the shear forces at the pile head increased up to 20.0 m pile length and then, slightly decreased with the increasing shear force at the layer interface. These decreases in the shear force values are negligible after 10D embedment length into the bottom layer.

In the third soil profile (V$_{s1}$ = 150 m/s, V$_{s2}$ = 760 m/s), the shear forces at the pile head remained almost constant. Besides, the shear forces at the layer interface and the maximum shear forces showed fluctuations with increasing pile length and there was not a uniform increase or decrease. However, these changes in the shear force values are negligible after 3D and 4D embedment lengths into the bottom layer, respectively.

5.3.3. Earthquake-3

For the third input signal (earthquake-3), twenty analyses were performed in two different layered soil profiles. In these soil profiles, loose sand (V$_s$ = 150 m/s) and dense sand (V$_s$ = 300 m/s) layers were used in two different combinations. In these analyses, ten different pile length ranging from 10.0 to 32.0 m were analyzed in the soil layers having an identical thickness of 20.0 m. The results of these analyses are presented in the following sections.

5.3.3.1. Accelerations

The graphs containing the accelerations in the soil layers are presented in Figure 5.45. The accelerations in the free field analyses and kinematic interaction analyses are presented together for each soil profile.
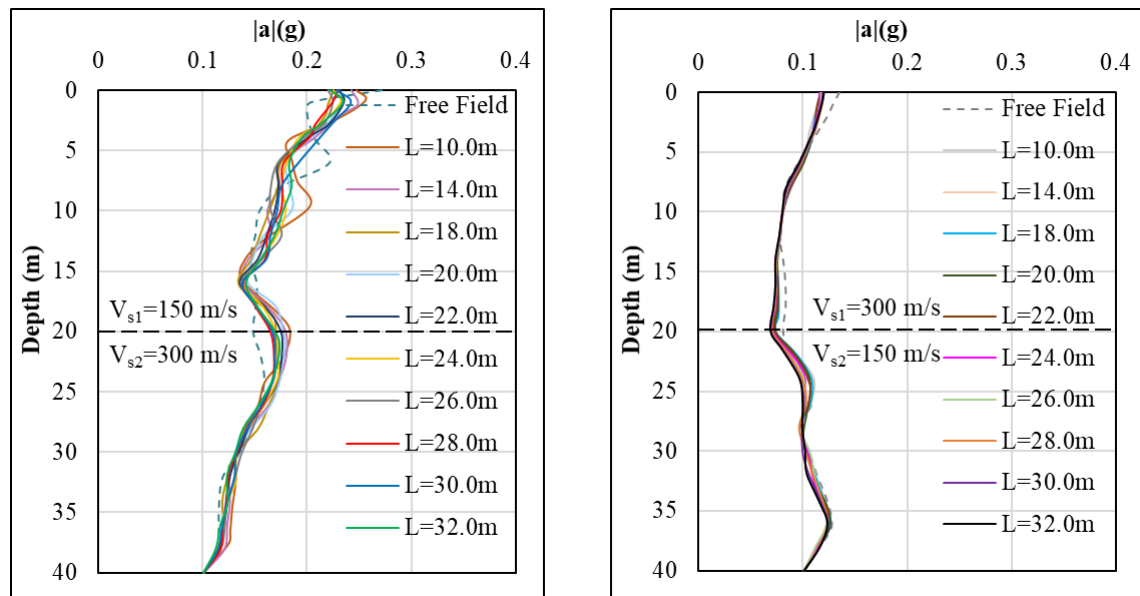
Figure 5.45. Influence of the pile length on the accelerations

As can be seen in the acceleration graphs, the accelerations in the soil remained almost constant regardless of the length of the piles. Among all scenarios examined, analyses with this input signal have the smallest variations in the acceleration values since the kinematic interaction effects decreased with the decreasing PGA.

5.3.3.2. Bending Moments

The bending moment diagrams for each soil profile and each pile length are presented in Figure 5.46.
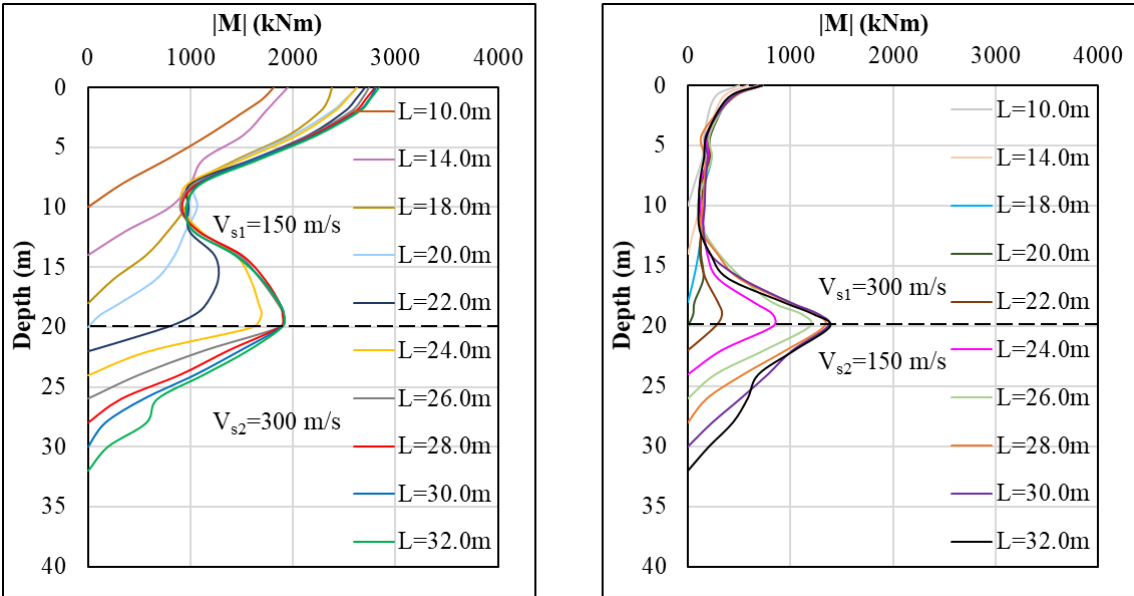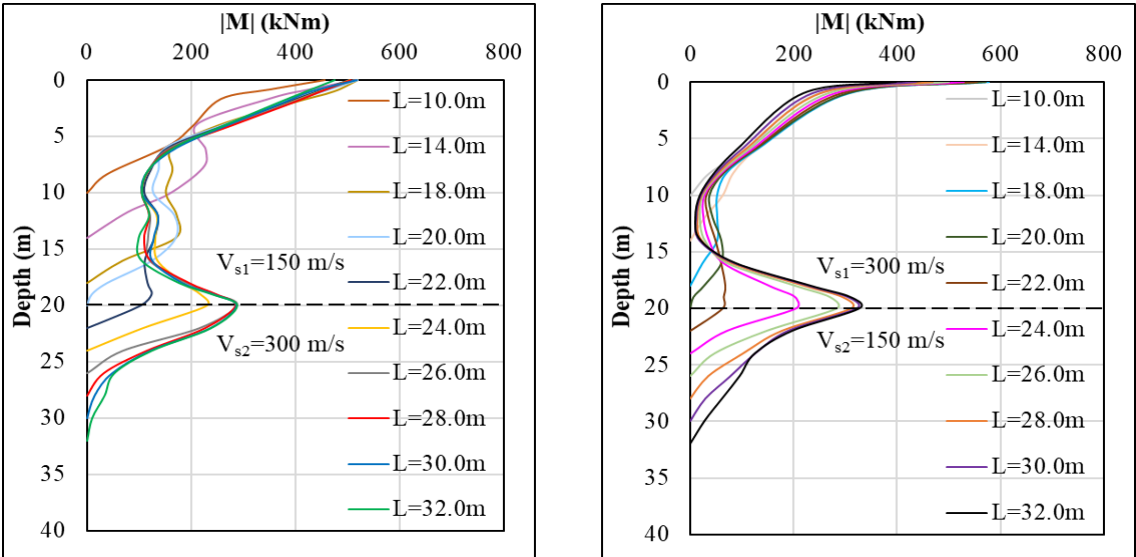

Figure 5.46. Influence of the pile length on the bending moments

The variations in the bending moments at the pile head and layer interface for different pile lengths can be seen more clearly in Figure 5.47.
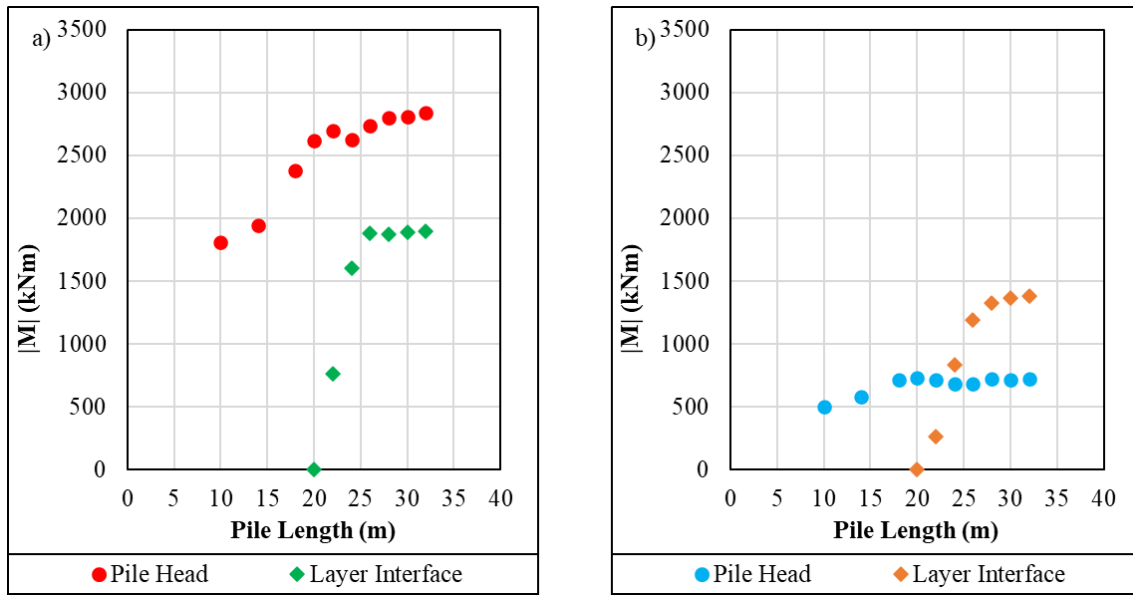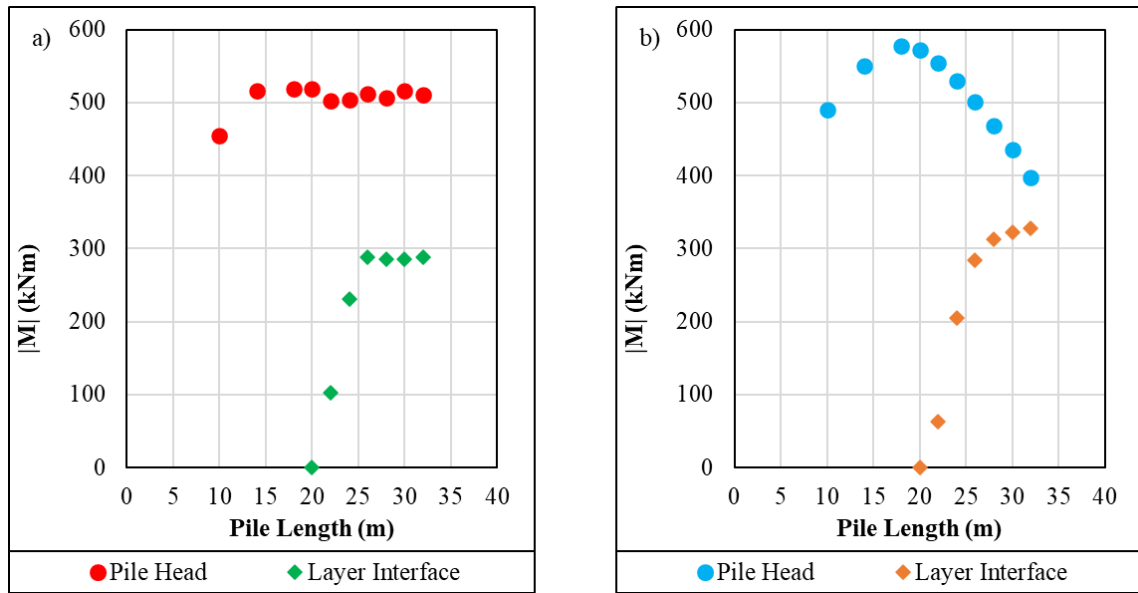

Figure 5.47. Bending moment variations at the pile head and layer interface for each pile length (a) $V_{s1} = 150$ m/s, $V_{s2} = 300$ m/s, b) $V_{s1} = 300$ m/s, $V_{s2} = 150$ m/s

It was observed that in the first soil profile ($V_{s1} = 150$ m/s, $V_{s2} = 300$ m/s), the bending moments at the pile head remained almost constant. Only a slight increase was observed when the pile length was increased from 10.0 m to 14.0 m. Besides, the bending moments at the layer interface increased up to 6D embedment length and remained almost constant after this length.

In the second soil profile ($V_{s1} = 300$ m/s, $V_{s2} = 150$ m/s), the bending moments at the pile head increased up to 20.0 m pile length and then, it decreased with the increasing bending moments at the layer interface. Additionally, it can be seen that the bending moments at the layer interface increased up to 8D embedment length and remained almost constant after this length.

It can be concluded that the changes in the bending moments along the pile became negligible (i.e., less than 10%) after 6D and 8D embedment lengths into the bottom layer for the first and second soil profiles, respectively.

111

5.3.3.3. Shear Forces

The shear force diagrams for each soil profile and each pile length are presented in Figure 5.48.
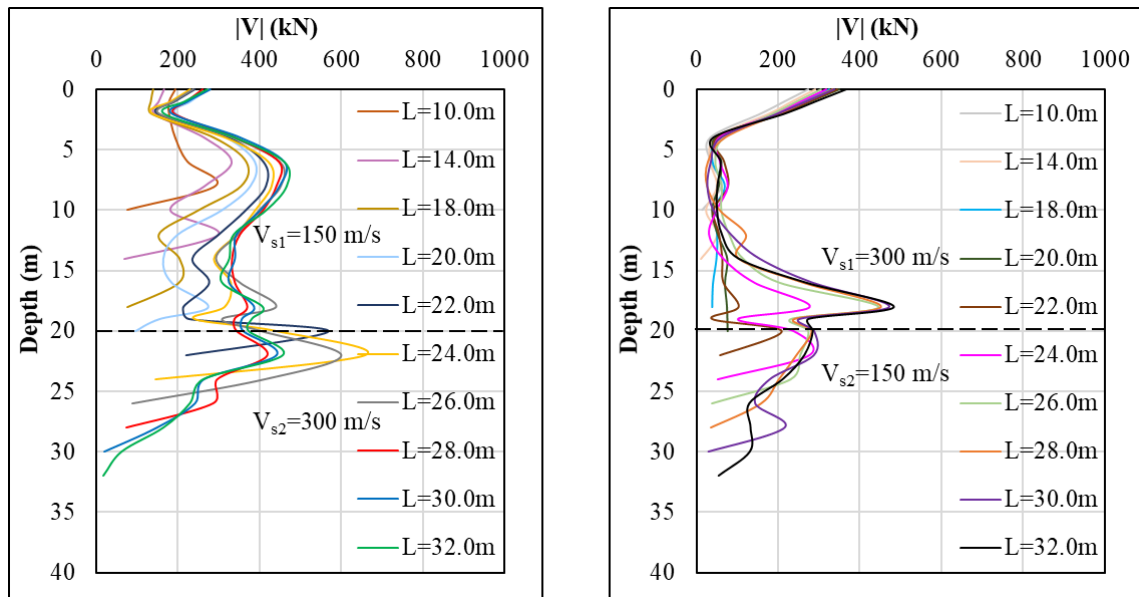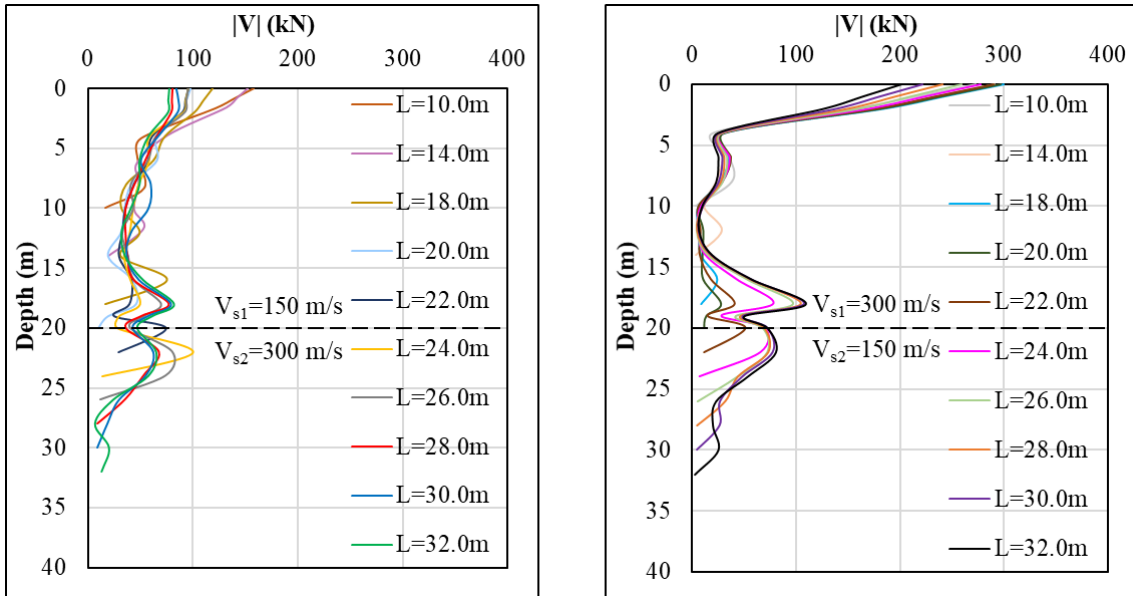

Figure 5.48. Influence of the pile length on the shear forces

The variations in the maximum shear forces and the shear forces at the pile head and layer interface for different pile lengths can be seen more clearly in Figure 5.49.
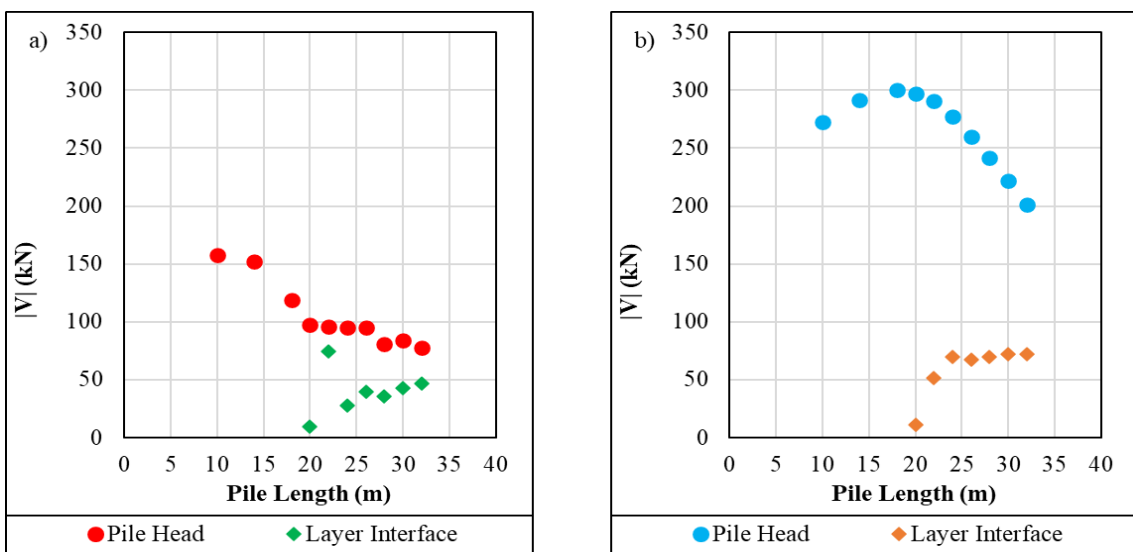
Figure 5.49. Variations of the shear forces at the pile head and layer interface for each pile length (a) $V_{s1} = 150$ m/s, $V_{s2} = 300$ m/s, b) $V_{s1} = 300$ m/s, $V_{s2} = 150$ m/s)

It was observed that <u>in the first soil profile (V_{s1} = 150 m/s, V_{s2} = 300 m/s)</u>, there were fluctuations in the shear force values. Although the shear forces did not show a uniform increase or decrease with increasing pile length, it can be said that the fluctuations in the shear force values are negligible (i.e., less than 10%) after 6D embedment length.

<u>In the second soil profile (V_{s1} = 300 m/s, V_{s2} = 150 m/s)</u>, it was observed that the shear forces at the layer interface generally increased as the pile length increased up to 4D embedment length into the bottom layer and then, remained almost constant. On the other hand, it was observed that the shear forces at the pile head increased up to 20.0 m pile length and then, it slightly decreased with the increasing shear force at the layer interface.

5.4. Influence of the Soil Stiffness

To understand the effect of the soil stiffness on the analysis results, soil profiles consist of layers having different shear wave velocities (150, 300 and 760 m/s) were analyzed. The results of the analyses are presented in the following sections.

5.4.1. Accelerations

Sample acceleration-depth graphs from the analyses with earthquake-2 input signal are presented in Figure 5.50.
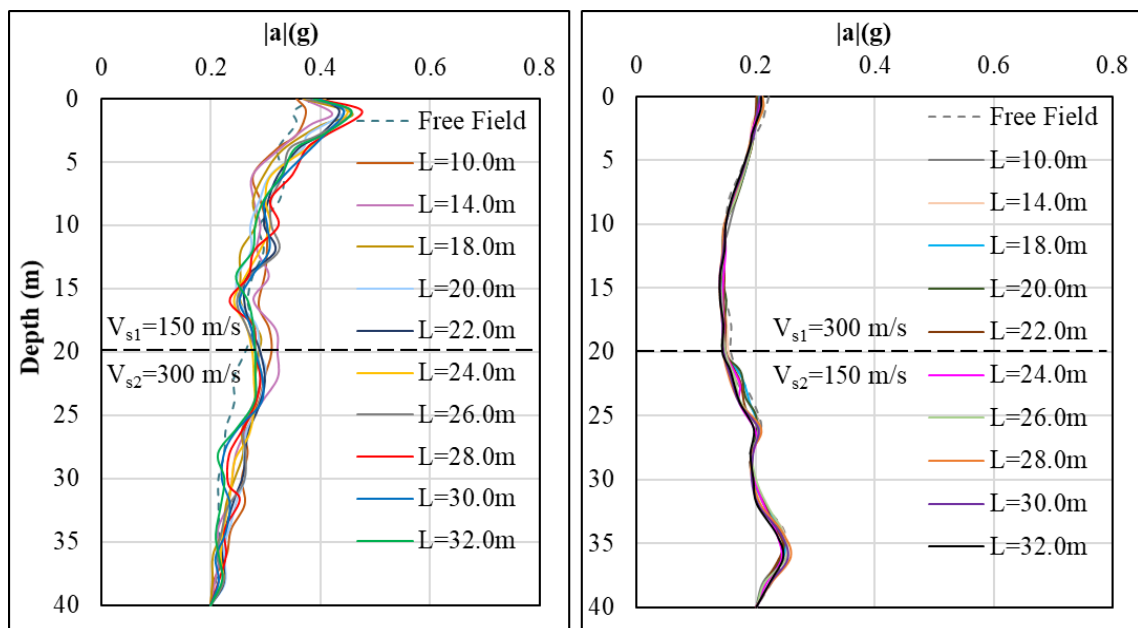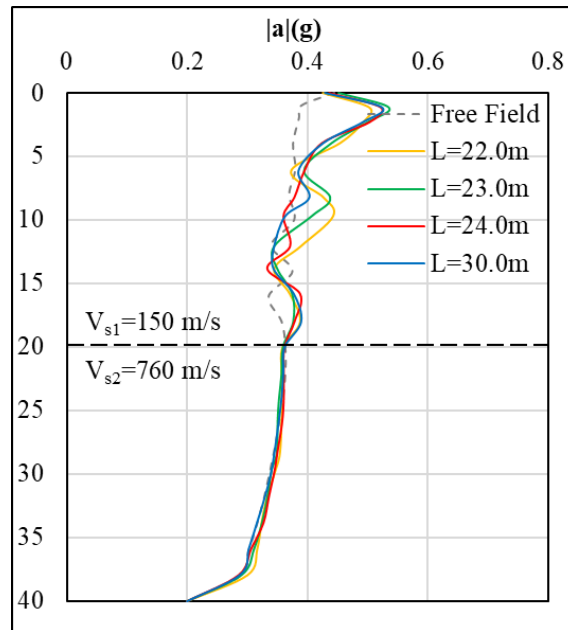
Figure 5.50. Influence of the soil stiffness on the accelerations

It was observed that the stiffness difference between the layers has a significant effect on the accelerations. According to the analysis results, it was observed that the soil profiles having loose sand layer at the top and dense sand layer at the bottom (V_{s1} = 150 m/s, V_{s2} = 300 m/s) experienced greater accelerations than the soil profiles having dense sand layer at the top and loose sand layer at the bottom (V_{s1} = 300 m/s, V_{s2} = 150 m/s). The stiffness of the soil affects how much it amplifies the accelerations. Loose sand layer amplifies the accelerations more than dense sand layer. In addition, the stiffness of the soil directly affects the deformations under seismic loading. Since the loose sand layer showed more deformations, this situation led to higher wave reflections and higher accelerations near the pile head in the soil profiles having loose sand layer at the top and dense sand layer at the bottom (V_{s1} = 150 m/s, V_{s2} = 300 m/s).

Furthermore, since the soil profile where loose sand layer at the top and rock layer at the bottom (V_{s1} = 150 m/s, V_{s2} = 760 m/s) has greater stiffness difference at the layer interface compared to the first two soil profiles, this soil profile has experienced higher levels of accelerations than the other two soil profiles.

5.4.2. Bending Moments

In the analyses with the input signals of earthquake-1 & 2, the bending moments acting on the pile were greater in the soil profiles having loose sand layer at the top and dense sand layer at the bottom (V_{s1} = 150 m/s, V_{s2} = 300 m/s) compared to the soil profiles having dense sand layer at the top and loose sand layer at the bottom (V_{s1} = 300 m/s, V_{s2} = 150 m/s). Furthermore, the effect of stiffness difference between the layers was observed more clearly in the bending moments. Since the soil profile where loose sand layer at the top and rock layer at the bottom (V_{s1} = 150 m/s, V_{s2} = 760 m/s) has greater stiffness difference at the layer interface compared to the first two soil profiles, piles in this soil profile has experienced much (almost 2-3 times) greater bending moments than the other two soil profiles. In the analyses with the earthquake-3 input signal (PGA = 0.2 g), the difference between the bending moments diminished and piles experienced almost the same bending moment values. Sample bending moment diagrams from the analyses with earthquake-2 input signal are presented in Figure 5.51.
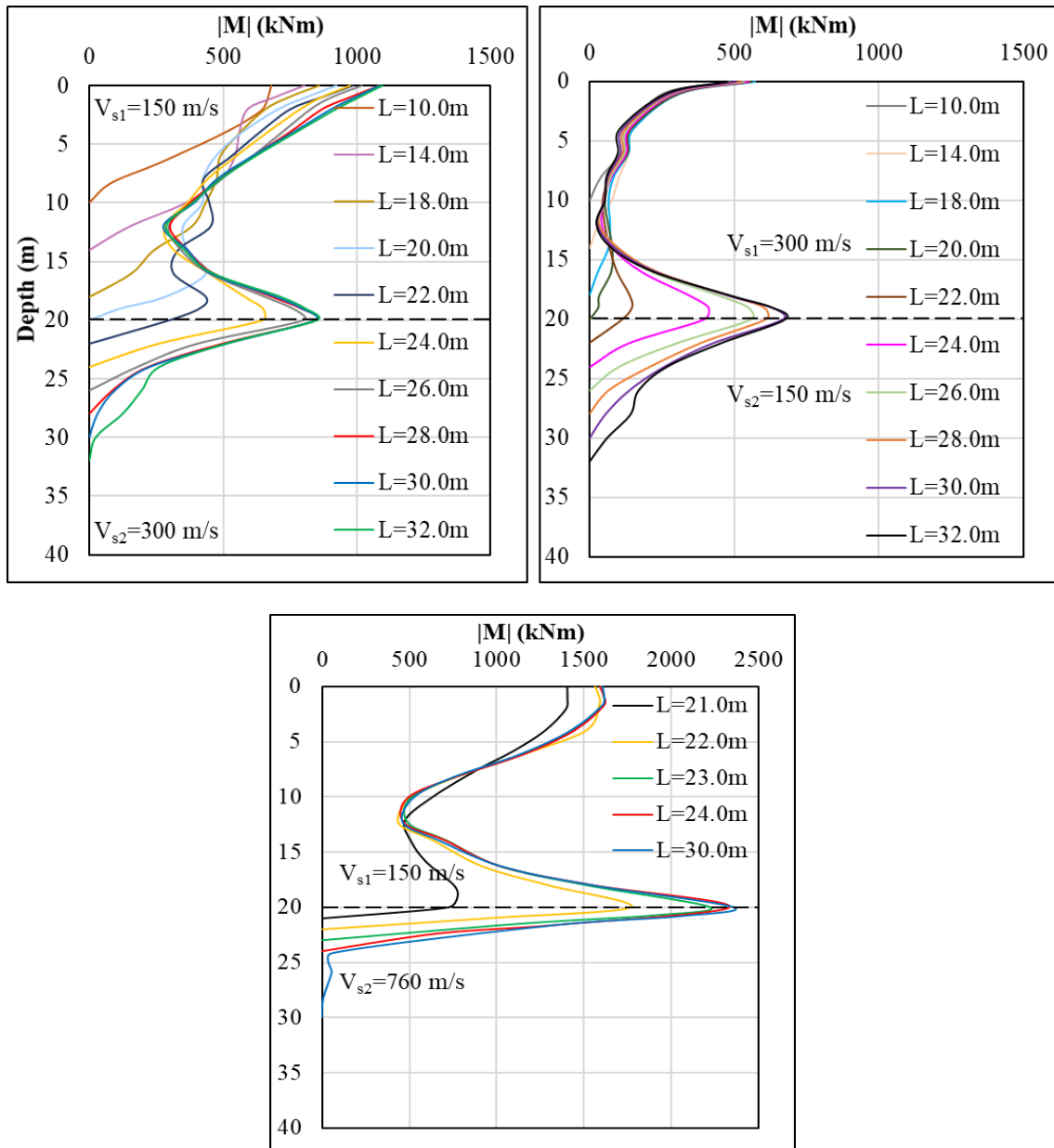
Figure 5.51. Influence of the soil stiffness on the bending moments

5.4.3. Shear Forces

For the shear forces, although a uniform trend could not be observed, a general comment can be made on the influence of the soil stiffness. It was observed that while the shear forces at the pile head were generally greater in the soil profiles having dense sand layer at the top and loose sand layer at the bottom (V_{s1} = 300 m/s, V_{s2} = 150 m/s), the shear forces along the pile shaft were generally greater in the soil profiles having loose sand layer at the top and dense sand layer at the bottom (V_{s1} = 150 m/s, V_{s2} = 300 m/s), compared to the second soil profile (V_{s1} = 300 m/s, V_{s2} = 150 m/s). Moreover, the effect

of stiffness difference between the layers was observed clearly in the shear forces, too. Since the soil profile where loose sand layer at the top and rock layer at the bottom (V_{s1} = 150 m/s, V_{s2} = 760 m/s) has greater stiffness difference at the layer interface compared to the first two soil profiles, piles in this soil profile has experienced much (almost 2-3 times) greater shear forces than the other two soil profiles. As in the bending moments, in the analyses with the earthquake-3 input signal (PGA = 0.2 g), the difference between the shear forces decreased.

Sample shear force diagrams from the analyses with earthquake-2 input signal are presented in Figure 5.52.
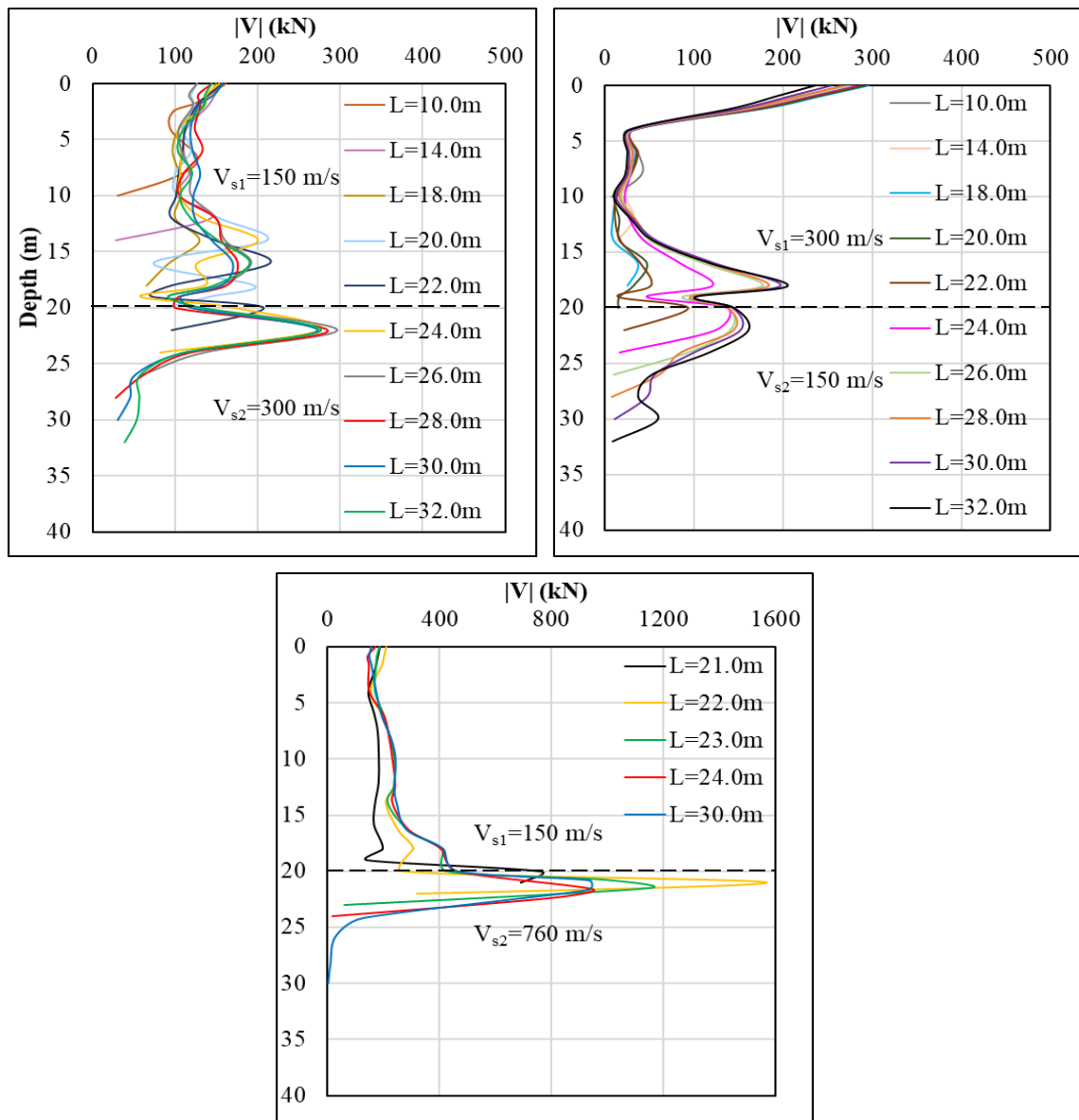
Figure 5.52. Influence of the soil stiffness on the shear forces

5.5. Influence of the Peak Ground Acceleration

Three distinct input signals, called as Earthquake-1, Earthquake-2 and Earthquake-3, having peak ground accelerations of 0.8 g, 0.4 g, 0.2 g, respectively are employed in the analyses to assess the effect of the earthquake PGA on the analysis results. Sample acceleration-depth graphs, bending moment diagrams and shear force diagrams from the analyses performed in this study for each input signal are presented in Figure 5.53 through Figure 5.55.
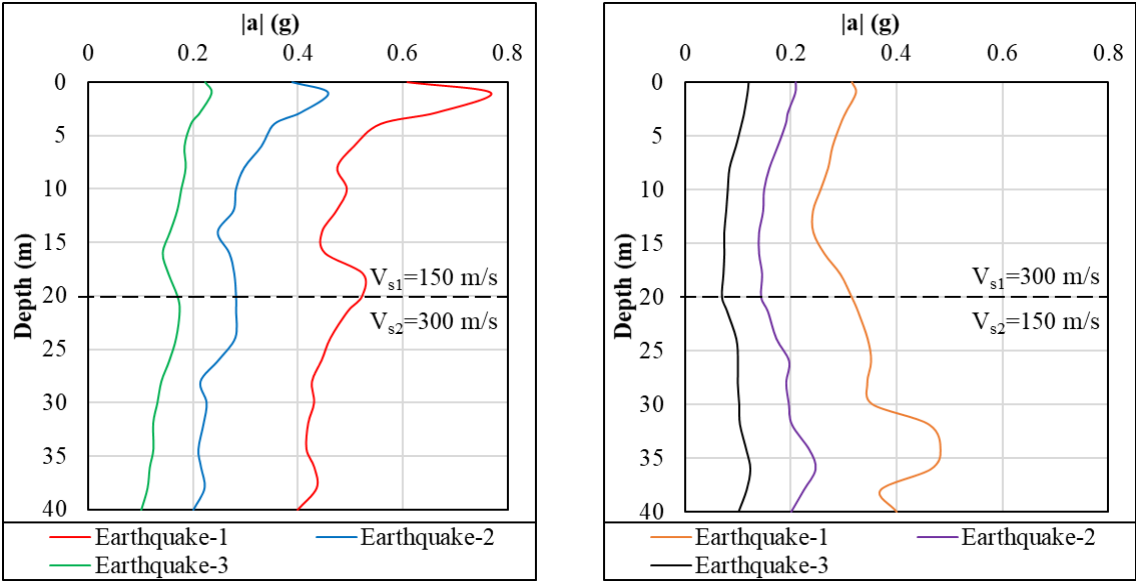
Figure 5.53. Influence of the earthquake PGA on the accelerations
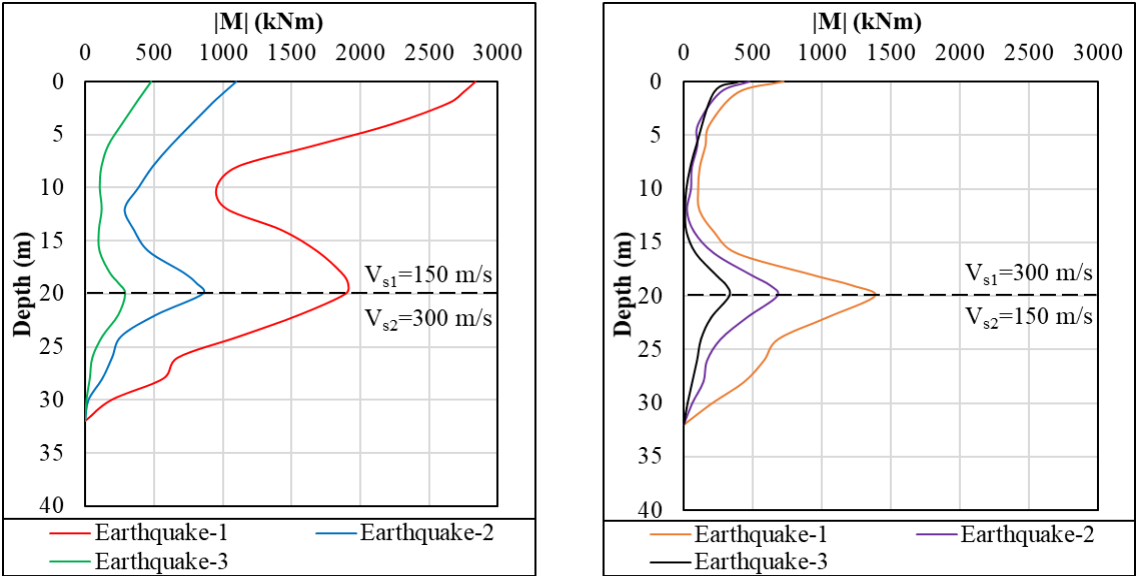
Figure 5.54. Influence of the earthquake PGA on the bending moments

118
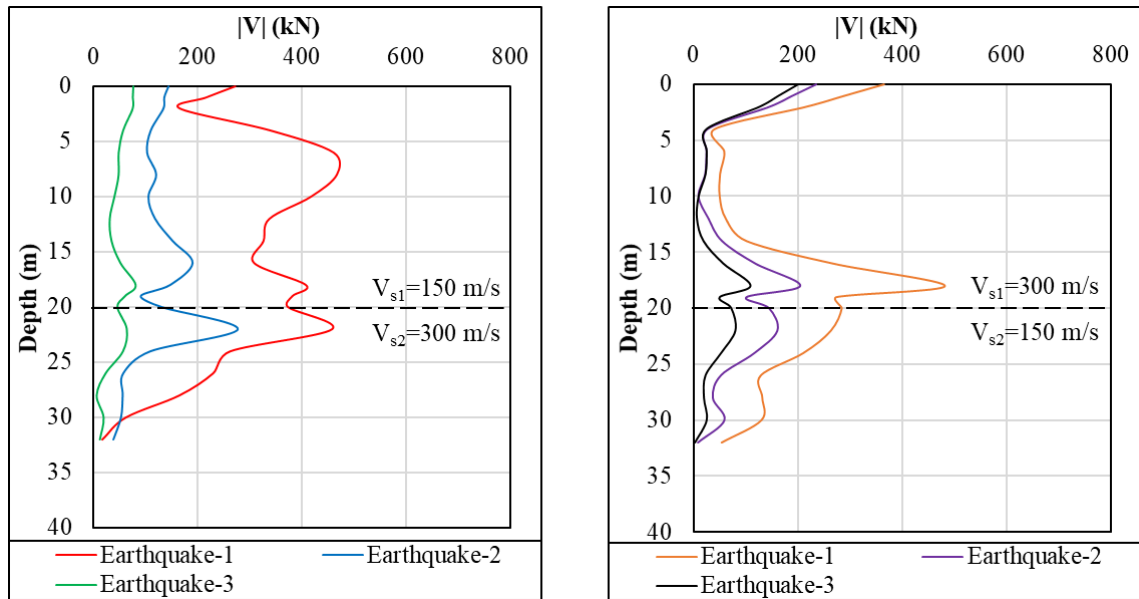
Figure 5.55. Influence of the earthquake PGA on the shear forces

The analysis results clearly demonstrate that the magnitude of the earthquake accelerations directly affects the results of the analyses, as expected. It was observed that the accelerations in the soil, as well as the bending moments and shear forces acting on the piles, increased as the earthquake PGA increased.

6. CONCLUSIONS AND RECOMMENDATIONS

The kinematic interaction between the piles and soils was examined in this comprehensive study. A thorough parametric study was performed by considering distinct variables such as soil stiffness, earthquake PGA and pile properties (diameter, spacing and length). Dynamic analysis in the scope of this study were performed using Plaxis 2D finite element software. In the analyses, in the layered soil profiles composed of different combinations of loose sand, dense sand and rock units, piles having diameters of 0.8, 1.0 and 1.2 m, spacings of 3D, 4D and 6D and lengths varying between 10.0-32.0 m were analyzed. In order to investigate the influence of pile length on the analysis results, piles with both varying and constant embedment length into the bottom layer were analyzed. For the case of varying pile embedment length into the bottom layer, ten different pile lengths ranging from 10.0 to 32.0 m were analyzed in the soil layers having identical thicknesses of 20.0 m ($H_1 = H_2 = 20$ m). For the case of piles with constant 3 m embedment length into the bottom layer, five different pile lengths varying between 18.0-32.0 m were used and the layer thicknesses were determined according to the pile length ($H_1 = (L - 3)$ m, $H_2 = (40 - H_1)$ m). Furthermore, three different earthquake input signals, called as earthquake-1, 2 and 3, which have PGA values of 0.8 g, 0.4 g and 0.2 g, respectively, were used in this parametric study. These input signals were obtained by scaling the peak ground acceleration of the rock outcrop ground motion history of Kobe (1995) earthquake. After completion of the analyses, the accelerations in the soils and the internal forces (bending moments and shear forces) acting on the piles were compared to investigate the influence of the variables on the analysis results.

6.1. Findings

The main findings obtained in the parametric study are summarized below:

Influence of the Pile Diameter:

Pile diameter has a significant effect on the bending moments and shear forces acting on the piles. It was observed that both bending moments and shear forces increased as the pile diameter increases due to increased flexural rigidity and increased interaction area between the piles and soils.

Furthermore, when the bending moments and shear forces were normalized as $\frac{M \times s}{EI}$ and $\frac{V}{A}$, respectively, it was observed that both bending moments and shear forces did not change significantly for different pile diameters in each soil profiles. The magnitudes of the bending moments were quite similar when the effects of the material stiffness (E), geometric properties (inertia) and spacing were excluded. Similarly, the magnitudes of the shear forces were quite similar when the effects of pile cross sectional area were excluded.

Influence of the Pile Spacing:

The bending moments and shear forces acting on the piles increased with increasing pile spacing. Nevertheless, the effect of pile spacing was not as significant as the effect of pile diameter. The increase in the bending moments can be attributed to the increased interaction between the soils and piles, as a result of the increase in soil volume affecting each pile.

Influence of the Pile Length:

In the analyses which were carried out to examine the influence of the pile length (for the condition of constant 3 m pile embedment length into the bottom layer): The results of the analyses demonstrated that the bending moments at the pile head generally remained almost constant and the bending moments near the layer interfaces showed slight increases with increasing pile length. Moreover, it can be stated that shear forces at layer interface slightly increased with increasing pile length. On the other hand, it was observed that while the shear forces at the pile head did not change significantly in the first soil profile (V_{s1} = 150 m/s, V_{s2} = 300 m/s), they decreased with increasing pile length in the second soil profile (V_{s1} = 300 m/s, V_{s2} = 150 m/s).

In the analyses performed to investigate the influence of pile length (for the condition of varying pile embedment length into the bottom layer): It was observed that as the pile length increases, the bending moments at the layer interfaces increased up to a certain pile length and remained nearly constant after that pile length in all analysis cases. The changes in the bending moment at the layer interface were negligible (i.e., less than 10%) after 6D, 8D and 3D embedment lengths into the bottom layer in the first, second and third soil profiles, respectively for each input signal.

Note: In the first soil profile: V_{s1} = 150 m/s, V_{s2} = 300 m/s, in the second soil profile: V_{s1} = 300

m/s, V_{s2} = 150 m/s, in the third soil profile: V_{s1} = 150 m/s, V_{s2} = 760 m/s)

The bending moments at the pile head increased up to a certain pile length and remained almost constant after that pile length in all analysis cases in the soil profiles having loose sand layer at the top / dense sand layer at the bottom and loose sand layer at the top / rock layer at the bottom. For the soil profiles having loose sand layer at the top / dense sand layer at the bottom, the changes in the bending moment at the pile head were negligible (i.e., less than 10%) after 2D and 6D embedment lengths into the bottom layer, for the Earthquake-1 and Earthquake-2 input signals, respectively. In the analyses of Earthquake-3 input signal, only a slight increase was observed when the pile length increased from 10.0 m to 14.0 m. The bending moments at the pile head remained almost constant after this pile length. Furthermore, in the soil profiles having loose sand layer at the top / rock layer at the bottom, the changes in the bending moment at the pile head were negligible after 2D embedment length into the bottom layer.

In the soil profiles having dense sand layer at the top / loose sand layer at the bottom, the accelerations in the soils were not affected considerably by the changes in pile properties. There were only little fluctuations in the acceleration values.

For the earthquake-1 input signal, bending moments at the pile head increased up to 18.0m pile length and remained almost constant after this length. On the other hand, for the earthquake-2 and earthquake-3 input signals, analysis results demonstrated that the bending moments at the pile head increased until the pile reached the layer interface (20.0 m pile length) and then, slightly decreased with the increasing bending moments at the layer interface.

Moreover, based on the analysis results, the shear forces acting on the pile did not show a uniform increase or decrease with increasing pile length. Despite the fluctuations in the shear force values, it was noted that the changes in the shear force values also were negligible after certain pile embedment lengths into the bottom layer. The detailed explanations for the variations in shear forces were provided in Section-5.

In conclusion, it was observed that although both bending moments and shear forces changed with varying pile lengths, the changes in both bending moments and shear forces were negligible after certain pile lengths for all analysis cases.

Influence of Layer Stiffness Contrast:

In addition, it was observed that the stiffness difference between the layers has also a significant effect on the accelerations. The analysis results showed that the soil profiles having loose sand at the top / dense sand at the bottom experienced greater accelerations than the soil profiles having dense sand layer at the top / loose sand layer at the bottom. Furthermore, since the soil profile where loose sand layer at the top and rock layer at the bottom has greater stiffness difference at the layer interface compared to the first two soil profiles, this soil profile experienced higher levels of accelerations than the other two soil profiles. In addition, since the stiffness of the soil directly affects the deformations under seismic loading, the loose sand layer showed more deformations and this situation led to higher wave reflections and higher accelerations near the pile head in the soil profiles having loose sand layer at the top and dense sand layer at the bottom (V_{s1} = 150 m/s, V_{s2} = 300 m/s).

In the analyses with the input signals of earthquake-1 & 2, the bending moments acting on the pile were greater in the soil profiles having loose sand layer at the top and dense sand layer at the bottom compared to the soil profiles having dense sand layer at the top and loose sand layer at the bottom. Furthermore, the effect of stiffness difference between the layers was observed more clearly in the bending moments in the soil profile where the top layer was loose sand and the bottom layer was rock. Since this soil profile has greater stiffness difference at the layer interface compared to the first two soil profiles, piles in this soil profile were exposed to much (almost 2-3 times) greater bending moments than the other two soil profiles. In the analyses with the earthquake-3 input signal (PGA = 0.2 g), the difference between the bending moments diminished and the piles experienced almost the same bending moment values.

It was observed that while the shear forces at the pile head were generally greater in the soil profiles having dense sand layer at the top / loose sand layer at the bottom, the shear forces along the pile shaft were generally greater in the soil profiles having loose sand layer at the top and dense sand layer at the bottom. Moreover, since the soil profile where loose sand layer at the top and rock layer at the bottom has greater stiffness difference at the layer interface, piles in this soil profile experienced much (almost 2-3 times) greater shear forces than the other two soil profiles. Similar to the bending moments, in the

analyses with the earthquake-3 input signal (PGA = 0.2 g), the difference between the shear forces decreased.

<u>Influence of the Peak Ground Acceleration:</u>

The peak ground acceleration of the earthquakes has also a considerable effect on the analysis results, as expected. It was observed that the accelerations in the soil, as well as the bending moments and shear forces acting on the piles, increased as the earthquake PGA increased.

In conclusion, a comprehensive parametric study was performed in this thesis study focusing on the influence of the soil parameters and pile properties on the kinematic interaction between piles and soils. The influence of distinct variables on the analysis results were discussed thoroughly to be able to provide a sample guide for the future kinematic interaction analyses. It should also be noted that the results in this study valid for the specific model parameters provided in the study.

6.2. Recommendations for Future Studies

For the future researches, this study can be improved by considering the situations mentioned below:

- Analyses can be conducted within 3D model geometries involving the superstructure to obtain more precise results.

- The soil profile combinations used in the analyses can be expanded using different clay and rock layers. Moreover, homogeneous soil layers can also be examined.

- The groundwater and soil liquefaction can be considered to examine the influence of them on the kinematic interaction between the pile and soil.

- A real case study containing experimental data for the soils and piles can be performed to validate the model parameters with the field data. Conducting a case study enables the appropriate selection of input signals corresponding to actual site conditions for the purpose of evaluating how soils and structures respond to various earthquake scenarios, in compliance with seismic design regulations outlined in different codes.

7. REFERENCES

AASHTO, AASHTO LRFD Bridge Design Specifications, 3rd Edition, American Association of State Highway and Transportation Officials, Washington, D.C., 2006.

Albusoda, B. S. and Salem, L. A. K., Australian Journal of Basic and Applied Sciences 10 (12) (2016) 240-247.

Anand, V. and Kumar, S. R. S., Seismic Soil-structure Interaction: A State-of-the-Art Review, Structures 16 (2018) 317-326.

Anonymous, What Happens During an Earthquake, https://www.scienceexchange. caltech.edu/topics/earthquakes/what-causes-earthquake (Date accessed: May 23, 2024).

Asli, S. J., Saadatinezhad, M. and Saffari, H., Comparing the Performance of Substructure and Direct Methods to Estimate the Effect of SSI on Seismic Response of Mid-Rise Structures, International Journal of Geotechnical Engineering (2019).

Bapir, B., Abrahamczyk, L., Wichtmann, T. and Sarmiento, L. F. P., Soil-Structure Interaction: A State-of-the-Art Review of Modeling Techniques and Studies on Seismic Response of Building Structures, Frontiers in Built Environment 9 (2023).

Benz, T., Small-Strain Stiffness of Soils and its Numerical Consequences, Ph.D. Thesis, University of Stuttgart, Stuttgart, 2006.

Beskos, D. E., Applications of the Boundary Element Method in Dynamic Soil-Structure Interaction. Developments in Dynamic Soil-Structure Interaction, Gülkan, P., Clough, R. W., (eds.), Kluwer Academic Publishers, Dordrecht, 61-90, 1993.

Birand, A., Ergun, U., Erol, U., CE 366 Foundation Engineering 1, Middle East Technical University, Ankara, 2011.

Boominathan, A., Varghese, R., Nair, S. K., Soil Structure Interaction Analysis of Pile Foundations Subjected to Dynamic Loads. Geotechnics for Natural and Engineered Sustainable Technologies, Krishna, A. M., Dey, A., Sreedeep, S., (eds.) Springer, Singapore, 45-61, 2018.

Burland, J. B., Shaft Friction of Piles in Clay-A Simple Fundamental Approach, Ground Engineering 6 (3) (1973) 30-42.

Çimen, Ö. and Osmanoğlu, U., An Investigation of the Dynamic Behavior of Piled Raft Foundation Systems Constituted on Sandy Soil: The Example of TRNC-Lefke, Konya Journal of Engineering Sciences 9 (3) (2021) 686-701.

Coyle, H. M., and Castello, R. R., New Design Correlations for Piles in Sand, Journal of the Geotechnical Engineering Division 107 (7) (1981) 965-986.

Czichos, H., Saito, T., Smith, L., (eds.) Springer Handbook of Materials Measurement Methods, Springer, Berlin, 2006.

Darendeli, M. B., Development of a New Family of Normalized Modulus Reduction and Material Damping Curves, Ph.D. Thesis, The University of Texas, Austin, 2001.

Das, B. M., Principles of Geotechnical Engineering, 7th Edition, Cengage Learning, Stamford, 2010.

Dezi, F., Carbonari, S. and Leoni, G., Kinematic Bending Moments in Pile Foundations, Soil Dynamics and Earthquake Engineering 30 (3) (2010) 119-132.

Dikmen, U., Statistical Correlations of Shear Wave Velocity and Penetration Resistance for Soils, Journal of Geophysics and Engineering, 6 (2009) 61-72.

Fan, K., Gazetas, G., Kaynia, A., Kausel, E. and Ahmad, S., Kinematic Seismic Response of Single Piles and Pile Groups, Journal of Geotechnical Engineering 117 (12) (1991) 1860-1879.

Fellenius, B. H. and Altaee, A. A., Critical Depth: How it came into being and why it does not exist, Proceedings of the Institution of Civil Engineers-Geotechnical Engineering 113 (2) (1995) 107-111.

FEMA, A Practical Guide to Soil-Structure Interaction, Applied Technology Council, United States, 2020.

Firoozi, A. A. and Firoozi, A. A., Soil-Structure Interaction: Understanding and Mitigating Challenges, Challenges in Foundation Engineering – Civil Engineering, IntechOpen, United Kingdom, 1-33, 2024.

Fu, F., Fundamentals of Tall Building Design, Design and Analysis of Tall and Complex Structures, Butterworth-Heinemann, an imprint of Elsevier, United Kingdom, 5-80, 2018.

Ge, J., Exploring the Finite Difference Method in Geotechnical Engineering, Journal of Geology & Geophysics 12 (5) (2023).

Giannakos, S., Gerolymos, N. and Gazetas, G., Cyclic Lateral Response of Piles in Dry Sand: Finite Element Modeling and Validation, Computers and Geotechnics 44 (2012) 116-131.

Haeri, S. M., Kavand, A., Rahmani, I. and Torabi, H., Response of A Group of Piles to Liquefaction-Induced Lateral Spreading by Large Scale Shake Table Testing, Soil Dynamic and Earthquake Engineering 38 (7) (2012) 25-45.

Hamada, M., Damage to Piles by Liquefaction-Induced Ground Displacements, 3rd U.S. Conference Lifeline Earthquake Engineering, ASCE, Los Angeles, 1172-1181, 1991.

Hardin, B. O. and Drnevich, V. P., Shear Modulus and Damping in Soils, Journal of Soil Mechanics and Foundation Division 98 (1972) 667-692.

Hasancebi, N and Ulusay, R., Empirical Correlations Between Shear Wave Velocity and Penetration Resistance for Ground Shaking Assessments, Bulletin of Engineering Geology and the Environment 66 (2007) 203-213.

Herreros, J., P., Dynamic soil-structure interaction of pile foundations: experimental and numerical study, Ph.D. Thesis, École Centrale de Nantes, Nantes, 2020.

Hudson, M. B., Idriss, I. M., Beikae, M., QUAD4M - A Computer Program to Evaluate the Seismic Response of Soil Structures Using Finite Element Procedures Incorporating a Compliant Base, Department of Civil & Environmental Engineering, California, 1994.

Imai, T., P- and S-wave Velocities of the Ground in Japan, Proceedings of the 9th International Conference on Soil Mechanics and Foundation Engineering 2, 127–132, 1977.

Imai, T., Tonouchi, K., Correlation on N-value with S-Wave Velocity and Shear Modulus, Proc. 2nd European Symposium of Penetration Testing, 57-72, 1982.

Ishihara, K., Soil Behavior in Earthquake Geotechnics, Clarendon Press, Oxford, 1996.

Jimenez, G. A. L., Static and Dynamic Behavior of Pile Supported Structures in Soft Soil, Ph.D. Thesis, Grenoble Alpes University, Grenoble, 2016.

Joyner, W. B. and Chen, A. T. F., Calculation of Nonlinear Ground Response in Earthquake, Bulletin of Seismological Society of America 65 (1975) 1315-1336.

Kausel, E., Early History of Soil-Structure Interaction, Soil Dynamics and Earthquake Engineering 30 (2009) 822-832.

Kavazanjian, E. Jr., Matasovic, N., Hadj-Hamou, T., H., Sabatini, P. J., FHWA

Administration, Design Guidance: Geotechnical Earthquake Engineering for Highways, Volume 1-Design Principles, FHWA-SA-97-076, U.S. Department of Transportation, Federal Highway Administration, 1997.

Kawamura, S., Nishizawa, T., Wada, K., Damage to Piles due to Liquefaction Found by Excavation Twenty Years after Earthquake, Nikkei Architecture, Tokyo, 130-134, 1985.

Khari, M., Kassim, K. A., Adnan, A. and Moayedi, H., Kinematic Bending Moments of Piles Under Seismic Motions, Asian Journal of Earth Sciences 7 (1) (2014) 1-9.

Kimmerling, R. E., Federal Highway Administration, U.S. Department of Transportation, Geotechnical Engineering Circular 6, Shallow Foundations, Report No. FHWA-SA-02-054, 2002.

Kramer S. L., Geotechnical Earthquake Engineering, Prentice Hall, New Jersey, 1996.

Kramer, S. L., Stewart, J. P., Geotechnical Aspects of Seismic Hazards, Earthquake Engineering, CRC Press, Florida, Chapter 4, 2004.

Kuhlemeyer, R. L. and Lysmer, J., Finite Element Method Accuracy for Wave Propagation Problems. Journal of the Soil Mechanics and Foundations Division (1973) 421-427.

Kulhawy, F.H., Mayne, P.W., Manual on Estimating Soil Properties for Foundation Design (No. EPRI-EL-6800), Electric Power Research Inst., Palo Alto, California, 1990.

Kwaak, V. D. B., Modeling of Dynamic Pile Behaviour During an Earthquake Using Plaxis 2D: Embedded Beam (Row), Master Thesis, Delft University of Technology, Delft, 2015.

Kwok, A. O. L., Stewart, J. P., Hashash, Y., M. A., Matasovic, N., Pyke, R., Wang, Z. and Yang, Z., Use of Exact Solutions of Wave Propagation Problems to Guide Implementation of Nonlinear Seismic Ground Response Analysis Procedures, Journal of Geotechnical and Geoenvironmental Engineering 133 (11) (2007) 1385-1398.

Lee, S. H., Regression Models of Shear Wave Velocities, Journal of the Chinese Institute of Engineers 13 (1990) 519-532.

Lin, Y. Y. and Miranda, E., Kinematic Soil-Structure Interaction Effects on Maximum Inelastic Displacement Demands of SDOF Systems, Bulleting Earthquake Engineering 6 (2007) 241-259.

Lysmer, J., Kuhlemeyer, R. L., Finite Dynamic Model for Infinite Media, Engineering Mechanics Division ASCE, 95, 859–877, 1969.

Makris, N. and Gazetas, G., Dynamic Pile-Soil-Pile Interaction. Part II: Lateral and Seismic Response, Earthquake Engineering and Structural Dynamics 21 (1992) 145-162.

Menglin, L., Huaifeng, W., Chen, X. and Yongmei, Z., Structure-Soil-Structure Interaction: Literature Review, Soil Dynamics and Earthquake Engineering 31 (2011) 1724-1731.

Meyerhof, G. G., Bearing Capacity and Settlement of Pile Foundations, Journal of the Geotechnical Engineering Division 102 (3) (1976) 197-228.

NAVFAC, Foundation and Earth Structures, Design Manual 7.2, U.S. Department of the Navy, Virginia, 1984.

NIST, Soil-Structure Interaction for Building Structures, Applied Technology Council, the Consortium of Universities Gaithersburg, 2012.

Obrzud, R. F., Truty, A., The Hardening Soil Model - a Practical Guidebook, Z Soil.PC 100701 report, Preverenges, 2018.

Ohta, T., Hara, A., Niwa, M., and Sakano, T., Elastic Shear Moduli as Estimated from N-value, Proc. 7th Ann. Convention of Japan Society of Soil Mechanics and Foundation Engineering, 265-268, 1972.

Ohta, Y. and Goto, N., Empirical Shear Wave Velocity Equations in Terms of Characteristic Soil Indexes, Earthquake Engineering and Structural Dynamics 6 (1978) 167–187.

Ordu, E. and Özkan, M. T., Kazıklı Temellerin Deprem Performanslarının Üç Boyutlu Sonlu Elemanlar Yöntemi ile İncelenmesi, İTÜ Dergisi 5 (2) (2006) 27-34.

Öztürk Kardoğan, P. S. and Onur, M. İ., Uç ve Sürtünme Kazıklarının Deprem Kuvvetleri Altında Davranışının Modellenmesi, Eskişehir Teknik Üniversitesi Bilim ve Teknoloji Dergisi 6 (2018) 117-123.

Pinto, P. A., Study of Constitutive Models for Soils Under Cyclic Loading, Master Thesis, Technic University of Lisbon, Lisbon, 2012.

Plaxis, Plaxis 2D Material Models Manual, Bentley, 2022.

Plaxis, Plaxis 2D Reference Manual, Bentley, 2022.

Plaxis, Plaxis 2D Scientific Manual, Bentley, 2022.

Puri, N., Prasad, H. D. and Jain, A., Prediction of Geotechnical Parameters Using

Machine Learning Techniques, Procedia Computer Science 125 (2018) 509-517.

Schanz, T., Vermeer, P.A., Bonnier, P.G., The Hardening-Soil Model: Formulation and Verification. Beyond 2000 in Computational Geotechnics, Balkema, Rotterdam. 281–290, 1999.

Shafiqu, Q. S. M. and Sa'ur, R. H. M., Numerical Analysis of a Pile-Soil System Under Earthquake Loading, Al-Nahrain Journal for Engineering Science 20(2) (2017) 446-451.

Sharudin, E. S., Yunus, N. Z. M., Marto, A., Jusoh, S. N., Ahmad, K., Kasim, F., Abdullah, R. A. and Hezmi, M. A., Rock Bearing Resistance of Bored Piles Socketed into Rock, Jurnal Teknologi 78 (8) (2016) 45-51.

Sluis, J., Validation of Embedded Pile Row in Plaxis 2D, Master Thesis, Delft University of Technology, Delft, 2012.

Sluys, L. J., Wave Propagation, Localisation and Dispersion in Softening Solids, Ph.D. Thesis, Delft University of Technology, Delft, 1992.

Sucuoğlu, H., Akkar, S., Basic Earthquake Engineering, Springer International Publishing, Switzerland, 2014.

Suzuki, H., Tokimatsu, K. and Tabata, K., Factors Affecting Stress Distributions of 3×3 Pile group in Dry Sand Based on Three-Dimensional Large Shaking Table Tests, Soils and Foundations 54 (4) (2014) 699-712.

Sykora, D. E. and Stokoe, K. H., Correlations of in-Situ Measurements in Sands of Shear Wave Velocity, Soil Dynamics and Earthquake Engineering 20 (1983) 125–136.

Tomlinson, M. J., The Adhesion of Piles Driven in Clay Soils, Proceedings of 5th International Conference, ISSMGE, London, Vol. 2, 66-71, 1957.

USGS, Earthquake Hazards Program, https://www.usgs.gov/glossary/earthquake-hazards-program (Date accessed: May 2, 2024).

Vesic, A. S., Design of Pile Foundations, NCHRP Synthesis 42, Transportation Research Board, Washington, D.C., 1977.

Vijayvergiya, V. N., Focht, J. A., A new way to predict the capacity of piles in clay, Proceedings of 4th Annual Offshore Technology Conference, Houston, 865-874, 1972.

Wolff, T. F., Pile Capacity Prediction Using Parameter Functions, ASCE Geotechnical Special Publication 23 (1989) 96–106.

Wolf, J. P., Soil-Structure-Interaction Analysis in Time Domain, Nuclear Engineering and Design 111 (3) (1989).

Yasuda, S., Yoshida, N., Kiku, H., Adachi, K., A Simplified Practical Method for Evaluating Liquefaction Induced Flow, Proceedings of the 7th U.S.-Japan Workshop on Earthquake Resistant Design of Lifeline Facilities and Countermeasures against Liquefaction, New York, 311-320, 1999.

Yiğit, M. A., Onur, M. İ. and Balaban, E., Investigation of Soil Pile Interaction Parameters in Piled Foundations, Journal of the Faculty of Engineering and Architecture of Gazi University 37 (2) (2021) 625-639.

Yu, K. H., Kadarman, A. H. and Djojodihardjo, H., Development and Implementation of Some BEM Variants- A Critical Review, Engineering Analysis with Boundary Elements (2010).

Zein, Z. H., Jaber, L. and Temsah, Y, Dynamic Soil-Structure Interaction Analysis: Detecting the Reliability of Modelling the Piles as a Plate Element for a Multistory Building Resting on Deep Foundation, BAU Journal - Science and Technology 2 (2) (2021).

APPENDICES

APPENDIX A – Soil Parameters

$V_{s1} = 150$ m/s, $V_{s2} = 300$ m/s, $H_1 = H_2 = 20.0$ m

Material set			
Identification number		1	2
Identification		Loose Sand	Dense Sand
Soil model		HS small	HS small
Drainage type		Drained	Drained
Colour		RGB 183, 215, 167	RGB 224, 200, 189
Comments			

Unit weights			
γ_{unsat}	kN/m³	17,00	21,00
γ_{sat}	kN/m³	17,00	21,00

Void ratio			
e_{init}		0,5000	0,5000
n_{init}		0,3333	0,3333

Rayleigh damping			
Input method		SDOF equivalent	SDOF equivalent
Rayleigh α		0,05890	0,05890
Rayleigh β		0,3183E-3	0,3183E-3
ξ_1	%	0,5000	0,5000
ξ_2	%	0,5000	0,5000
f_1	Hz	1,250	1,250
f_2	Hz	3,750	3,750

Material set			
Identification number		1	2
Identification		Loose Sand	Dense Sand
Soil model		HS small	HS small
Drainage type		Drained	Drained
Colour		RGB 183, 215, 167	RGB 224, 200, 189
Comments			

Stiffness			
E_{50}^{ref}	kN/m²	6580	26,72E3

Stiffness			
E_{oed}^{ref}	kN/m²	6580	26,72E3
E_{ur}^{ref}	kN/m²	19,74E3	80,16E3
v_{ur}		0,2000	0,2000
Alternatives			
Use alternatives		False	False
C_c		0,05249	0,01293
C_s		0,03057	0,01046
e_{init}		0,5000	0,5000
Stress-dependency			
power (m)		0,7000	0,7000
p_{ref}	kN/m²	100,0	100,0
Small-strain			
G_0^{ref}	kN/m²	41,97E3	114,8E3
$Y_{0.7}$		0,6345E-3	0,4335E-3
Strength			
Shear			
c'_{ref}	kN/m²	0,000	0,000
φ' (phi)	°	29,00	39,00
ψ (psi)	°	0,000	9,000
Depth-dependency			
c'_{inc}	kN/m²/r	0,000	0,000
y_{ref}	m	0,000	0,000
Dilatancy cut-off			
Dilatancy cut-off		False	False
e_{min}		1,000E-9	1,000E-9
e_{max}		999,0	999,0
Tension			
Tension cut-off		True	True
Tensile strength	kN/m²	0,000	0,000
Miscellaneous			
Use defaults		True	True

V$_{s1}$ = 150 m/s, V$_{s2}$ = 300 m/s, H$_1$ = (L-3) m, H$_2$ = (40-H$_1$) m, L = 18.0 m

Material set			
Identification number		1	2
Identification		Loose Sand	Dense Sand
Soil model		HS small	HS small
Drainage type		Drained	Drained
Colour		RGB 183, 215, 167	RGB 224, 200, 189
Comments			

Unit weights			
γ_{unsat}	kN/m³	17,00	21,00
γ_{sat}	kN/m³	17,00	21,00

Void ratio			
e_{init}		0,5000	0,5000
n_{init}		0,3333	0,3333

Rayleigh damping			
Input method		SDOF equivalent	SDOF equivalent
Rayleigh α		0,06409	0,06409
Rayleigh β		0,2926E-3	0,2926E-3
ξ_1	%	0,5000	0,5000
ξ_2	%	0,5000	0,5000
f_1	Hz	1,360	1,360
f_2	Hz	4,080	4,080

Material set			
Identification number		1	2
Identification		Loose Sand	Dense Sand
Soil model		HS small	HS small
Drainage type		Drained	Drained
Colour		RGB 183, 215, 167	RGB 224, 200, 189
Comments			

Stiffness			
E_{50}^{ref}	kN/m²	8050	27,89E3

Stiffness			
E_{oed}^{ref}	kN/m²	8050	27,89E3
E_{ur}^{ref}	kN/m²	24,15E3	83,67E3
v_{ur}		0,2000	0,2000
Alternatives			
Use alternatives		False	False
C_c		0,04291	0,01238
C_s		0,02498	0,01002
e_{init}		0,5000	0,5000
Stress-dependency			
power (m)		0,7000	0,7000
p_{ref}	kN/m²	100,0	100,0
Small-strain			
G_0^{ref}	kN/m²	51,33E3	119,8E3
$\gamma_{0.7}$		0,4759E-3	0,4079E-3
Strength			
Shear			
c'_{ref}	kN/m²	0,000	0,000
φ' (phi)	°	29,00	39,00
ψ (psi)	°	0,000	9,000
Depth-dependency			
c'_{inc}	kN/m²/r	0,000	0,000
y_{ref}	m	0,000	0,000
Dilatancy cut-off			
Dilatancy cut-off		False	False
e_{min}		1,000E-9	1,000E-9
e_{max}		999,0	999,0
Tension			
Tension cut-off		True	True
Tensile strength	kN/m²	0,000	0,000
Miscellaneous			
Use defaults		True	True

V$_{s1}$ = 150 m/s, V$_{s2}$ = 300 m/s, H$_1$ = (L-3) m, H$_2$ = (40-H$_1$) m, L = 20.0 m

Material set			
Identification number		1	2
Identification		Loose Sand	Dense Sand
Soil model		HS small	HS small
Drainage type		Drained	Drained
Colour		RGB 183, 215, 167	RGB 224, 200, 189
Comments			

Unit weights			
γ_{unsat}	kN/m³	17,00	21,00
γ_{sat}	kN/m³	17,00	21,00

Void ratio			
e_{init}		0,5000	0,5000
n_{init}		0,3333	0,3333

Rayleigh damping			
Input method		SDOF equivalent	SDOF equivalent
Rayleigh α		0,06220	0,06220
Rayleigh β		0,3014E-3	0,3014E-3
ξ_1	%	0,5000	0,5000
ξ_2	%	0,5000	0,5000
f_1	Hz	1,320	1,320
f_2	Hz	3,960	3,960

Material set			
Identification number		1	2
Identification		Loose Sand	Dense Sand
Soil model		HS small	HS small
Drainage type		Drained	Drained
Colour		RGB 183, 215, 167	RGB 224, 200, 189
Comments			

Stiffness			
E_{50}^{ref}	kN/m²	7380	27,41E3

Stiffness			
E_{oed}^{ref}	kN/m²	7380	27,41E3
E_{ur}^{ref}	kN/m²	22,14E3	82,23E3
v_{ur}		0,2000	0,2000
Alternatives			
Use alternatives		False	False
C_c		0,04680	0,01260
C_s		0,02725	0,01020
e_{init}		0,5000	0,5000
Stress-dependency			
power (m)		0,7000	0,7000
p_{ref}	kN/m²	100,0	100,0
Small-strain			
G_0^{ref}	kN/m²	47,03E3	117,7E3
$\gamma_{0.7}$		0,5394E-3	0,4181E-3
Strength			
Shear			
c'_{ref}	kN/m²	0,000	0,000
φ' (phi)	°	29,00	39,00
ψ (psi)	°	0,000	9,000
Depth-dependency			
c'_{inc}	kN/m²/r	0,000	0,000
y_{ref}	m	0,000	0,000
Dilatancy cut-off			
Dilatancy cut-off		False	False
e_{min}		1,000E-9	1,000E-9
e_{max}		999,0	999,0
Tension			
Tension cut-off		True	True
Tensile strength	kN/m²	0,000	0,000
Miscellaneous			
Use defaults		True	True

$V_{s1} = 150$ m/s, $V_{s2} = 300$ m/s, $H_1 = (L-3)$ m, $H_2 = (40-H_1)$ m, $L = 22.0$ m

Material set			
Identification number		1	2
Identification		Loose Sand	Dense Sand
Soil model		HS small	HS small
Drainage type		Drained	Drained
Colour		RGB 183, 215, 167	RGB 224, 200, 189
Comments			

Unit weights			
γ_{unsat}	kN/m³	17,00	21,00
γ_{sat}	kN/m³	17,00	21,00

Void ratio			
e_{init}		0,5000	0,5000
n_{init}		0,3333	0,3333

Rayleigh damping			
Input method		SDOF equivalent	SDOF equivalent
Rayleigh α		0,05985	0,05985
Rayleigh β		0,3133E-3	0,3133E-3
ξ_1	%	0,5000	0,5000
ξ_2	%	0,5000	0,5000
f_1	Hz	1,270	1,270
f_2	Hz	3,810	3,810

Material set			
Identification number		1	2
Identification		Loose Sand	Dense Sand
Soil model		HS small	HS small
Drainage type		Drained	Drained
Colour		RGB 183, 215, 167	RGB 224, 200, 189
Comments			

Stiffness			
E_{50}^{ref}	kN/m²	6820	26,95E3

Stiffness			
E_{oed}^{ref}	kN/m²	6820	26,95E3
E_{ur}^{ref}	kN/m²	20,46E3	80,85E3
v_{ur}		0,2000	0,2000
Alternatives			
Use alternatives		False	False
C_c		0,05064	0,01282
C_s		0,02949	0,01037
e_{init}		0,5000	0,5000
Stress-dependency			
power (m)		0,7000	0,7000
p_{ref}	kN/m²	100,0	100,0
Small-strain			
G_0^{ref}	kN/m²	43,50E3	115,8E3
$\gamma_{0.7}$		0,6028E-3	0,4284E-3
Strength			
Shear			
c'_{ref}	kN/m²	0,000	0,000
φ' (phi)	°	29,00	39,00
ψ (psi)	°	0,000	9,000
Depth-dependency			
c'_{inc}	kN/m²/r	0,000	0,000
y_{ref}	m	0,000	0,000
Dilatancy cut-off			
Dilatancy cut-off		False	False
e_{min}		1,000E-9	1,000E-9
e_{max}		999,0	999,0
Tension			
Tension cut-off		True	True
Tensile strength	kN/m²	0,000	0,000
Miscellaneous			
Use defaults		True	True

V$_{s1}$ = 150 m/s, V$_{s2}$ = 300 m/s, H$_1$ = (L-3) m, H$_2$ = (40-H$_1$) m, L = 28.0 m

Material set			
Identification number		1	2
Identification		Loose Sand	Dense Sand
Soil model		HS small	HS small
Drainage type		Drained	Drained
Colour		RGB 183, 215, 167	RGB 224, 200, 189
Comments			

Unit weights			
γ_{unsat}	kN/m³	17,00	21,00
γ_{sat}	kN/m³	17,00	21,00

Void ratio			
e_{init}		0,5000	0,5000
n_{init}		0,3333	0,3333

Rayleigh damping			
Input method		SDOF equivalent	SDOF equivalent
Rayleigh α		0,05419	0,05419
Rayleigh β		0,3460E-3	0,3460E-3
ξ_1	%	0,5000	0,5000
ξ_2	%	0,5000	0,5000
f_1	Hz	1,150	1,150
f_2	Hz	3,450	3,450

Material set			
Identification number		1	2
Identification		Loose Sand	Dense Sand
Soil model		HS small	HS small
Drainage type		Drained	Drained
Colour		RGB 183, 215, 167	RGB 224, 200, 189
Comments			

Stiffness			
E_{50}^{ref}	kN/m²	5630	25,67E3

Stiffness			
E_{oed}^{ref}	kN/m²	5630	25,67E3
E_{ur}^{ref}	kN/m²	16,89E3	77,01E3
v_{ur}		0,2000	0,2000
Alternatives			
Use alternatives		False	False
C_c		0,06135	0,01345
C_s		0,03572	0,01089
e_{init}		0,5000	0,5000
Stress-dependency			
power (m)		0,7000	0,7000
p_{ref}	kN/m²	100,0	100,0
Small-strain			
G_0^{ref}	kN/m²	35,90E3	110,3E3
$Y_{0.7}$		0,7932E-3	0,4591E-3
Strength			
Shear			
c'_{ref}	kN/m²	0,000	0,000
φ' (phi)	°	29,00	39,00
ψ (psi)	°	0,000	9,000
Depth-dependency			
c'_{inc}	kN/m²/r	0,000	0,000
y_{ref}	m	0,000	0,000
Dilatancy cut-off			
Dilatancy cut-off		False	False
e_{min}		1,000E-9	1,000E-9
e_{max}		999,0	999,0
Tension			
Tension cut-off		True	True
Tensile strength	kN/m²	0,000	0,000
Miscellaneous			
Use defaults		True	True

$V_{s1} = 150$ m/s, $V_{s2} = 300$ m/s, $H_1 = (L-3)$ m, $H_2 = (40-H_1)$ m, $L = 32.0$ m

Material set			
Identification number		1	2
Identification		Loose Sand	Dense Sand
Soil model		HS small	HS small
Drainage type		Drained	Drained
Colour		RGB 183, 215, 167	RGB 224, 200, 189
Comments			

Unit weights			
γ_{unsat}	kN/m³	17,00	21,00
γ_{sat}	kN/m³	17,00	21,00

Void ratio			
e_{init}		0,5000	0,5000
n_{init}		0,3333	0,3333

Rayleigh damping			
Input method		SDOF equivalent	SDOF equivalent
Rayleigh α		0,05137	0,05137
Rayleigh β		0,3650E-3	0,3650E-3
ξ_1	%	0,5000	0,5000
ξ_2	%	0,5000	0,5000
f_1	Hz	1,090	1,090
f_2	Hz	3,270	3,270

Material set			
Identification number		1	2
Identification		Loose Sand	Dense Sand
Soil model		HS small	HS small
Drainage type		Drained	Drained
Colour		RGB 183, 215, 167	RGB 224, 200, 189
Comments			

Stiffness			
E_{50}^{ref}	kN/m²	5080	24,90E3

Stiffness			
E_{oed}^{ref}	kN/m²	5080	24,90E3
E_{ur}^{ref}	kN/m²	15,24E3	74,70E3
v_{ur}		0,2000	0,2000
Alternatives			
Use alternatives		False	False
C_c		0,06799	0,01387
C_s		0,03959	0,01123
e_{init}		0,5000	0,5000
Stress-dependency			
power (m)		0,7000	0,7000
p_{ref}	kN/m²	100,0	100,0
Small-strain			
G_0^{ref}	kN/m²	32,36E3	107,0E3
$\gamma_{0.7}$		0,9201E-3	0,4796E-3
Strength			
Shear			
c'_{ref}	kN/m²	0,000	0,000
φ' (phi)	°	29,00	39,00
ψ (psi)	°	0,000	9,000
Depth-dependency			
c'_{inc}	kN/m²/r	0,000	0,000
y_{ref}	m	0,000	0,000
Dilatancy cut-off			
Dilatancy cut-off		False	False
e_{min}		1,000E-9	1,000E-9
e_{max}		999,0	999,0
Tension			
Tension cut-off		True	True
Tensile strength	kN/m²	0,000	0,000
Miscellaneous			
Use defaults		True	True

$V_{s1} = 150$ m/s, $V_{s2} = 760$ m/s, $H_1 = H_2 = 20.0$ m

Material set

Identification number		1
Identification		Loose Sand
Soil model		HS small
Drainage type		Drained
Colour		RGB 183, 215, 167
Comments		

Unit weights

γ_{unsat}	kN/m³	17,00
γ_{sat}	kN/m³	17,00

Void ratio

e_{init}		0,5000
n_{init}		0,3333

Rayleigh damping

Input method		SDOF equivalent
Rayleigh α		0,07398
Rayleigh β		0,2534E-3
ξ_1	%	0,5000
ξ_2	%	0,5000
f_1	Hz	1,570
f_2	Hz	4,710

Material set

Identification number		1
Identification		Loose Sand
Soil model		HS small
Drainage type		Drained
Colour		RGB 183, 215, 167
Comments		

Stiffness

E_{50}^{ref}	kN/m²	6580

Stiffness		
E_{oed}^{ref}	kN/m²	6580
E_{ur}^{ref}	kN/m²	19,74E3
v_{ur}		0,2000
Alternatives		
Use alternatives		False
C_c		0,05249
C_s		0,03057
e_{init}		0,5000
Stress-dependency		
power (m)		0,7000
p_{ref}	kN/m²	100,0
Small-strain		
G_0^{ref}	kN/m²	41,97E3
$\gamma_{0.7}$		0,6345E-3
Strength		
Shear		
c'_{ref}	kN/m²	0,000
φ' (phi)	°	29,00
ψ (psi)	°	0,000
Depth-dependency		
c'_{inc}	kN/m²/r	0,000
y_{ref}	m	0,000
Dilatancy cut-off		
Dilatancy cut-off		False
e_{min}		1,000E-9
e_{max}		999,0
Tension		
Tension cut-off		True
Tensile strength	kN/m²	0,000
Miscellaneous		
Use defaults		True

Material set

Identification number		2
Identification		Rock
Soil model		Mohr-Coulomb
Drainage type		Drained
Colour		RGB 115, 156, 160
Comments		

Unit weights

γ_{unsat}	kN/m³	25,00
γ_{sat}	kN/m³	25,00

Void ratio

e_{init}		0,5000
n_{init}		0,3333

Rayleigh damping

Input method		SDOF equivalent
Rayleigh α		0,07398
Rayleigh β		0,2534E-3
ξ_1	%	0,5000
ξ_2	%	0,5000
f_1	Hz	1,570
f_2	Hz	4,710

Material set

Identification number		2
Identification		Rock
Soil model		Mohr-Coulomb
Drainage type		Drained
Colour		RGB 115, 156, 160
Comments		

Stiffness

E'_{ref}	kN/m²	3,680E6

Stiffness		
ν (nu)		0,2500
Alternatives		
G_{ref}	kN/m²	1,472E6
E_{oed}	kN/m²	4,416E6
Depth-dependency		
E'_{inc}	kN/m²/r	0,000
y_{ref}	m	0,000
Wave velocities		
V_s	m/s	760,0
V_p	m/s	1316
Strength		
Shear		
c'_{ref}	kN/m²	50,00
φ' (phi)	°	30,00
ψ (psi)	°	0,000
Depth-dependency		
c'_{inc}	kN/m²/r	0,000
y_{ref}	m	0,000
Tension		
Tension cut-off		True
Tensile strength	kN/m²	0,000
Excess pore pressure calculation		
Determination		v-undrained definition
ν_u definition method		Direct
$\nu_{u,equivalent}$ (nu)		0,4950
Skempton B		0,9833
$K_{w,ref}/n$	kN/m²	144,3E6
Material set		
Identification number		2
Identification		Rock
Soil model		Mohr-Coulomb

$V_{s1} = 300$ m/s, $V_{s2} = 150$ m/s, $H_1 = H_2 = 20.0$ m

Material set			
Identification number		1	2
Identification		Loose Sand	Dense Sand
Soil model		HS small	HS small
Drainage type		Drained	Drained
Colour		RGB 194, 189, 179	RGB 232, 224, 201
Comments			

Unit weights			
γ_{unsat}	kN/m³	17,00	21,00
γ_{sat}	kN/m³	17,00	21,00

Void ratio			
e_{init}		0,5000	0,5000
n_{init}		0,3333	0,3333

Rayleigh damping			
Input method		SDOF equivalent	SDOF equivalent
Rayleigh α		0,05890	0,05890
Rayleigh β		0,3183E-3	0,3183E-3
ξ_1	%	0,5000	0,5000
ξ_2	%	0,5000	0,5000
f_1	Hz	1,250	1,250
f_2	Hz	3,750	3,750

Material set			
Identification number		1	2
Identification		Loose Sand	Dense Sand
Soil model		HS small	HS small
Drainage type		Drained	Drained
Colour		RGB 194, 189, 179	RGB 232, 224, 201
Comments			

Stiffness			
E_{50}^{ref}	kN/m²	2760	52,43E3

Stiffness			
E_{oed}^{ref}	kN/m²	2760	52,43E3
E_{ur}^{ref}	kN/m²	8280	157,3E3
ν_{ur}		0,2000	0,2000
Alternatives			
Use alternatives		False	False
C_c		0,1251	6,588E-3
C_s		0,07287	5,332E-3
e_{init}		0,5000	0,5000
Stress-dependency			
power (m)		0,7000	0,7000
P_{ref}	kN/m²	100,0	100,0
Small-strain			
G_0^{ref}	kN/m²	17,57E3	225,2E3
$\gamma_{0.7}$		2,202E-3	0,1655E-3
Strength			
Shear			
c'_{ref}	kN/m²	0,000	0,000
φ' (phi)	°	29,00	39,00
ψ (psi)	°	0,000	9,000
Depth-dependency			
c'_{inc}	kN/m²/r	0,000	0,000
y_{ref}	m	0,000	0,000
Dilatancy cut-off			
Dilatancy cut-off		False	False
e_{min}		1,000E-9	1,000E-9
e_{max}		999,0	999,0
Tension			
Tension cut-off		True	True
Tensile strength	kN/m²	0,000	0,000
Miscellaneous			
Use defaults		True	True

V$_{s1}$ = 300 m/s, V$_{s2}$ = 150 m/s, H$_1$ = (L-3) m, H$_2$ = (40-H$_1$) m, L = 18.0 m

Material set			
Identification number		1	2
Identification		Loose Sand	Dense Sand
Soil model		HS small	HS small
Drainage type		Drained	Drained
Colour		RGB 194, 189, 179	RGB 232, 224, 201
Comments			

Unit weights			
γ_{unsat}	kN/m³	17,00	21,00
γ_{sat}	kN/m³	17,00	21,00

Void ratio			
e_{init}		0,5000	0,5000
n_{init}		0,3333	0,3333

Rayleigh damping			
Input method		SDOF equivalent	SDOF equivalent
Rayleigh α		0,05419	0,05419
Rayleigh β		0,3460E-3	0,3460E-3
ξ_1	%	0,5000	0,5000
ξ_2	%	0,5000	0,5000
f_1	Hz	1,150	1,150
f_2	Hz	3,450	3,450

Material set			
Identification number		1	2
Identification		Loose Sand	Dense Sand
Soil model		HS small	HS small
Drainage type		Drained	Drained
Colour		RGB 194, 189, 179	RGB 232, 224, 201
Comments			

Stiffness			
E_{50}^{ref}	kN/m²	2980	64,13E3

Stiffness			
E_{oed}^{ref}	kN/m²	2980	64,13E3
E_{ur}^{ref}	kN/m²	8940	192,4E3
v_{ur}		0,2000	0,2000
Alternatives			
Use alternatives		False	False
C_c		0,1159	5,386E-3
C_s		0,06749	4,359E-3
e_{init}		0,5000	0,5000
Stress-dependency			
power (m)		0,7000	0,7000
p_{ref}	kN/m²	100,0	100,0
Small-strain			
G_0^{ref}	kN/m²	19,00E3	275,5E3
$\gamma_{0.7}$		1,969E-3	0,1241E-3
Strength			
Shear			
c'_{ref}	kN/m²	0,000	0,000
φ' (phi)	°	29,00	39,00
ψ (psi)	°	0,000	9,000
Depth-dependency			
c'_{inc}	kN/m²/m	0,000	0,000
y_{ref}	m	0,000	0,000
Dilatancy cut-off			
Dilatancy cut-off		False	False
e_{min}		1,000E-9	1,000E-9
e_{max}		999,0	999,0
Tension			
Tension cut-off		True	True
Tensile strength	kN/m²	0,000	0,000
Miscellaneous			
Use defaults		True	True

$V_{s1} = 300$ m/s, $V_{s2} = 150$ m/s, $H_1 = (L-3)$ m, $H_2 = (40-H_1)$ m, $L = 20.0$ m

Material set			
Identification number		1	2
Identification		Loose Sand	Dense Sand
Soil model		HS small	HS small
Drainage type		Drained	Drained
Colour		RGB 194, 189, 179	RGB 232, 224, 201
Comments			

Unit weights			
γ_{unsat}	kN/m³	17,00	21,00
γ_{sat}	kN/m³	17,00	21,00

Void ratio			
e_{init}		0,5000	0,5000
n_{init}		0,3333	0,3333

Rayleigh damping			
Input method		SDOF equivalent	SDOF equivalent
Rayleigh α		0,05608	0,05608
Rayleigh β		0,3344E-3	0,3344E-3
ξ_1	%	0,5000	0,5000
ξ_2	%	0,5000	0,5000
f_1	Hz	1,190	1,190
f_2	Hz	3,570	3,570

Material set			
Identification number		1	2
Identification		Loose Sand	Dense Sand
Soil model		HS small	HS small
Drainage type		Drained	Drained
Colour		RGB 194, 189, 179	RGB 232, 224, 201
Comments			

Stiffness			
E_{50}^{ref}	kN/m²	2885	58,75E3

Stiffness			
E_{oed}^{ref}	kN/m²	2885	58,75E3
E_{ur}^{ref}	kN/m²	8655	176,3E3
v_{ur}		0,2000	0,2000
Alternatives			
Use alternatives		False	False
C_c		0,1197	5,879E-3
C_s		0,06971	4,758E-3
e_{init}		0,5000	0,5000
Stress-dependency			
power (m)		0,7000	0,7000
P_{ref}	kN/m²	100,0	100,0
Small-strain			
G_0^{ref}	kN/m²	18,39E3	252,4E3
$\gamma_{0.7}$		2,062E-3	0,1407E-3
Strength			
Shear			
c'_{ref}	kN/m²	0,000	0,000
φ' (phi)	°	29,00	39,00
ψ (psi)	°	0,000	9,000
Depth-dependency			
c'_{inc}	kN/m²/m	0,000	0,000
y_{ref}	m	0,000	0,000
Dilatancy cut-off			
Dilatancy cut-off		False	False
e_{min}		1,000E-9	1,000E-9
e_{max}		999,0	999,0
Tension			
Tension cut-off		True	True
Tensile strength	kN/m²	0,000	0,000
Miscellaneous			
Use defaults		True	True

V$_{s1}$ = 300 m/s, V$_{s2}$ = 150 m/s, H$_1$ = (L-3) m, H$_2$ = (40-H$_1$) m, L = 22.0 m

Material set			
Identification number		1	2
Identification		Loose Sand	Dense Sand
Soil model		HS small	HS small
Drainage type		Drained	Drained
Colour		RGB 194, 189, 179	RGB 232, 224, 201
Comments			

Unit weights			
γ_{unsat}	kN/m³	17,00	21,00
γ_{sat}	kN/m³	17,00	21,00

Void ratio			
e_{init}		0,5000	0,5000
n_{init}		0,3333	0,3333

Rayleigh damping			
Input method		SDOF equivalent	SDOF equivalent
Rayleigh α		0,05796	0,05796
Rayleigh β		0,3235E-3	0,3235E-3
ξ_1	%	0,5000	0,5000
ξ_2	%	0,5000	0,5000
f_1	Hz	1,230	1,230
f_2	Hz	3,690	3,690

Material set			
Identification number		1	2
Identification		Loose Sand	Dense Sand
Soil model		HS small	HS small
Drainage type		Drained	Drained
Colour		RGB 194, 189, 179	RGB 232, 224, 201
Comments			

Stiffness			
E_{50}^{ref}	kN/m²	2800	54,35E3

Stiffness			
E_{oed}^{ref}	kN/m²	2800	54,35E3
E_{ur}^{ref}	kN/m²	8400	163,1E3
v_{ur}		0,2000	0,2000
Alternatives			
Use alternatives		False	False
C_c		0,1234	6,355E-3
C_s		0,07183	5,143E-3
e_{init}		0,5000	0,5000
Stress-dependency			
power (m)		0,7000	0,7000
p_{ref}	kN/m²	100,0	100,0
Small-strain			
G_0^{ref}	kN/m²	17,83E3	233,5E3
$\gamma_{0.7}$		2,156E-3	0,1572E-3
Strength			
Shear			
c'_{ref}	kN/m²	0,000	0,000
φ' (phi)	°	29,00	39,00
ψ (psi)	°	0,000	9,000
Depth-dependency			
c'_{inc}	kN/m²/n	0,000	0,000
y_{ref}	m	0,000	0,000
Dilatancy cut-off			
Dilatancy cut-off		False	False
e_{min}		1,000E-9	1,000E-9
e_{max}		999,0	999,0
Tension			
Tension cut-off		True	True
Tensile strength	kN/m²	0,000	0,000
Miscellaneous			
Use defaults		True	True

$V_{s1} = 300$ m/s, $V_{s2} = 150$ m/s, $H_1 = (L-3)$ m, $H_2 = (40-H_1)$ m, L = 28.0 m

Material set			
Identification number		1	2
Identification		Loose Sand	Dense Sand
Soil model		HS small	HS small
Drainage type		Drained	Drained
Colour		RGB 194, 189, 179	RGB 232, 224, 201
Comments			

Unit weights			
γ_{unsat}	kN/m³	17,00	21,00
γ_{sat}	kN/m³	17,00	21,00

Void ratio			
e_{init}		0,5000	0,5000
n_{init}		0,3333	0,3333

Rayleigh damping			
Input method		SDOF equivalent	SDOF equivalent
Rayleigh α		0,06409	0,06409
Rayleigh β		0,2926E-3	0,2926E-3
ξ_1	%	0,5000	0,5000
ξ_2	%	0,5000	0,5000
f_1	Hz	1,360	1,360
f_2	Hz	4,080	4,080

Material set			
Identification number		1	2
Identification		Loose Sand	Dense Sand
Soil model		HS small	HS small
Drainage type		Drained	Drained
Colour		RGB 194, 189, 179	RGB 232, 224, 201
Comments			

Stiffness			
E_{50}^{ref}	kN/m²	2570	44,85E3

Stiffness			
$E_{oed}{}^{ref}$	kN/m²	2570	44,85E3
$E_{ur}{}^{ref}$	kN/m²	7710	134,6E3
v_{ur}		0,2000	0,2000
Alternatives			
Use alternatives		False	False
C_c		0,1344	7,701E-3
C_s		0,07826	6,233E-3
e_{init}		0,5000	0,5000
Stress-dependency			
power (m)		0,7000	0,7000
p_{ref}	kN/m²	100,0	100,0
Small-strain			
$G_0{}^{ref}$	kN/m²	16,37E3	192,7E3
$\gamma_{0.7}$		2,436E-3	0,2069E-3
Strength			
Shear			
c'_{ref}	kN/m²	0,000	0,000
φ' (phi)	°	29,00	39,00
ψ (psi)	°	0,000	9,000
Depth-dependency			
c'_{inc}	kN/m²/m	0,000	0,000
y_{ref}	m	0,000	0,000
Dilatancy cut-off			
Dilatancy cut-off		False	False
e_{min}		1,000E-9	1,000E-9
e_{max}		999,0	999,0
Tension			
Tension cut-off		True	True
Tensile strength	kN/m²	0,000	0,000
Miscellaneous			
Use defaults		True	True

V$_{s1}$ = 300 m/s, V$_{s2}$ = 150 m/s, H$_1$ = (L-3) m, H$_2$ = (40-H$_1$) m, L = 32.0 m

Material set			
Identification number		1	2
Identification		Loose Sand	Dense Sand
Soil model		HS small	HS small
Drainage type		Drained	Drained
Colour		RGB 194, 189, 179	RGB 232, 224, 201
Comments			

Unit weights			
γ_{unsat}	kN/m³	17,00	21,00
γ_{sat}	kN/m³	17,00	21,00

Void ratio			
e_{init}		0,5000	0,5000
n_{init}		0,3333	0,3333

Rayleigh damping			
Input method		SDOF equivalent	SDOF equivalent
Rayleigh α		0,06927	0,06927
Rayleigh β		0,2707E-3	0,2707E-3
ξ_1	%	0,5000	0,5000
ξ_2	%	0,5000	0,5000
f_1	Hz	1,470	1,470
f_2	Hz	4,410	4,410

Material set			
Identification number		1	2
Identification		Loose Sand	Dense Sand
Soil model		HS small	HS small
Drainage type		Drained	Drained
Colour		RGB 194, 189, 179	RGB 232, 224, 201
Comments			

Stiffness			
E_{50}^{ref}	kN/m²	2440	40,43E3

Stiffness			
E_{oed}^{ref}	kN/m²	2440	40,43E3
E_{ur}^{ref}	kN/m²	7320	121,3E3
v_{ur}		0,2000	0,2000
Alternatives			
Use alternatives		False	False
C_c		0,1416	8,544E-3
C_s		0,08243	6,915E-3
e_{init}		0,5000	0,5000
Stress-dependency			
power (m)		0,7000	0,7000
p_{ref}	kN/m²	100,0	100,0
Small-strain			
G_0^{ref}	kN/m²	15,55E3	173,6E3
$\gamma_{0.7}$		2,622E-3	0,2400E-3
Strength			
Shear			
c'_{ref}	kN/m²	0,000	0,000
φ' (phi)	°	29,00	39,00
ψ (psi)	°	0,000	9,000
Depth-dependency			
c'_{inc}	kN/m²/m	0,000	0,000
y_{ref}	m	0,000	0,000
Dilatancy cut-off			
Dilatancy cut-off		False	False
e_{min}		1,000E-9	1,000E-9
e_{max}		999,0	999,0
Tension			
Tension cut-off		True	True
Tensile strength	kN/m²	0,000	0,000
Miscellaneous			
Use defaults		True	True

APPENDIX B – Vertical Pile Capacities

Table B.1. Vertical Pile Capacities ($V_{s1} = 150$ m/s, $V_{s2} = 300$ m/s, $H_1 = H_2 = 20$ m)

Pile Properties		Skin Friction per Unit Length		Tip Resistance, Q_P (kN)
L (m)	D (m)	q_{s1} (kN/m)	q_{s2} (kN/m)	
10.0	1.0	55.3	-	1201.7
14.0		74.6	-	1682.3
18.0		93.2	-	1802.5
20.0		99.4	-	12016.6
22.0		99.4	224.3	12016.6
24.0				
26.0				
28.0				
30.0				
32.0	0.8	71.6	143.6	6152.5
	1.0	99.4	224.3	12016.6
	1.2	126.6	323.0	20764.7

Table B.2. Vertical Pile Capacities ($V_{s1} = 300$ m/s, $V_{s2} = 150$ m/s, $H_1 = H_2 = 20$ m)

Pile Properties		Skin Friction per Unit Length		Tip Resistance, Q_P (kN)
L (m)	D (m)	q_{s1} (kN/m)	q_{s2} (kN/m)	
10.0	1.0	92.4	-	9896.0
14.0		129.3	-	13854.4
18.0		161.6	-	14844.0
20.0		173.2	-	2226.6
22.0		173.2	197.4	2226.6
24.0				
26.0				
28.0				
30.0				
32.0	0.8	124.1	126.3	1140.0
	1.0	173.2	197.4	2226.6
	1.2	219.5	284.3	3847.6

Table B.3. Vertical Pile Capacities (V_{s1} = 150 m/s, V_{s2} = 300 m/s, H_1 = (L-3) m, H_2 = (40-H_1) m)

Pile Properties		Skin Friction per Unit Length		Tip Resistance, Q_p (kN)
L (m)	D (m)	q_{s1} (kN/m)	q_{s2} (kN/m)	
18.0	1.0	79.9	224.3	12016.6
20.0		89.3		
22.0		96.7		
28.0		111.9		
32.0		118.5		

Table B.4. Vertical Pile Capacities (V_{s1} = 300 m/s, V_{s2} = 150 m/s, H_1 = (L-3) m, H_2 = (40-H_1) m)

Pile Properties		Skin Friction per Unit Length		Tip Resistance, Q_p (kN)
L (m)	D (m)	q_{s1} (kN/m)	q_{s2} (kN/m)	
18.0	1.0	138.6	197.4	2226.6
20.0		154.9		
22.0		167.7		
28.0		194.0		
32.0		205.4		

Table B.5. Vertical Pile Capacities (V_{s1} = 150 m/s, V_{s2} = 760 m/s, H_1 = H_2 = 20 m)

Pile Properties		Skin Friction per Unit Length		Tip Resistance, Q_p (kN)
L (m)	D (m)	q_{s1} (kN/m)	q_{s2} (kN/m)	
21.0	1.0	99.9	1570.0	-
22.0				
23.0				
24.0				
30.0				